LEVEL II

AD A098264

DTIC FILE COPY

DTIC ELECTE APR 28 1981 S D C

DISTRIBUTION STATEMENT A
Approved for public release;
Distribution Unlimited

NIELSEN ENGINEERING
AND RESEARCH, INC.

OFFICES: 510 CLYDE AVENUE / MOUNTAIN VIEW, CALIFORNIA 94043 / TELEPHONE (415) 968-9457

81 4 27 003

(12)

COPY NO. 14

EXPERIMENTAL RESULTS ON VORTICITY SHEDDING AT THE EDGE OF A FLAT PLATE IN TWO-DIMENSIONAL FLOW

by

S. B. Spangler, R. G. Schwind,
and K. Owen

NEAR TR 224
September 1980

Technical Report
For the period May, 1978 to March, 1980

Prepared under Contract No. N00014-78-C-0388

for

OFFICE OF NAVAL RESEARCH
Arlington, Virginia 22217

by

NIELSEN ENGINEERING & RESEARCH, INC.
510 Clyde Avenue, Mountain View, CA 94043
Telephone (415) 968-9457

Unclassified

SECURITY CLASSIFICATION OF THIS PAGE (When Data Entered)

REPORT DOCUMENTATION PAGE	READ INSTRUCTIONS BEFORE COMPLETING FORM
1. REPORT NUMBER	2. GOVT ACCESSION NO. AD-A098264 / 3. RECIPIENT'S CATALOG NUMBER
4. TITLE (and Subtitle) (6) EXPERIMENTAL RESULTS ON VORTICITY SHEDDING AT THE EDGE OF A FLAT PLATE IN TWO-DIMENSIONAL FLOW	5. TYPE OF REPORT & PERIOD COVERED (9) Interim Technical Report 1 May 79 -30 Mar 80 / (14) NEAR-TR-224 / 6. PERFORMING ORG. REPORT NUMBER
7. AUTHOR(s) (10) S. B. Spangler, R. G. Schwind, and K. Owen	8. CONTRACT OR GRANT NUMBER(s) (15) N00014-78-C-0388
9. PERFORMING ORGANIZATION NAME AND ADDRESS Nielsen Engineering & Research, Inc. 510 Clyde Avenue Mountain View, CA 94043 (16) RF41411	10. PROGRAM ELEMENT, PROJECT, TASK AREA & WORK UNIT NUMBERS 62241N RF 41-411-801 NR 212-253
11. CONTROLLING OFFICE NAME AND ADDRESS Office of Naval Research 800 N. Quincy Arlington, VA 22217 (12) 1521 (11)	12. REPORT DATE Sep[illegible] 1980 / 13. NUMBER OF PAGES 150
14. MONITORING AGENCY NAME & ADDRESS (if different from Controlling Office) (17) RF41411801	15. SECURITY CLASS. (of this report) Unclassified / 15a. DECLASSIFICATION/DOWNGRADING SCHEDULE

16. DISTRIBUTION STATEMENT (of this Report)

Approved for public release; distribution unlimited.

17. DISTRIBUTION STATEMENT (of the abstract entered in Block 20, if different from Report)

18. SUPPLEMENTARY NOTES

19. KEY WORDS (Continue on reverse side if necessary and identify by block number)

Vorticity
Vortex Shedding
Two-Dimensional Flow

20. ABSTRACT (Continue on reverse side if necessary and identify by block number)

A two-dimensional test was performed on a flat plate normal to a low subsonic flow to investigate the relationship between the vorticity shed at an edge and the vorticity appearing in the shear layer adjacent to the edge. Both a sharp and a rounded edge were provided on the plate. A splitter plate was used to create a steady wake flow behind the plate. The measurements made were velocities in the flow field, static pressures on the model —> next page

DD FORM 1 JAN 73 1473

Unclassified 381783

SECURITY CLASSIFICATION OF THIS PAGE (When Data Entered)

Block 20 (Continued)

upstream and downstream surfaces, and surface flow visualization. A laser velocimeter was used to obtain the velocity measurements. Analysis of the data was performed to calculate circulation and vorticity transport rate in the flow adjacent to the edge and vorticity transport rate of the flow separating from the edge.

PREFACE

This technical report covers the work performed under Contract N00014-78-C-0388 from May 1, 1978 through March 30, 1980. Significant cooperation was furnished by the Ames Research Center in conducting a test program in the 2- by 2-Foot Wind Tunnel. Specifically, we wish to express appreciation to Dr. Gary Chapman for his guidance and sponsorship of the test program and Mr. Earl Keener for the conduct of the test program, both of whom are members of the NASA staff.

Dr. Robert Whitehead and Mr. David Siegel, Office of Naval Research, were the Navy Scientific Officers.

This Document Contains
Missing Page/s That Are
Unavailable In The
Original Document

OR are
Blank pgs
that have
Been Removed

**BEST
AVAILABLE COPY**

TABLE OF CONTENTS

TABLE OF CONTENTS (Concluded)

LIST OF TABLES

LIST OF FIGURES

LIST OF FIGURES (Concluded)

EXPERIMENTAL RESULTS ON VORTICITY SHEDDING AT THE EDGE OF A FLAT PLATE IN TWO-DIMENSIONAL FLOW

by

S. B. Spangler, R. G. Schwind, and K. Owen

1. INTRODUCTION

Over the last several years, the requirement for good handling qualities of high-speed fighters at high angles of attack has led to the use of strakes, or leading-edge extensions. These have relatively sharp edges which produce flow separation and a leading-edge vortex system at high angles of attack. The vortex system interacts with the wing flow field to maintain lift to considerably higher angles of attack than for a wing without a strake.

The fluid mechanics of the leading-edge separating flow, the roll-up of the shear layer into a vortex, and the influence of the vortex on the flow about the strake and wing are poorly understood. In particular, strake design for a particular aircraft development program is an empirical process involving intuition and a great deal of wind tunnel testing.

The Office of Naval Research initiated a program at Nielsen Engineering & Research, Inc. (NEAR) to make a fundamental study of the fluid mechanics of flow over strakes. The overall objectives of the program are to develop a greater knowledge and understanding of the rate of shedding of vorticity at the edge and to develop methods for predicting the shedding rate. As a part of this program, experiments have been run at the Ames Research Center, NASA, on a two-dimensional model having both sharp and rounded edges. This report describes the test program and its results.

2. DESCRIPTION OF EXPERIMENT

This section contains a description of the test program, including the models, instrumentation, and flow conditions. An initial discussion on the general approach is given to show the rationale for the selection of the model configuration.

2.1 Approach

The flow over a three-dimensional strake/body configuration at moderate to high angles of attack is a steady flow exhibiting separation along the strake leading edges and roll-up of the vorticity in the shear layers into concentrated vortices above the leading edges. An essential feature of the problem is the viscous part: the boundary layer on the windward side of the strake that contains most of the vorticity leaving the edge and the lower speed viscous flow on the leeward side that also contains vorticity leaving the edge. A full consideration of the problem involves dealing with three-dimensional turbulent boundary layer growth on the windward side and the complicated three-dimensional separated flow on the leeward side dominated by the organized flow in the main leading-edge vortex.

Since prediction of shedding rate is an important aspect of the problem, it is desirable to start with a simple case in which the boundary-layer characteristics can be predicted with reasonable certainty, at least on the windward side, in order to provide some capability to compare measured and predicted shedding rates. The case selected is a two-dimensional experiment in which a model with a flat face facing upstream was placed across a wind tunnel test section. The flat face was selected over a more typical aircraft cross section of a cylinder with strakes because the windward side flow and boundary-layer development between the windward side stagnation line and the edge is more predictable than the cylinder/strake

combination, which would probably have flow separation in the corner formed by the intersection of the strake with the cylinder.

The model was supported at the ends on glass windows through which laser beams of a laser velocimeter (LV) could pass to measure velocities adjacent to the edges. Pressure measurements were made along the windward face and, to a lesser extent, on the leeward side, to define the pressure gradients under which the boundary layer develops. A splitter plate was used on the downstream side of the plate to obtain a steady flow in the shear layer and prevent the development of an unsteady wake vortex system that would otherwise develop behind the plate. Preliminary measurements were made in the NEAR Water/Wind Tunnel to select the splitter plate length.

The models were tested in the 2- by 2-Foot Transonic Wind Tunnel at Ames Research Center, NASA. This tunnel is not highly scheduled, is used primarily for research work, has an LV system, and has been used in similar kinds of tests on flow over two-dimensional shapes. The use of the tunnel was provided through the cooperation and interest of the technical staff of the Aerodynamics Division of Ames Research Center.

2.2 Models

Two models were tested. The configurations are shown in figure 1(a). The models consist of three pieces: a face piece, a support plate, and a splitter plate. The latter two pieces are common to both models. The two face pieces differ in edge radius, with one being sharp-edged and one rounded as shown. The rounded one was thicker, and thus it extended forward to $x = -0508$ cm [see fig. 1(a)]. The face pieces were fastened to the support piece with screws countersunk into the front of the face pieces, with the depression filled with wax and

smoothed. A 5 cm (2 inch) section at the center of the 61 cm (24 inch) span of the model was left without screws to provide a smooth surface at the center of the model where the velocity and pressure measurements were taken.

The support plate (used with both face pieces) was made with a cavity within which was laid the tubing connected to the pressure taps on the front and rear parts of the model. The tubing was led out the ends of the model through small holes in the center of the windows. The aft end of the support plate was dovetailed and fastened to the splitter plate with screws, countersunk and filled.

The splitter plate was made initially of a length such that the overall model length was 30.5 cm (12.5 inches) or 6 face widths. This length was selected based on information in the literature (ref. 1) indicating the length necessary to eliminate the unsteady wake behind a flat plate normal to the stream. It was also the maximum length permitted by the location of the wind tunnel sting which was used to support the trailing edge of the splitter plate.

Initial tests in the 2- by 2-Foot Tunnel showed high vibration levels characteristic of an unsteady wake. A 50.8 cm (20 inch) length of additional splitter plate was then added to the original splitter plate when an old short sting was located, so that trailing-edge support could still be achieved. Subsequent flow visualization tests indicated reattachment to occur about 3 cm aft of the original trailing edge. The step between the original and added splitter plates due to different thicknesses was blended with Devcon to provide a smooth transition between the two thicknesses of plate.

The model was supported at both ends of the support plate with pins that fitted into existing holes in the windows. A general arrangement of the test section is shown in figure 1(b)

and a close view of the window is shown in figure 1(c). The trailing edge was supported at its center with the short sting and sting support of the tunnel. In addition the outboard trailing edges of the splitter plate were fastened to the tunnel wall with angle brackets. With the longer splitter plate, the flexibility to change the attitude of the model slightly with the sting support to ensure orienting the face at zero angle of attack was lost. However, the face pressure with the final mounting arrangement showed essentially zero misalignment.

The locations of the pressure taps on the models are shown in figures 2-5. Figure 2 shows the locations on the face of the sharp-edge model. Most of the taps are concentrated at the center of the model, Row A [fig. 2(b)]. There are 13 taps over the half-width on which the velocity measurement were made, with the most outboard tap being .19 cm (.075 in.) from the sharp edge. It was not possible to place all the taps in a single row at the midspan station because of lack of space in the thin tip section, so the taps were staggered off the centerline as shown. Several taps were placed on the other half-width to examine the asymmetry of the pressures on the face. One tap (No. 18) was placed on the downstream side of the plate near the tip. A number of taps were placed at other stations along the span to assess the two-dimensionality of the flow, as shown.

Similar information is shown in figure 3 for the round-edge plate. In this case, taps were placed around the edge as well as on the top surface, with a spacing of 15 degrees around the edge.

Two pressure taps were placed in the support plate at the center station spanwise. The locations of these two stations are shown in figure 4.

Three pressure taps were placed on the splitter plate at midspan. The locations are shown in figure 5. These taps were placed on the side on which the velocity measurements were taken. The tubes for these three pressure taps were led aft along the opposite side of the plate back to the sting and out of the tunnel.

The tubing leaving the tunnel was connected into a standard scanivalve arrangement which is part of the data acquisition system for the facility. A one-second dwell time was used with the scanivalves in stepping through the ports. The length of tubing was such that all dynamic effects were damped out, and only steady state values were obtained. A series of 12.5 psi pressure transducers were used. The pressure data acquisition process includes a pressure check before and after a test series to identify leaky or blocked pressure taps. The pressure transducer output was digitized and processed in near-real-time and displayed in the control room.

Two Kulite high-frequency-response pressure transducers were used to assess the unsteadiness of the flow around the model. One was mounted on the front face of the model about 5 cm from the midspan station and about 1 cm from the center-line of the model. The second was mounted on the support plate about midway between the two static taps 32 and 33 shown on figure 4 but 5 cm from the midspan station.

The two transducers have a diameter of 2.3 mm (.090 inch) and were mounted from the rear of the surface such that the transducer surface was recessed approximately 3 mm (0.12 inch) from the exterior of the model surface. The hole size in the model at the transducers is approximately 1.8 mm (.070 inch). The transducers were statically calibrated in the 0 to 2 psi range. The output of the transducers was recorded on an FM four track tape recorder. The frequency response of the system is limited by the recording tape drive speed to about 5 KHz.

The coordinate system for the results presented in subsequent sections is shown in figure 1. The coordinates are centered on the midpoint of the sharp-edge front face, with x positive downstream and y positive up. For the round-edge face piece, the same physical location is used, but because of the greater thickness of the face piece, the front face is located at x = -0.508 cm (-0.2 inch).

2.3 Laser Velocimeter

Velocity measurements were made with a laser velocimeter. Figure 6 is a schematic of the laser velocimeter system designed for the Ames 2- by 2-Foot Transonic Wind Tunnel. This fringe-mode velocimeter is a dual-color system utilizing the 4880 Angstrom and 5145 Angstrom lines of an argon-ion laser. One spectral line is used to measure the streamwise velocity component, the other to measure the vertical velocity component. Bragg-cell frequency shifting necessary for probing highly turbulent and separated flow regions is incorporated in both spectral lines. The frequency offsets also facilitate the direct measurement of the vertical velocity component (i.e., ±45° beam orientations to resolve the vertical velocity are unnecessary).

As seen in figure 6, most of the optical components are located outside the tunnel plenum chamber, where color separation, Bragg-cell frequency shifting, and the establishment of the four-beam matrix are accomplished. Only the transmitting optics, collecting lens, and photo detectors are mounted inside the plenum chamber. Two traversing systems are shown inside the plenum chamber. The one on the opposite side of the test section from the laser holds the collecting lens and photo detectors for forward-scatter light collection. The traversing system on the laser side of the test section supports the transmitting lenses. Mirrors fixed to this traversing system

permit three-dimensional scanning of the velocimeter's sensing volume; the optics outside the plenum chamber remain stationary. Both traversing systems are driven with computer-controlled stepper motors. The effective sensing volume is approximately ellipsoidal, 200 μm in diameter and 3 mm long, with the long axis aligned in the cross stream direction.

Signal processing was accomplished with single-particle burst counters and the individual realizations from the two channels were simultaneously recorded. The mean velocities and turbulence intensities were calculated as follows:

$$\bar{u} = \sum_{i=1}^{N} u_i/N \tag{1}$$

$$\bar{v} = \sum_{i=1}^{N} v_i/N \tag{2}$$

$$\overline{u'^2} = \sum_{i=1}^{N} (u_i^2/N) - \bar{u}^2 \tag{3}$$

$$\overline{v'^2} = \sum_{i=1}^{N} (v_i^2/N) - \bar{v}^2 \tag{4}$$

Naturally occurring particles in the tunnel were used for light scattering. In this facility, lubrication oil within the drive system vaporizes and then condenses in the tunnel circuit to provide a generous supply of scattering centers. Previous measurements across a normal shock have shown that these particles are small enough in size (estimated to be 1 μm) to give very good response to a step change in velocity at sonic speeds. At each point in the flow, generally several hundred velocity realizations were used to calculate the flow properties given in Equations (1)-(4).

An analysis was performed to evaluate the confidence level on the velocity measurements. The approach is based on Gaussian probablity statistics from reference 2 and is described briefly in Appendix A. Typical results are given for measurements made in the outer flow and shear layer. The curves of figure A-1 can be used with the calculated rms velocity values in Tables I-IV to estimate confidence levels for any of the measurements.

2.4 Test Conditions

The 2- by 2-Foot Transonic Wind Tunnel is a variable density tunnel having a capability of 3 atmospheres of pressure and a continuously variable Mach number range from 0.2 to 1.4. The original test plan envisioned tests of both models at Mach numbers of .25 and .5 and at least two Reynolds numbers, one of which is the highest available value. The low Mach number was selected to provide as nearly an incompressible case as the tunnel would permit and the higher Mach number was selected to introduce some compressibility into the data.

A number of difficulties occurred, including the problem with the splitter plate noted previously, which limited the number of test conditions that could be run. In addition, a tunnel dynamic pressure limitation prevented operation at high combined Mach and Reynolds numbers. As a result, data were obtained under the following conditions.

Model	Reynolds No.	Mach No.
sharp edge	$.25 \times 10^6$	.25
sharp edge	$.15 \times 10^6$	.5
round edge	$.25 \times 10^6$	.25
round edge	$.15 \times 10^6$	.5

In addition, a small amount of velocity and pressure data was obtained for the sharp edge model at M = .25 and Re = .063 × 10^6.

3. EXPERIMENTAL DATA

This section presents the data obtained in the experiment. Included is information on pressures, velocities and flow visualization.

3.1 Pressures

The pressure data consist of steady state measurements of a number of static pressure taps, with locations as shown in section 2.1, and two high-frequency-response Kulite transducer tape records.

Representative static pressure data for the front face are shown in figure 7 for the various combinations of models and flow conditions. In each case a pressure variation is shown for the upper (positive-y) half of the face containing the greatest number of taps, and the values at corresponding points on the lower (negative-y) half are also shown. For the sharp-edge model, data are also shown for a spanwise station 2.8 half-face-widths from the midspan, which show excellent agreement with the midspan data.

Figure 7(d) shows pressure data not only on the front face but also on the rounded edge and the two static taps on the support plate. In this case the abscissa is distance along the surface rather than along the y direction, with the two being identical out to .875 b/2. In the range of .875 b/2 to 1.2 b/2, the angular locations are also shown, as indicated in the sketch. The location of separation as deduced from the flow visualization photographs (section 3.3) is also marked at an angle of about 45 degrees.

The pressure data in figure 7 for negative y values generally agree well with the positive y pressures, which indicates that the front surface of the model was aligned reasonably well with the normal to the flow direction.

The results in figures 7(b), (c), and (d) show pressure coefficients near y=0 with values greater than unity. An explanation could not be found. The results were repeatible and are felt to be due to some aspect of the tunnel pressure data acquisition and processing system.

Spanwise variations of the static pressures at three locations on the models are shown in figure 8. The three locations are the centerline of the front face, a line along the front face at y/(b/2) = .4, and the aftmost row of static taps on the support plate in the recirculation region. The data for the sharp edge model [figs. 8(a) and (b)] are similar in that the spanwise variations along the front face are very small and the variations in the separated region are significant. In the separated region (the lower curves) the pressure coefficients are negative and show the static pressure decreasing with distance away from the centerspan of the model, which would indicate a spanwise flow away from the centerspan towards the tips of the model.

The data for the round-edge model [fig. 8(c)] show somewhat more variation across the span on the front surface and a similar behavior on the rear surface.

The streamwise variation of static pressure on the support and splitter plates is shown in figure 9. Again the two sharp edge cases [figs. 9(a) and (b)] show similar results, with pressure recovery to nearly free-stream pressure within 16 half-face-widths distance aft of the face. The round-edge results [fig. 9(c)] show a more upstream recovery which does not agree with the flow visualization results (section 3.3). The data at x/(b/2) = 6.5 are believed to be in error.

Static pressure data for the round edge model at $M = 0.5$ were not obtained because of a problem with the data acquisition system during that part of the test.

Representative traces of the unsteady Kulite transducers are shown in figure 10 for each of the five cases for the transducer in the separated region on the support plate and for one case on the front surface. A band representing a fraction of the free-stream dynamic pressure is shown on all traces, as is a time scale. On the front surface (bottom trace), the amplitude of the pressure fluctuation is less than one-half percent of q.

In the separated region, the amplitude is the order of 10 percent of q.

These unsteady pressure data were processed on electronic signal analyzer equipment to obtain autocorrelation and power spectral density information. The data tape was replayed through a variable gain and then through 18 db/octave Butterwork filters which had high and low pass settings of 1 Hz and 20 kHz, respectively. The signals were then fed into a Saicor 42A, 400 line correlator where the auto and cross correlation functions, defined as

$$R_{xx} = \lim_{T\to\infty} \frac{1}{T} \int_0^T P_x(t) P_x(t + \tau) dt$$

and

$$R_{xy} = \lim_{T\to\infty} \frac{1}{T} \int_0^T P_x(t) P_y(t + \tau) dt$$

were determined, where τ is the time delay. Spectra were obtained using a Honeywell SAI 52C, 400 line real time spectrum analyzer in the form

$$\psi_P^2\ [f, f + \Delta f] = \lim_{T \to \infty} \frac{1}{T} \int_0^T P_x^2(t, f, \Delta f)\, dt$$

where Δf is the frequency range of each line. Some typical results are shown in figures 11-14.

Figure 11 shows autocorrelation coefficients as a function of time delay for the sharp-edge model at M = 0.25. For zero time delay the correlation coefficient by definition is unity, and it drops off with increasing time delay. For the transducer on the front face [fig. 11(a)] there is a distinct periodic content to the pressure fluctuation which occurs with a frequency of about 500 Hz and shows 10 cycles in the 20 millisecond sampling time. There may also be a periodic content with a frequency of about 60 Hz, but the sampling time was not sufficiently long to verify this. The transducer in the separated region on the support plate [fig. 11(b)] does not exhibit the 500 Hz content, but is more characteristic of a turbulent flow with a wide spectrum of frequencies. This difference in behavior between front and rear transducers was typical of all the cases examined.

The power spectral density results for the same test case are shown in figure 12. In this case both the front and rear transducers show a distinct energy content in the flow at about 500 Hz, with probably a harmonic at about 1000 Hz. The front transducer energy peak at 500 Hz is about the same as that of the low frequency energy, whereas the rear transducer energy peak at 500 Hz is about 12 db below the low frequency value, or about 1/16 the energy in the low frequency flow. The low energy level is probably responsible for lack of any noticable frequency content in the autocorrelation.

Figure 13 shows the power spectral density results for the round edge model at the same Mach number. Again there is a peak

at about 500 Hz with a smaller peak at 1000 Hz. There is a small peak at about 5 kHz which is typical of the round edge model results, although the energy level at this frequency is very low. The peak at 9.5 kHz did not appear in most of the power density curves and is probably due to some source of spurious noise or signal in the tape.

Figure 14 shows power spectral density results for the sharp edge model at M = 0.5. There is a major source of energy at about 1000 Hz, with some harmonics at higher frequencies. Again, the 1000 Hz peak is typical of all of the M = 0.5 results for both sharp- and round-edge models.

A Strouhal number was calculated for each of the two Mach numbers based on the two frequencies noted above, the free-stream velocity, and width of the front face of the model. The results are as follows:

$$\text{for } M = 0.25,\ St = \frac{fb}{V} = .299$$

$$\text{for } M = 0.5,\ St = .297$$

The results of the tests done by Fage and Johansen (ref. 3) for a sharp edge flat plate normal to the flow show a Strouhal number of 0.146 based on the frequency with which a vortex of one sign is transported in the wake behind the model. The Fage tests did not employ a splitter plate and the wake developed a definite periodicity, as in the wake behind a cylinder. If the Fage value is doubled to account for a complete cycle of shedding, the agreement with the Strouhal number based on the power spectrum frequencies is very good.

3.2 Velocities

All velocity measurements were made at the midspan station ($z = 0$). The two components measured were the axial (u) and the vertical (v) velocity. The data acquisition rate varied considerably during the tests, depending on the density level in the tunnel and the power output of the drive system, both of which influenced the amount of oil leakage from the drive system which provided the seeding particles for the flow. The range of data rates (scattering particles crossing the measurement volume) were several counts per second to about 500 counts per second. For the data in the outer flow and shear layer, a sufficient sampling time was allowed to obtain several hundred counts at a given point. In the low velocity recirculation region, the data rates were much lower and as few as 50 counts were obtained in some cases. In general, the data acquisition rate was not sufficiently high to resolve any motion of the shear layer behind the model.

The data were acquired and processed by a HP 9830 computer, which calculated the average and rms values of the two velocity components. Both the raw data and the calculated values were recorded on floppy-disk magnetic storage which could be accessed for later processing. Also recorded in the computer were potentiometer outputs indicating the position of the measurement volume in model coordinates. The computer was also used to drive the optics to position the measurement volume through stepper motors. A position calibration was done before and after a series of LV measurements.

The positions of the velocity measurements for the models and flow conditions are shown in figure 15. Each dot represents a position at which LV measurements were obtained. In some cases, repeat measurements were made, which are indicated by two or three dots close together, side by side. The dashed

lines in these figures represent the approximate boundary of the shear layer, as deduced from the velocity measurements.

The tabular data for velocities are listed in Tables I through V. The listing consists of a point number, the two coordinates of the point, the average values of the two velocity components, and their rms values.

Some typical plots of variations of the velocity components with distance are shown in figures 16 and 17. Figure 16 shows u and v velocities for the sharp-edge model. The u profile in figure 16(a) is shown at $x/(b/2) = 0.5$, which is relatively close to the edge where the shear layer is rather thin. There is a small negative velocity in the recirculation region, a very steep gradient in the shear layer, and a small overshoot at the outer edge of the layer. Some repeat points are shown on the plot indicating small differences except at $y/(b/2) = 1.4$. If the shear layer is moving slightly, or if the LV measurement volume is not in exactly the same place, the differences in repeat data would be larger in the high gradient region than outside the shear layer.

The v curves are shown in figure 16(b): one close to the tip at $y/(b/2) = 1.1$ where the shear layer is very thin and one further from the tip at $y/(b/2) = 1.6$. These curves should show zero values far upstream and downstream ($x \to \pm\infty$) with high values only in the vicinity of the edge. The magnitudes and gradients near $y = b/2$ are much greater than those further from the edge, although in both cases there is a large change in velocity through the outer edge of the shear layer.

Some results for the round-edge model are shown in figure 17. Figure 17(a) shows three sets of u data: two very close to the edge and one well downstream of the edge. The data for $x/(b/2) = -0.1$ are upstream of the shear layer and do not show the high gradients of the shear layer edge, whereas the

data for x/(b/2) = +0.1 do show the steep gradient. The repeat data show reasonably good agreement. The vertical velocity variations shown in figure 17(b) indicate a sharp gradient near the edge as in the sharp edge model, but the gradients at y/(b/2) = 1.6 are less severe than in the sharp-edge case.

Some examples of repeat data were shown in figures 16 and 17. The repeatability was generally quite good except in regions of high velocity gradient. In the experiment, a vertical scan of the LV system was made along constant x lines, and generally the repeat points were taken at a different time in the experiment. In processing and analyzing the velocity data, the sequence in which the velocity measurements were taken was taken into account in selecting the duplicate points to be deleted, and those points were retained which represent a systematic sweep in y at one time in the experiment. The points which were dropped are marked in the data presented in Tables I-V.

In order to get some insight into the unsteadiness of the shear layer, some histograms of the velocity measurements were examined. Some typical results are shown in figure 18. These are plots of the number of occurrences of a given velocity as the measurement volume sits at a given point in the flow, nondimensionalized by the number of occurrences of the most frequently observed velocity. Figure 18(a) shows u/V and v/V data for the sharp edge model at three vertical locations: one at the inner edge, one in the center, and one at the outer edge of the shear layer. Typically, the inner and outer edge data show relatively sharp peaks and narrow widths, whereas the center data show a broader curve.

If the shear layer were oscillating with some amplitude about a measurement point, as shown in the sketch below, the

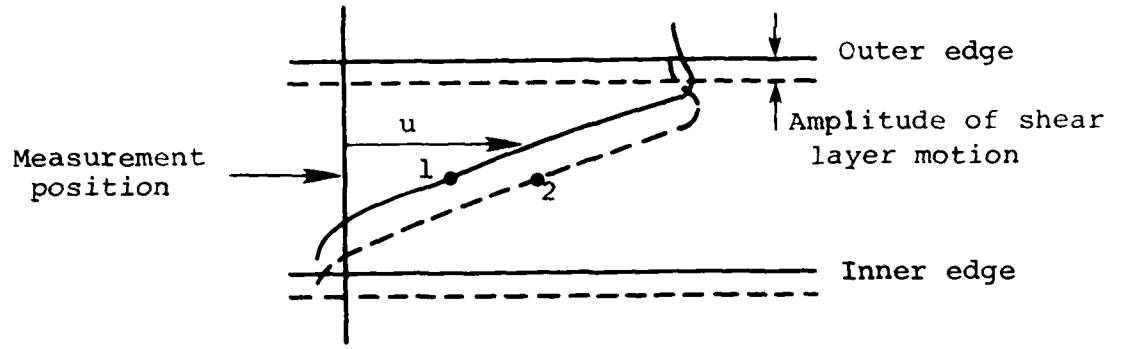

histogram would tend to show two peaks with velocities at values 1 and 2. The top center curve of figure 18(a) tends to show this behavior, with peaks at .15 and .40. If one uses the appropriate mean velocity curve [similar to that of figure 16(a)] to calculate the amplitude of motion required to change the velocity at the measuring point from .15V to .40V, the resulting value is .38 mm (.015 inch), which is 1.5% of the model half-width.

The round edge model histogram data are shown in figure 18(b). Qualitatively, these show the same trends, except the second peak for the u velocity in the shear layer is much lower than the first peak Probably the velocity fluctuations at a given point are due to a combination of small, shear-layer position variations and turbulence in the flow.

3.3 Flow Visualization

Surface flow visualization was performed on both the sharp edge and round edge models at the completion of the velocity data acquisition periods. A mixture of carbon black, oil, and kerosene was "painted" on the top and front surface of the models and the models were run about 15 minutes at the low

Mach number flow condition, at which time the oil pattern had dried. Photographs were then taken of the flow patterns on the surface. Qualitatively, the surface flow patterns on both the sharp and round edge models were very similar. Because of the short time available for the model change from the sharp to round edge configuration, more detailed photographs were obtained of the round edge configuration, and these are included with this report as figure 19.

An overall view of the top of the plate is shown in figure 19(a). The edge of the face piece is just in view at the top of the photograph and the flow direction is top to bottom. The straight horizontal line across the model near the face piece edge at the top of the photograph is the parting line between the support plate and splitter plate. The dark horizontal band near the center of the photograph is the devcon blending between the original splitter plate and the added, thicker plate. The tubing for the static pressure tap for the underside of the splitter plate is on the lower part of the photograph and the fitting for the trailing-edge sting support is seen at the bottom.

It is clear that the flow in the low speed recirculating region is not two dimensional. The white dashed ink line across the plate is the approximate reattachment line and the aft boundary of the recirculating region. The flow that leaves this line has an inboard component for both the forward moving recirculating flow and the aftward-moving attached flow.

As the recirculating flow moves forward towards the front edge, it approaches a secondary separation line located approximately at the parting line between the splitter and support plates. The white ink arrow in the upper left corner indicates the location of this line.

The remaining major feature of the flow shown is a pair of vortices (the dark spots), one at each end (spanwise) of the plate close to the top of the photograph, at the ends of the secondary separation line. These were caused by the interaction of the flow over the model with the tunnel side-wall boundary layers passing over the windows. These vortices effectively acted as a sink for the recirculating flow.

Figure 19(b) shows a close up photograph of the secondary separation line at the center span of the model. This region is near the top center of figure 19(a). In figure 19(b), the edge of the face piece is along the left side of the photograph, and the free-stream flow direction is from left to right. The two straight vertical lines are the parting lines between the face piece, support plate, and splitter plate. The center span of the model ($z = 0$) is very close to the horizontal dashed line near the center of the photograph. The forward moving recirculating flow moves from right to left and approaches a secondary separation line, shown by the white vertical dashed ink lines. At the center, spanwise, of the model, the flow stagnates and leaves an accumulation of carbon black. Away from the center, the surface flow turns rapidly to form a three-dimensional separation line (the vertical dashed ink lines).

This figure also shows a secondary reattachment line along the left side of the figure which coincides very closely with the parting line between the face piece and support plate. The curved white ink lines near the left edge of the photograph help show the surface flow directions in the secondary recirculation region.

The flow pattern at center span that is implied by these surface flows is shown in the sketch below. Primary separation (PS) occurs at the edge and forms a large recirculation region,

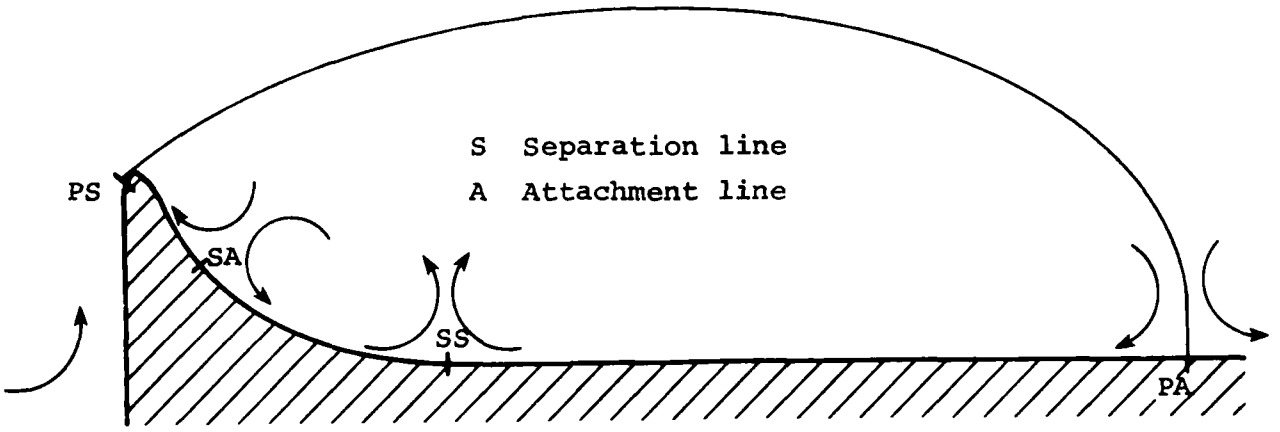

with primary reattachment (PA) well aft on the splitter plate. As the recirculating flow moves forward, it approaches a secondary separation line (SS). There is a corresponding secondary reattachment line (SA) just downstream of the edge and a secondary recirculation flow between SA and SS.

Figure 19(c) shows an enlarged view of the round edge of the face piece. The orientation is the same as in figure 19(b), with the free-stream flow direction from left to right. The left half of the photograph shows the surface flow pattern on the front surface of the face piece and indicates a two-dimensional flow approaching the edge. The flow visualization results for both the sharp and round edge models showed a two dimensional flow over the entire span of the model. The right half of the photograph (out of focus) shows the rear curved surface of the face piece and the parting line between the face piece and support plate. The primary separation line shows as a vertical line near the center of the photograph. In the lower center of the photograph are seen the static pressure taps near the edge [fig. 3(a)]. The white ink arrow points to the tap 45 degrees around the edge, which is closest to the separation line. This tap location is also shown on figure 7(d) as the location of separation. The spanwise length of edge in view in this photograph is about 6 cm (2.5 inches).

These results indicate that the attached flow on the front of the model is two dimensional, the flow in the recirculation region is largely three dimensional, and the surface flow at mid-span, which is where the velocity measurements were made, lies in a plane of symmetry normal to the span which divides the recirculating flow into two regions that have spanwise velocity components directed outward towards the two ends of the model.

4. METHODS OF ANALYSIS

Several methods of analysis were used to evaluate the velocity data. These are discussed in this section.

4.1 Contour Integration

The circulation around any closed contour in the flow can be calculated by the following expression

$$\frac{\Gamma}{bV} = \frac{1}{bV} \oint \vec{V}_s \cdot d\vec{s} \qquad (11)$$

This calculation was made for a number of contours, mostly consisting of a streamwise length $\Delta x/(b/2)$ of 0.1 and a height sufficient to cover the shear layer. Some calculations were also made in the flow upstream of the model to determine the circulation in the tunnel flow approaching the model.

In addition to the circulation, the net flow into the same contours was calculated according to the following expression

$$\frac{Q}{bV} = \frac{1}{bV} \oint \vec{V}_s \cdot \vec{n}\, ds \qquad (12)$$

The purpose of making these net flow calculations was to assess the accuracy of the velocity data used in the contour integrations for circulation [Eq. (11)], since the net flow through a contour ought to be zero.

4.2 Vorticity

The vorticity at a point in a two dimensional flow can be calculated as

$$\frac{\zeta(b/2)}{V} = \frac{\partial(v/V)}{\partial\left(\frac{x}{b/2}\right)} - \frac{\partial(u/V)}{\partial\left(\frac{y}{b/2}\right)} \tag{13}$$

In order to calculate the velocity derivatives, two approaches were used. In the first, the velocity data were spline-fitted to obtain an analytical expression that could be differentiated to get the derivatives required in Equation (13).

In general, this procedure worked well for the streamwise velocity component (u), but in many cases the vertical velocity derivatives were not satisfactory. Typical examples are shown in figures 20 and 21. Figure 20(a) shows a computer-generated plot of the u variation with y and 20(b) shows the resulting derivative variation determined from the spline fit. The results show the steep gradient in velocity through the shear layer, the overshoot at the outer edge of the shear layer, and the large derivative values. The gradients in velocity are largest near the edge of the layer and decrease with increasing distance downstream along the shear layer.

Figure 21(a) shows the v variation with x and figure 21(b) shows the resulting derivatives, as evaluated from the spline fit. Typically the v component is small in the upstream flow, rises in the flow near the edge, reaches a peak at the outer edge of the shear layer and falls very rapidly through the

outer part of the shear layer to essentially zero at the inner edge of the shear layer. Generally, the v variations with x were not as smooth as the u variations with y, which are reflected in the derivative calculations, as shown in figure 21(b).

Various types of spline-fit codes were used with the velocity data, and the free parameters used to control the fit and the smoothing were varied to attempt to obtain a satisfactory analytical description of the velocity derivatives. This procedure proved successful generally only for the u derivatives, and the values used were the spline-fit results. For most of the v velocities, the plot and crossplot approach described below was used.

In order to obtain a smooth and systematic set of v component derivatives, the v velocity data were plotted by hand. Figure 22 shows some results of a sequence of plots to obtain values of the v derivative at $x/(b/2) = 0.5$ for the sharp edge model. Generally, the spatial distribution of data [fig. 15(b)] favored initial plots of v/V versus $y/(b/2)$, as shown in figure 22(a). These were then used with the data to obtain smoothed plots of v/V versus $x/(b/2)$ for constant values of $y/(b/2)$ and to interpolate for intermediate $y/(b/2)$ values where no data were available [fig. 22(b)]. In cases where no intermediate y data were obtained, linear interpolation was used. The slopes were obtained graphically to construct a curve of the v derivatives versus $y/(b/2)$, as shown in figure 22(c).

The results of these calculations are values of the vorticity at various y values through the shear layer at a series of axial stations downstream of the front face. These

values were then used in the following way. An "integrated value of vorticity" through the shear layer was obtained from the following expression

$$\frac{\gamma}{V} = \int_1^2 \left[\frac{\zeta(b/2)}{V}\right] d\,\frac{y}{b/2} \tag{14}$$

where the stations 1 and 2 are the inner and outer edges of the shear layer, respectively. The inner and outer edges were taken (approximately) as the points where $\partial u/\partial y$ were zero. At the outer edge, the second zero slope point beyond the overshoot was used.

For purposes of comparison with the circulation values obtained from the contour integrations, and "average vorticity" was calculated from the velocity derivative data at the various axial stations considered, as follows.

$$\frac{\Gamma}{bV} = \frac{1}{2}\iint \frac{\zeta(b/2)}{V}\, d\left(\frac{y}{b/2}\right) d\left(\frac{x}{b/2}\right) \cong \frac{\Delta\left(\frac{x}{b/2}\right)}{2}\,\frac{\gamma}{V} \tag{15}$$

where $\Delta\left(\frac{x}{b/2}\right)$ is typically 0.1, which is the spacing used in the data acquisition and the streamwise width of the strip used for the circulation contour integrations.

Finally, a streamwise rate of transport of vorticity over the height of the shear layer past a given axial station was calculated from the following expression

$$R = \int_1^2 \left(\frac{u}{V}\right) \frac{\zeta(b/2)}{V}\, d\left(\frac{y}{b/2}\right) \tag{16}$$

where again the stations 1 and 2 are the edges of the shear layer, as before.

4.3 Thin Shear Layer Approximation

For a thin shear layer in parallel flow with a velocity profile shown in the sketch below, the vorticity can be

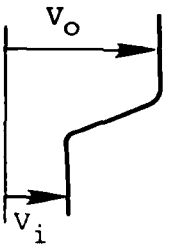

expressed in terms of the outer and inner velocities as

$$\frac{\gamma}{V} = \frac{V_o}{V} - \frac{V_i}{V} \tag{17}$$

and the rate of transport of vorticity as

$$R = \left(\frac{V_o + V_i}{2V}\right) \frac{\gamma}{V} \tag{18}$$

As an approximate check on the vorticity calculations made with the velocity derivatives, "thin shear layer" quantities were calculated at various x stations using for the outer and inner velocities the vector sum of the u and v velocities at the outer and inner edges of the shear layer in Equation (17) and using that vorticity with the u components in the transport equation, Equation (18), to get the streamwise transport rate.

4.4 Boundary-Layer Vorticity

A boundary layer is developed on the upstream surface of the model. As this boundary layer leaves the surface at the edge or at the separation point on the round edge model, its vorticity is convected into the shear layer. The rate of transport of this upstream surface vorticity is given by the following:

$$R = \int_0^1 \left(\frac{u}{v}\right) \frac{\partial u/V}{\partial y/\delta} \, d\left(\frac{y}{\delta}\right) = \frac{1}{2} \left(\frac{u_\delta}{V}\right)^2 \tag{19}$$

Further, the edge velocity u_δ is related to the local static pressure. For incompressible flow, the relation is simply expressed as

$$C_p = 1 - \left(\frac{u_\delta}{V}\right)^2 \tag{20}$$

At a free-stream Mach number of .25, the compressibility correction is small and can be neglected. At M = .5, the correction on u_δ is about 2 percent and may be included using the isentropic gas relations instead of Equation (20) to calculate u_δ from the measured C_p.

For the sharp-edge model, the pressure tap closest to the edge is at y/(b/2) = .965. The pressure coefficient is changing rapidly, however [fig. 7(b)]. The static pressure was measured on the rear surface a short distance from the edge (see fig. 4), and it seems reasonable to expect that this rear surface pressure is very close to the rear surface pressure right at the edge, because of the low velocities in the recirculation region. For the sharp edge, there should be no pressure difference across the edge. Thus, the pressure used in

Equation (20) to calculate the shedding rate in Equation (19) is the rear surface pressure at tap number 18. For the round edge model, the location of separation at M = .25 is known from the flow visualization, and the measured pressure at separation is used in Equations (19) and (20).

The average of several sets of pressures taken at each flow condition was used to calculate the shedding rate from Equations (19) and (20).

5. RESULTS

The results of the measurements and data analysis are described in this section, together with some discussion of the results. The presentation considers flow fields, vorticity, and vorticity transport.

5.1 Flow Fields

The flow fields are generally similar for both models and both Mach numbers. Plots of the velocity results are shown in figure 23. The velocities within the recirculation region are shown as vectors, with the tail of the vector at the measurement location, and the length and direction representing the magnitude and the direction of the measured velocity. The u component velocity data in the shear layer and outer flow are shown as profiles to illustrate the development of the shear layer. Some data, both in vector and profile form, are shown for the onset flow approaching the front surface. Note that the scale (upper left corners) is different by a factor of 5 between the velocity profile data in the shear layer and the vector data in the recirculation region, with the latter magnified because of the very low velocities there.

In order to gain some insight into flow ingestion into the shear layer, some analysis was made on the flow field data for the round edge model at M = 0.25. The data are those of figure 23(c). It is necessary to start at the wall on the downstream side of the model and analyze the flow, working toward the shear layer. First, it is known from the surface flow visualization that there is a secondary separation line at x/(b/2) = 2.1 and a secondary reattachment line at x/(b/2) = 0.1 (at the spanwise model center, z = 0). These are marked S and A, respectively in figure 23(c). The location of the boundary of this secondary recirculation region cannot be determined precisely because the LV system could not acquire data close to the model. A "nominal" dashed line approximately parallel to the measured vectors is shown connecting S and A in figure 23(c). In a two-dimensional flow, the flow between this dashed line and the model is a recirculating flow which would not enter the main shear layer. From the carbon black flow visualization previously described, it is known that there is some flow spanwise out of this region. This spanwise flow must be balanced by ingestion from the fluid in the primary recirculation region across the dashed line.

The short dashed line well above the A-S line is the u = 0 line in the shear layer. The flow between this line and some location within the secondary recirculation region is the forward moving recirculating flow, and that outside (above) the line is aft moving.

The recirculating flow rate moving forward between the wall and the u = 0 line at x/(b/2) = 2 was divided into four equal parts. In order to do this, the u velocity profile was extrapolated to zero at the wall. An attempt was then made at other x stations to integrate the flow starting at the wall and find the heights (y dimensions) encompassing the same four equal parts of the flow rate determined at x/(b/2) = 2.0. At the x/(b/2) = 2.55 station, the heights marked A, B, C, and D were

determined. Again the u-velocity profile was extrapolated to zero at the wall. Thus, the four solid lines marked A, B, C, and D between x/(b/2) of 2.0 and 2.55 become streamlines of the recirculating flow.

Forward of the x/(b/2) = 2.0 station, the same calculation process becomes dependent on the assumed boundary of the secondary recirculation region (the dashed line connecting S and A). The same procedure was used at x/(b/2) = 1.6, based on extrapolating the u-velocity profile to zero at the dashed line [y/(b/2) = 0.25]*. The solid lines were then extended forward to x/(b/2) = 1.6, as shown. This result shows that the flow between streamlines C and D all enters the shear layer between x/(b/2) of 1.6 and 2.0, and the flow between the wall and C enters the inner part of the shear layer upstream of x/(b/2) = 1.6.

A similar calculation was made at x/(b/2) = 0.4, using the assumed location of the secondary recirculation boundary shown in figure 23(c) [y/(b/2) = 0.70]. The forward moving rate of flow between y/(b/2) = .70 and the u = 0 line is about 90 percent of the flow rate between the wall and streamline A at x/(b/2) = 2, which indicates that streamline A would intersect the u = 0 line somewhat aft of x/(b/2) = 0.4.

Another calculation that can be made is to compute, for a given x station, the y coordinate in the shear layer at which the aft moving flow rate above the u = 0 line equals the forward moving recirculating flow rate from the u = 0 line down to the wall (or boundary of the secondary recirculation region). This calculation would indicate the relative proportion of the flow in the shear layer that is composed of ingested recirculation flow, as opposed to ingested free-stream flow. This was done for x/(b/2) values of 0.4, 1.6, 2, and 2.55, and

*The u value goes to zero somewhat below this dashed line, but as an approximation, the dashed line location was used.

the results are shown by the long dashed line in figure 23(c) noted "dividing streamline." The position of this curve between .4 and 1.6 is faired from the four calculated points.

At $x/(b/2) = 0.4$, the "dividing streamline" occurs at the point in the shear layer at which $u/V = 0.5$, at which point about 15 percent of the shear layer flow is ingested from the recirculation region. At $x/(b/2) = 2.0$, the "dividing streamline" occurs at $u/V = .8$, at which point about 50 percent of the flow is ingested from the recirculation region.

These results are only approximate. The lack of velocity data near the wall limits one's ability to define the secondary recirculation region boundary precisely, and the measured velocities are very small and have relatively large fluctuating components (Tables I-IV). Nevertheless, the assumptions made appear reasonable and do give useful information on the ingestion aspects of the shear layer flow.

5.2 Vorticity

Some contour calculations for circulation in the flow upstream of the model were made for the sharp-edge model at $M = 0.25$ to examine the character of the onset flow. The relationship used is Equation (11). The results are shown in figure 24, which show the contours as dashed lines. The calculated values near the center of the flow upstream of the model face show positive and negative values in adjacent contours. The velocities are relatively small and the continuity check performed on these contours in accordance with Equation (12) show very large flow imbalances (a net flux as high as 60 percent of the inflow), because of measurement uncertainties and spacing of the measurement locations. Consequently, these circulation values should only be viewed in a qualitative manner to indicate the vorticity content in this region of the flow.

The results at x = 0 off the tip of the model are self consistent, and the continuity checks on these contours show net flows of the order of one percent of the inflow. The circulations in these contours are the order of 5 percent of the values in the contours through the shear layer, one of which is shown on the right side of the figure and are of the same sign. This vorticity in the upstream tunnel flow may result from an unused probe support structure in the plenum section of the tunnel. This structure sheds a wake which is about in the correct position for flow passing through the contours off the tip of the model. To our knowledge, no tunnel-empty flow surveys have been made in this tunnel to confirm or deny the presence of vorticity in the test section flow.

Contour integrations for circulation in the shear layer were made at a number of axial stations along the shear layer for all test cases. For the most part, the contours used covered an axial distance $\Delta x/(b/2)$ of 0.1 and a lateral distance extending across the shear layer from the point (approximately) where $\partial u/\partial y = 0$ on the inner side to the point beyond the overshoot where $\partial u/\partial y = 0$ at the outer edge [see fig. 16(a) for a typical u profile]. One such contour is shown in figure 24. The value of the circulation is ascribed to the axial location of the midpoints (axially) of the contour. A summary of results for all cases is shown in figure 25.

There is a fair amount of scatter in all cases except the sharp-edge model at M = 0.5. A line has been drawn through these data to indicate the trend with axial distance.

Continuity checks using Equation (12) were made on all these contours to evaluate the circulation calculations. The contours for $x/(b/2) < 0.3$ showed net flows through the contour as high as 30 percent of the inflow. In this region, the shear

layer is very thin and the grid spacing of the velocity data was not small enough to resolve the velocities well.

For the sharp-edge model at M = 0.25, the two adjacent contours centered at x/(b/2) = 0.85 and 0.95 showed flow imbalances of +15 and -19 percent, respectively. The circulation values for these contours (fig. 25) are -.0855 and -.063, respectively. This result would indicate some problems with the measured velocities at x/(b/2) = 0.9, which are used with both contours.

The continuity checks for all other contours indicated flow imbalances of only a few percent of the inflow. In particular, the flow imbalances for the sharp-edge M = 0.5 case, which had the greatest consistency in circulation, were no different than the other cases.

The averages of the circulation values for each of the four cases are shown on the right side of figure 25. The values are very close and do not show any trend with respect to Mach number or edge radius.

Three data points are shown from the work of Fage and Johansen (ref. 3). Their model was a sharp-edge flat plate of about the same face width-to-length ratio as the present model, spanning a low speed tunnel, but had no splitter plate. The contours used by the authors were longer streamwise, so their circulation values were reduced by the axial length ratio to correspond to $\Delta x/(b/2) = 0.1$. The Fage data have the same level as the present data. No measurements were made further downstream by Fage, because of the unsteadiness associated with the periodic wake development.

Figure 26 shows some typical results for velocity and the construction of the velocity derivatives and vorticity at an axial station x/(b/2) = 1.0 for the sharp edge model. The velocity data are shown in figures 26(a) and (b). In order to

obtain the v-velocity derivatives at various y values, it was necessary to plot v/V versus x/(b/2) at as many y stations as the data permit, as shown in figure 26(b), and interpolate on velocities to get derivative values at intermediate y values. Generally, the gradients in velocity are most severe near the model tip, and the greatest uncertainty in their determination occurs there. Also, the u-velocity profiles were more easily defined [fig. 26(a)] than the v-velocity profiles [fig. 26(b)]. As is shown in figure 26(c), the u-velocity derivatives are generally larger than the v-velocity derivatives, so the greater uncertainty in the v derivatives does not carry over directly into the vorticity calculation. The vorticity distribution is shown in figure 26(d). The (negative) vorticity is highest in the high u-gradient region, and there is a small region of positive vorticity in the overshoot region at the outer edge of the shear layer. The rate of transport of vorticity, figure 26(e), is generally similar to the vorticity distribution but more peaked.

Some additional results for circulation are shown in figure 27. In this case, a circulation is calculated from the velocity data using Equation (15) by first calculating velocity derivatives and vorticity at various y values through the shear layer for a given x value, and dividing by the area of the contour to obtain an "average vorticity" for comparison with the contour integrations. In the results shown in figure 27, the two values of contour integration circulation on either side of a given x station are averaged to obtain a single value of circulation for comparison with the velocity derivative value at that x station. In almost all cases, two sets of values agree within a few percent, with the velocity derivative values smaller than the contour integration values. Fage and Johansen (ref. 3) found nearly identical results with respect to agreement between the two sets of values for their experiment.

Some results for integrated vorticity are shown in figure 28. The results using the velocity derivative data were calculated using Equation (14), and the "thin shear layer" results were obtained using Equation (17). The two sets of results show the same trends with x distance, although the thin shear layer approximations are 10 to 15 percent lower than the velocity derivative results.

5.3 Vorticity Transport

Vorticity transport rate was calculated in three ways. First, the rate at which upstream boundary layer vorticity leaves the separation point at the edge of the model was calculated in accordance with the discussion of section 4.4. This shedding rate depends only on the static pressure at the point where the boundary-layer flow leaves the surface. For the three cases where pressure data are available, the pressure coefficients at separation are the following:

Edge Condition	M	C_p (separation)
Sharp	0.25	-.60
Sharp	0.5	-.50
Rounded	0.25	-.59

In the low Mach number cases, the effect of compressibility is negligible and the incompressible relationship between pressure and boundary layer edge velocity was used [Eq. (20)]. At M = 0.5, there is some effect of compressibility, and the isentropic gas relations were used.

The second method used to calculate transport rate is Equation (16). This method makes use of the velocity derivatives to calculate vorticity and its transport rate at various axial stations along the shear layer.

The third method is the thin shear layer approximation described in section 4.3.

The results of these calculations are shown in figure 29. The thin shear layer results show the same trend with x as the velocity derivative results, but are consistently lower in value by 10 to 20 percent. These results are very similar to those of Fage and Johansen (ref. 3), who found differences of 8 to 15 percent between the two sets of results. The upstream surface boundary-layer shedding rate results are shown as straight lines indicating the level of shedding.

Nearest the model edge [$0.2 < x/(b/2) < 0.4$] the transport rate based on velocity derivatives is approximately 80 percent of the edge shedding rate. The low value of 0.4 at $x/(b/2) = 0.2$ for the sharp edge model at $M = 0.5$ appears inconsistent with the data at larger x values and is probably due to the lack of accuracy in calculating the velocity gradients near the edge where the shear layer is very thin and the gradients high.

One possible reason for the result that the shear layer vorticity transport rate just downstream of the edge is only 80 percent of the calculated rate being shed from the upstream model surface at the separation point on the edge is that vorticity of an opposite sign is being transported into the shear layer from the flow along the rear surface of the model. This vorticity is generated at the wall in the forward moving recirculating flow. Some calculations were made for the round edge model at $M = 0.25$ in the following way.

The flow field is that of figure 23(c). The velocity data at $x/(b/2) = 0.4$ were used in Equation (16) to obtain a vorticity transport rate for the forward moving recirculation flow between the $u = 0$ line at $y/(b/2) = 1.28$ and the edge of the secondary recirculation region at $y/(b/2) = 0.7$. The u-velocity

were extrapolated to u = 0 at y/(b/2) = 0.7. The resulting transport rate of the vorticity of positive sign forward through this x station is calculated to be R = 0.007, which is about 1 percent of the rate in the shear layer.

To this value must be added the (positive) vorticity which is produced at the wall between the secondary attachment line ["A" in fig. 23(c)] and the separation line for the forward moving flow, which is close to the line at the tip where the forward surface boundary layer separates. As a means of extimating this contribution, the velocity measurements nearest the surface were used as an indication of the velocities in the region just aft of the primary separation line. Figure 15(d) shows the locations of the following velocities.

x/(b/2)	y/(b/2)	u/V	v/V	$\sqrt{u^2 + v^2}/V$
0	1.025	-.11	.032	.115
.1	0.95	-.075	.027	.08
.2	0.8	-.026	-.001	.026

The surface pressure in this region is relatively uniform [fig. 7(d)]. If one assumes that a boundary layer on the rear surface separates with a local edge velocity u_δ/V = .115 and a shedding rate is calculated from Equation (19), the rear surface contribution is .007, which is also about one percent of the front surface rate, and the sume of these two effects is .014. Thus, these two rear surface contributions do not appear to be responsible for much of the 20 percent difference between the calculated front surface rate and the measured shear layer rate.

Another feature of interest in figure 29 is the increase in vorticity transport rate within the shear layer with increasing distance downstream of the edge. If the vorticity in the

shear layer were generated only at the edge, the transport rate would be uniform along the length of the shear layer. In fact, vorticity can enter the inner edge of the shear layer with the recirculation fluid ingested by the shear layer. If there is any vorticity in the onset flow, as was indicated by figure 24, this could also be ingested into the outer edge of the shear layer. Estimates were made of both the quantities, again for the case of the round edge model at M = 0.25.

For the outer flow, the vorticity transport rate, R, was calculated at x/(b/2) = -0.1 over the height from y/(b/2) = 1.1 to 2.0 using Equations (16) and (13). The v-derivative contributions were obtained from the velocities at x/(b/2) = 0, -0.1, and -0.2. The calculated transport rate was R = -.04. If this vorticity enters the outer edge of the shear layer, it could account for a portion of the (negative) increase shown in figure 29.

For the recirculating flow, the rate of transport of vorticity moving forward at x/(b/2) = 1.6 between the u = 0 line [y/(b/2) = 1.6] and y/(b/2) = 0.2 was calculated. This location was selected because of the velocity data available [fig. 15(d)]. The inner part of this region has positive vorticity which is part of the opposite-sense vorticity introduced from the recirculation region into the shear layer near the edge. The outer part of this region [in the approximate rage from y/(b/2) of 1.2 to 1.6] has negative vorticity moving forward at a rate R $\cong$ .02 (positive because of negative u velocity). In accordance with the flow reconstruction of figure 23(c), the negative vorticity enters the inner part of the shear layer over the x/(b/2) range from about 0.8 to 1.6, which would not account for all of the (negative) increase in R between x/(b/2) of 0.4 and 0.8 shown in figure 29.

6. CONCLUDING REMARKS

A two-dimensional test was performed on a flat plate at low subsonic speeds to investigate the relationship between the vorticity shed at an edge and the vorticity appearing in the flow field shear layer adjacent to the edge. The measurements made were velocities in the flow field, pressures on the model, and surface flow visualization. Two degrees of sharpness of the edge were tested.

The flow over the entire span of the front face was two dimensional. The resulting flow in the recirculation region on the model was not two dimensional. The velocity- and most of the pressure-measurements were taken at the center span of the model (center of the tunnel), which was shown by the flow visualization and pressures to be a plane of symmetry dividing two regions of flow having a spanwise component towards the ends of the model in the recirculating region. It is felt that the lack of two dimensionality in the recirculating flow behind the model had little influence on the results, because the measurement plane coincided with the plane of symmetry dividing the outboard flows towards the ends of the model and the measured velocities in the recirculation region are small ($u/v < 0.1$ and $v/u < 0.05$).

The flow appeared to be reasonably steady, particularly the flow outside the shear layer. The reattachment point of the recirculating flow was well forward of the splitter plate trailing edge. The histograms of the LV velocity data in the shear layer, and the spectral analysis of the surface pressures show indication of a small amount of energy in a frequency typical of a Strouhal shedding rate. However, the repeatability of the velocity measurements and the small magnitudes of these unsteady effects, within and outside of the shear layer,

indicate that the unsteady aspect of the flow should have little influence on the results.

The boundary layer on the model upstream surface is laminar. The only evidence to show any influence of Reynolds number on the shedding rate is the pressure data for the sharp-edge model at M = .25. The data show $C_p = -0.52$ at $Re = 0.063 \times 10^6$ and $C_p = -0.6$ at $Re = 0.25 \times 10^6$ at the static tap on the rear surface of the model closest to the edge [fig. 9(a)]. On the basis that this pressure is the value at the edge from which the upstream surface boundary-layer vorticity transport rate is computed, there is little change in the rate over this Reynolds number range.

The results of the experiment show that the vorticity transport rate measured in the shear layer close to the edge is about 80 percent of the predicted value in the upstream surface boundary layer at separation. The boundary-layer rate depends on u_δ, which in turn depends on the local pressure at separation. For the rounded edge case, the latter is well established from the behavior of the pressure distribution [fig. 7(d)] and the surface flow visualization. There is some question, however, for the sharp-edge case, because the pressure at the edge could not be measured.

An effort was made to locate data at the edge of a flat plate normal to the flow. The only source found is the work of Fage and Johansen (ref. 4). The plate cross section is as shown below, and no splitter plate was used. Although no

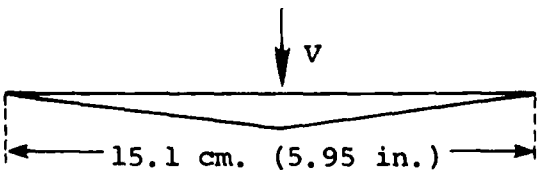

tables are given of static pressure tap location, it appears that the front surface static pressure was measured to within .02 to .03 b/2 of the edge. The C_p values are -0.7 nearest the edge on the front surface and -1.38 (essentially uniform) on the rear surface, whereas the present experiment shows -0.6 on the rear surface near the edge. One would expect the C_p on the rear surface to be greater (less negative) for the present experiment than for the Fage test because a splitter plate is known to reduce the drag considerably.

Fage also measured the velocity in the plane of the front surface a short distance off the tip and found that it agreed within 5 percent with a predicted velocity using the rear surface static pressure and the assumption that the total head in the flow just off the tip is free-stream total head. Thus, even though the rear surface static pressure is different in the Fage test, the assumption in the present case of using the rear surface pressure near the tip for purposes of calculating u_e is supported by the results of reference 4, and any discrepancy between calculated-boundary-layer and measured-shear-layer vorticity rates should not be attributable to use of an incorrect pressure at separation.

Vorticity of an opposite sign to that shed from the front surface boundary layer is produced at the edge by the forward moving recirculating flow along the splitter plate and model rear surface. Calculations indicate that the transport rate of the recirculating flow approaching the secondary reattachment point is roughly 2 percent of the forward surface shedding rate, whereas there is a difference of 20 percent between the calculated forward surface rate and the measured rate in the shear layer adjacent to the edge. Thus, the rear surface contributions appear to account only for a part of the differences between the measured shear layer rate and the calculated forward surface shedding rate.

Vorticity also enters the shear layer along both the outer surface (due to vorticity in the onset tunnel flow) and the inner surface. Estimates of the quantities of these transport rates indicate values generally smaller than the changes in transport rate measured along the shear layer.

As a final comment, it does not appear possible to account for the difference between the calculated shedding rate of the front surface boundary layer at separation and the measured rate in the shear layer just downstream of the edge. The u_ξ method [Eq. (19)] of calculating shedding rate at separation is an old concept (for instance, ref. 5) and has been used extensively. In these experiments, however, no direct measurement of the vorticity flux at separation could be made, so no check is available on how accurately the u_ξ method predicts the shedding rate at a separation point.

As a practical matter, an approach has been adopted in engineering analysis methods (for instance, ref. 6) in which the shedding rate is calculated as

$$R = \Lambda \frac{1}{2} \left(\frac{u_\xi}{V} \right)^2$$

where Λ is an empirical factor which is assigned a value based on experimental observations. For a cylinder in crossflow, for example, the value is 0.5 to 0.6, based on the vorticity which appears in the wake vortices. The "missing" vorticity is attributed to the rear surface boundary-layer/shear-flow and other unknown factors.

In the present experiment, the value of Λ based on the measurements obtained is approximately 0.8. This value appears to hold for both the sharp edge and rounded edge cases tested.

REFERENCES

1. Apelt, C. J. and Wert, G. S.: The Effects of Wake Splitter Plates on Bluff-Body Flow in the Range $10^4 < Re < 5 \times 10^4$. JMF, Vol. 71, Pt. 1, 1975, pp. 145-160.

2. Lindgren, B. W. and McElrath, C. W.: Introduction to Probability and Statistics. MacMillan, New York, 1959.

3. Fage, A. and Johansen, F. C.: The Structure of Vortex Sheets. Philosophical Magazine S7, Vol. 5, No. 28, Feb. 1928.

4. Fage, A. and Johansen, F. C.: On the Flow of Air Behind an Inclined Flat Plate of Infinite Span. ARC R&M No. 1104, Feb. 1927.

5. Goldstein, S.: Modern Developments in Fluid Dynamics. Vol. I, Ch. II, Oxford University Press, 1938.

6. Fidler, J. E.: Approximate Method for Estimating Wake Vortex Strength. AIAA Journal, Vol. 12, No. 5, May 1977.

APPENDIX A

STATISTICAL CONFIDENCE LEVELS IN VELOCITY DATA

Using relationships based on Gaussian probability statistics, estimates can be made of the confidence level in the laser velocimeter data as functions of the number of samples of a given measurement and the rms error. The theory and relationships are obtained from reference 2.

For a given Doppler frequency measurement, f_D, the error may be expressed as

$$|\bar{f}_D - \beta_D| < \frac{K_f S_f}{\sqrt{N}} \tag{A-1}$$

where β_D is the true mean frequency, K_f is a multiplier related to the confidence level and the Gaussian probability distribution, and N is the number of measurements. The quantity S_f is the calculated variance,

$$S_f^2 = \frac{1}{N}\left[\sum_{i=1}^{N} (f_i - \bar{f})^2\right] \tag{A-2}$$

and $\bar{f}$ is the calculated mean frequency

$$\bar{f}_D = \frac{1}{N}\left[\sum_{i=1}^{N} f_D\right] \tag{A-3}$$

From Equation (A-1), the error increases as the variance increases and decreases with the number of samples. The confidence level can thus be expressed as

$$\frac{|\bar{f} - \beta_D|}{\bar{f}_D} < \frac{K_f S_f}{\bar{f}_D \sqrt{N}} \qquad \text{(A-4)}$$

The relationship between the confidence level, the number of samples, the error in mean measurement, and the rms variation about the mean, σ, is shown in figure A-1.

In the outer flow and outer part of the shear layer, typically about 300 samples were taken at a given point and the rms level is the order of 8 percent of the mean velocity. For these values, figure A-1 shows that 50 percent of the measurements would be in error by less than four percent of the rms or .32 percent of the mean, and one percent would be in error by less than 15 percent of the rms or 1.2 percent of the mean.

For the measurements in the reverse flow region where the velocities are low ($u \approx 10$ m/sec. and $v \approx 1$ m/sec.), it was more difficult to obtain measurements because of fewer scattering particles. Typically, 50 samples were obtained, and the rms level was the order of 100 percent of the mean in u and 300 percent of the mean in v. For these values, figure A-1 shows that 50 percent of the u measurements would be in error by 10 percent of the mean and 50 percent of the v measurements would be in error by 30 percent of the mean.

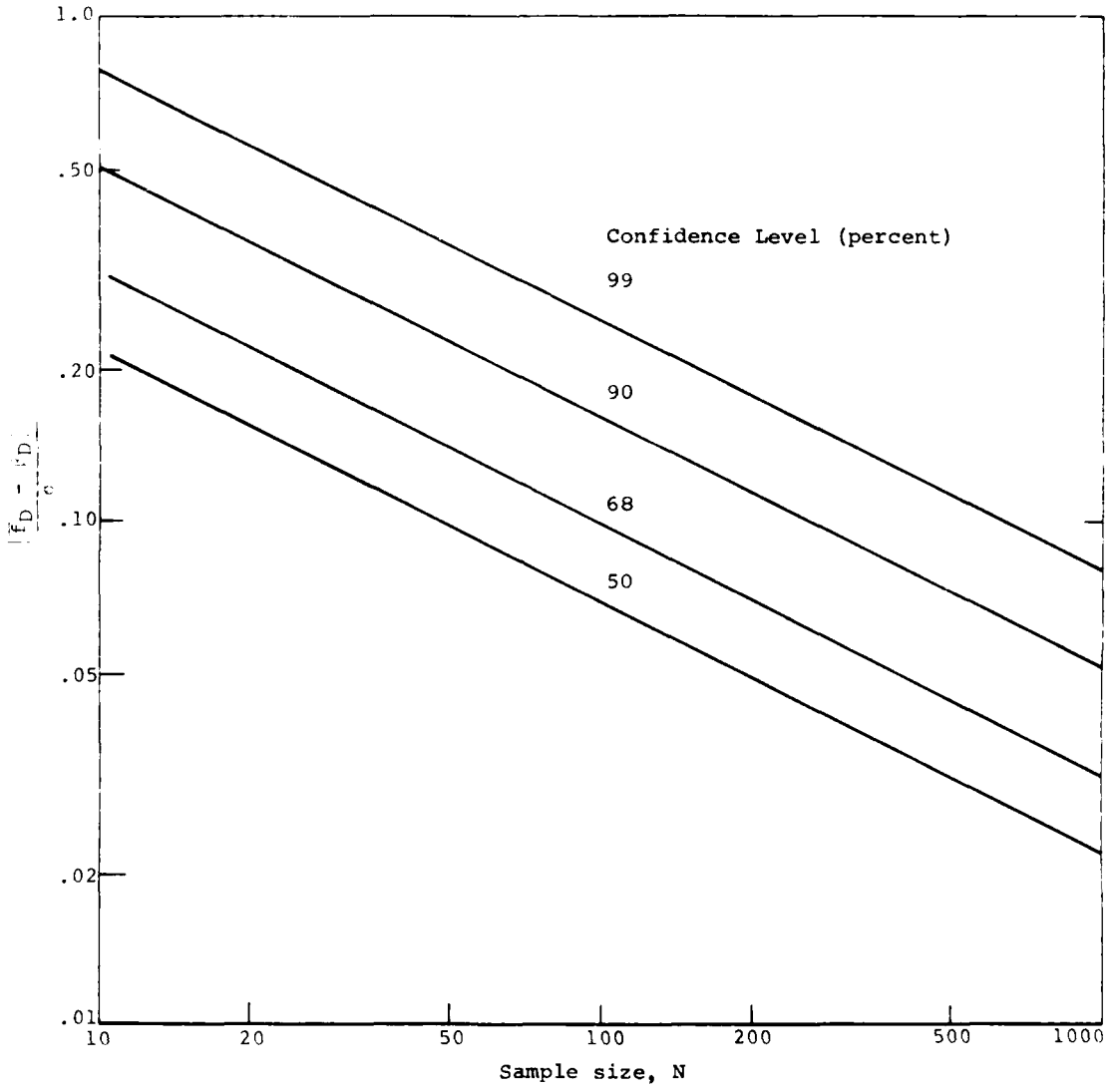

Figure A-1.- Variation of Mean Measurement Accuracy Parameter with Confidence Level and Sample Size.

TABLE I.- VELOCITY DATA FOR SHARP EDGE MODEL
M = 0.25, Re = .063 × 10^6

Pt	$\frac{x}{b/2}$	$\frac{y}{b/2}$	$\frac{u}{V}$	$\frac{u'}{V}$	$\frac{v}{V}$	$\frac{v'}{V}$
1	0.0	1.50000	0.73403	0.09241	0.59030	0.10427
2	0.0	2.00000	0.84582	0.10768	0.45444	0.14420
3	0.0	2.50000	0.90207	0.09441	0.38105	0.07574
4	0.0	1.50000	0.71054	0.12388	0.57785	0.12341
5	0.50000	1.50000	0.95197	0.16522	0.60921	0.08701
6	0.50000	1.25000	-0.12741	0.09699	0.01151	0.07186
7	0.50000	1.30000	-0.11097	0.10357	-0.00634	0.07973
8	0.50000	1.35000	-0.04568	0.13492	0.04838	0.09089
9	0.50000	1.40000	0.14784	0.22346	0.17085	0.11531
10	0.50000	1.45000	0.45009	0.29662	0.37999	0.12835
11	0.50000	1.50000	0.91698	0.19962	0.58478	0.09007
12	0.50000	1.60000	0.98086	0.09758	0.61719	0.08337
13	0.50000	2.00000	0.95409	0.13304	0.48849	0.11367

TABLE II.- VELOCITY DATA FOR SHARP EDGE MODEL
$M = .25$, $Re = .25 \times 10^6$

(*indicates points dropped from analysis)

Pt	$\frac{x}{b/2}$	$\frac{y}{b/2}$	$\frac{u}{V}$	$\frac{u'}{V}$	$\frac{v}{V}$	$\frac{v'}{V}$
14	0.50000	2.00000	0.95479	0.11731	0.42156	0.26609
15*	0.50000	1.50000	0.97769	0.18953	0.62799	0.11273
16	0.50000	1.25000	-0.09934	0.09829	0.01339	0.08067
17*	0.50000	1.30000	-0.09394	0.11085	-0.00716	0.08607
18*	0.50000	1.35000	-0.08384	0.11766	0.03464	0.08631
19*	0.50000	1.40000	0.06106	0.18941	0.11801	0.11743
20*	0.50000	1.45000	0.47358	0.29039	0.41733	0.21278
21*	0.50000	1.50000	0.98250	0.20996	0.65688	0.09969
22	1.00000	1.50000	-0.10709	0.12118	0.03253	0.09876
23	1.00000	1.60000	0.10733	0.23062	0.10568	0.11860
24	1.00000	1.65000	0.36003	0.30660	0.19551	0.14772
25	1.00000	1.70000	0.69387	0.32151	0.33924	0.13798
26	1.00000	1.75000	1.02078	0.22487	0.46360	0.12788
27	1.00000	1.80000	1.09864	0.13938	0.48826	0.10063
28	1.00000	2.00000	1.05390	0.12647	0.46137	0.18894
29	1.00000	1.40000	-0.14244	0.11590	0.01714	0.10204
30	2.00000	2.00000	0.63668	0.33760	0.14690	0.23156
31	2.00000	2.20000	1.12365	0.18835	0.12647	0.49331
32	2.00000	2.40000	1.15066	0.11837	0.27900	0.29779
33	2.00000	2.60000	1.13727	0.11484	0.32233	0.08384
34	2.00000	1.80000	0.04803	0.23544	0.03969	0.28605
35	2.00000	1.60000	-0.14620	0.15383	0.01362	0.21548
36	2.00000	1.40000	-0.16522	0.12341	0.02642	0.16674
37	2.00000	1.50000	-0.15395	0.13845	0.01069	0.19469
38	2.00000	1.70000	-0.09852	0.16217	-0.00975	0.24389
39	2.00000	1.90000	0.29180	0.30249	0.03147	0.30272
40	2.00000	2.10000	0.96430	0.28899	0.24789	0.20056
41	2.00000	2.30000	1.15124	0.12776	0.20878	0.42954
42	2.00000	2.50000	1.13187	0.12001	0.25857	0.39455
43	2.00000	1.55000	-0.13023	0.13269	0.02677	0.16945
44	2.00000	1.65000	-0.11343	0.15477	0.02466	0.20045
45	2.00000	1.75000	-0.02842	0.19434	0.04357	0.21923
46	2.00000	1.85000	0.15406	0.25587	0.05578	0.18624
47	2.00000	1.95000	0.46231	0.33736	0.11578	0.18729
48	2.00000	2.05000	0.81541	0.32186	0.19822	0.20115
49	2.00000	2.15000	1.06341	0.24025	0.24166	0.30860
50	2.00000	2.25000	1.15512	0.13751	0.22698	0.35557
51*	0.60000	1.60000	1.01597	0.22346	0.33220	0.51268
52*	0.60000	1.56000	0.96360	0.32727	0.52031	0.29756
53	0.0	1.50000	0.73309	0.07527	0.54568	0.06975
54	0.0	1.40000	0.69775	0.07351	0.60028	0.07762
55	0.0	1.30000	0.62248	0.08114	0.66299	0.07433
56	0.0	1.20000	0.51902	0.09394	0.72405	0.08596
57	0.0	1.10000	0.35897	0.12776	0.82421	0.09089

TABLE II.- Continued.

Pt	$\frac{x}{b/2}$	$\frac{y}{b/2}$	$\frac{u}{V}$	$\frac{u'}{V}$	$\frac{v}{V}$	$\frac{v'}{V}$
58	0.0	1.05000	0.21959	0.11966	0.86343	0.14314
59	0.0	1.60000	0.76679	0.06975	0.51691	0.06787
60	0.0	1.70000	0.78065	0.07421	0.48121	0.06646
61	0.0	1.80000	0.80930	0.06752	0.45902	0.07245
62	0.0	2.00000	0.83866	0.06411	0.40442	0.17297
63	0.0	2.20000	0.87165	0.07022	0.38445	0.06188
64	0.0	2.40000	0.88938	0.07093	0.34594	0.06764
65	0.0	3.00000	0.93001	0.07292	0.28147	0.05953
66	0.0	3.50000	0.95092	0.06670	0.24272	0.06036
67	0.10000	3.50000	0.95996	0.07938	0.23908	0.06047
68	0.10000	3.00000	0.93906	0.08525	0.29509	0.06177
69	0.10000	2.40000	0.92520	0.07245	0.33772	0.06458
70	0.10000	2.20000	0.89232	0.07081	0.39138	0.06764
71	0.10000	2.00000	0.87553	0.06482	0.42473	0.07104
72	0.10000	1.80000	0.83725	0.08419	0.44657	0.21148
73	0.10000	1.70000	0.82821	0.07081	0.49378	0.19587
74	0.10000	1.60000	0.81799	0.07093	0.53722	0.07351
75	0.10000	1.50000	0.77701	0.07363	0.57151	0.08748
76	0.10000	1.40000	0.73192	0.07574	0.62670	0.08114
77	0.10000	1.30000	0.64596	0.11813	0.69692	0.08267
78	0.10000	1.20000	0.67027	0.07316	0.81517	0.08983
79	0.30000	1.10000	-0.07832	0.08819	-0.00869	0.07104
80	0.30000	1.30000	0.33842	0.18248	0.39302	0.14185
81	0.30000	1.20000	-0.09324	0.09288	0.01080	0.06975
82*	0.30000	1.30000	0.26397	0.24859	0.41334	0.14972
83	0.30000	1.35000	0.87330	0.11085	0.64913	0.09136
84	0.30000	1.40000	0.86167	0.07821	0.64209	0.08948
85	0.30000	1.45000	0.84605	0.09958	0.61660	0.08325
86	0.30000	1.50000	0.84934	0.08079	0.61073	0.08243
87	0.30000	1.60000	0.86872	0.07410	0.55836	0.08584
88	0.30000	1.80000	0.87835	0.08760	0.49472	0.08220
89	0.30000	2.00000	0.90395	0.06858	0.42543	0.17825
90	0.30000	2.50000	0.92414	0.08971	0.35216	0.06411
91	0.30000	3.00000	0.93906	0.06740	0.29239	0.06423
92	0.30000	3.50000	0.95233	0.07034	0.24612	0.06858
93	0.30000	1.32500	0.71101	0.22346	0.60287	0.10604
94	0.40000	1.10000	-0.07421	0.09347	0.02525	0.08067
95	0.40000	1.30000	-0.07586	0.15312	0.04263	0.08666
96	0.40000	1.40000	0.76233	0.23755	0.54368	0.09347
97	0.40000	1.35000	0.21512	0.25552	0.26679	0.12612
98	0.40000	1.37500	0.41181	0.23344	0.41815	0.13563
99	0.40000	1.42500	0.90676	0.14995	0.60698	0.14760
100	0.40000	1.45000	0.92954	0.09077	0.61696	0.08185
101	0.40000	1.50000	0.90442	0.07703	0.59054	0.08795
102	0.40000	1.55000	0.88387	0.07609	0.58232	0.08748

TABLE II.- Continued.

Pt	$\frac{x}{b/2}$	$\frac{y}{b/2}$	$\frac{u}{V}$	$\frac{u'}{V}$	$\frac{v}{V}$	$\frac{v'}{V}$
103	0.40000	1.60000	0.89490	0.10016	0.57891	0.08725
104	0.40000	1.65000	0.90183	0.09394	0.55014	0.07562
105	0.40000	1.70000	0.91710	0.07785	0.53276	0.08314
106	0.40000	1.80000	0.91792	0.07245	0.47757	0.19375
107	0.40000	2.00000	0.92426	0.07457	0.44587	0.07186
108	0.40000	2.50000	0.93671	0.08372	0.35169	0.06177
109	0.40000	3.00000	0.95843	0.09394	0.30249	0.06106
110	0.40000	3.50000	0.97558	0.07915	0.25329	0.06517
111	0.50000	3.50000	0.99155	0.06811	0.26057	0.05953
112	0.50000	3.00000	0.97992	0.08419	0.31259	0.06282
113	0.50000	2.50000	0.97264	0.09899	0.36214	0.06623
114	0.50000	2.00000	0.95784	0.07116	0.43084	0.23978
115	0.50000	1.80000	0.95808	0.07468	0.50247	0.07774
116	0.50000	1.70000	0.95139	0.08995	0.54004	0.09535
117	0.50000	1.60000	0.94481	0.07574	0.56153	0.08619
118	0.50000	1.50000	0.97969	0.12024	0.56682	0.10310
119	0.50000	1.40000	0.18589	0.22839	0.20608	0.11743
120	0.50000	1.47500	0.90254	0.21031	0.54615	0.10744
121	0.50000	1.45000	0.71994	0.24624	0.45949	0.11731
122	0.50000	1.42500	0.40348	0.25364	0.34371	0.12224
123	0.50000	1.35000	-0.06047	0.13434	0.06353	0.09570
124	0.50000	1.30000	-0.11484	0.11942	0.01714	0.07961
125	0.50000	1.20000	-0.09887	0.09711	0.00423	0.07515
126	0.50000	1.00000	-0.08325	0.10510	-0.00505	0.07950
127	0.50000	0.80000	-0.06599	0.09793	-0.02255	0.05026
128	0.60000	0.80000	-0.06717	0.10251	0.00552	0.08807
129	0.60000	1.00000	-0.08607	0.10427	-0.00117	0.06717
130	0.60000	1.20000	-0.11519	0.10874	0.00705	0.07257
131	0.60000	1.40000	-0.03934	0.14890	0.04685	0.09136
132	0.60000	1.50000	0.65747	0.28124	0.41522	0.12318
133	0.60000	1.45000	0.24695	0.26667	0.17637	0.10803
134	0.60000	1.55000	0.99354	0.14655	0.53417	0.10615
135	0.60000	1.60000	0.98403	0.11649	0.54580	0.08549
136	0.60000	1.70000	0.97886	0.08995	0.53922	0.08842
137	0.60000	2.00000	0.97898	0.07961	0.45890	0.07797
138	0.60000	2.50000	0.98227	0.08901	0.37259	0.07515
139	0.60000	3.00000	0.96548	0.08126	0.32386	0.06834
140	0.60000	3.50000	0.96935	0.08419	0.27795	0.04897
141	0.80000	3.50000	0.98297	0.09535	0.26186	0.07550
142	0.80000	3.00000	0.98732	0.07961	0.31271	0.05636
143	0.80000	2.50000	0.98368	0.10122	0.36660	0.07691
144	0.80000	2.00000	0.99507	0.09488	0.49108	0.07504
145	0.80000	1.80000	1.00517	0.10639	0.51585	0.07621
146	0.80000	1.70000	1.02384	0.11531	0.50376	0.08960
147	0.80000	1.60000	0.72475	0.29251	0.44998	0.11132
148	0.80000	1.50000	0.06787	0.19904	0.10721	0.08513

TABLE II.- Continued.

Pt	$\frac{x}{b/2}$	$\frac{y}{b/2}$	$\frac{u}{\bar{V}}$	$\frac{u'}{\bar{V}}$	$\frac{v}{\bar{V}}$	$\frac{v'}{\bar{V}}$
149	0.80000	1.55000	0.27771	0.28077	0.25376	0.11907
150	0.80000	1.40000	-0.12435	0.11261	0.01750	0.09723
151	0.80000	1.20000	-0.12295	0.11226	0.00423	0.08678
152	0.80000	1.00000	-0.08819	0.10768	-0.01538	0.09969
153	0.20000	1.20000	0.25740	0.24460	0.38727	0.26456
154	0.20000	1.10000	-0.06611	0.08960	0.02208	0.06975
155	0.20000	1.15000	-0.09288	0.08877	-0.01444	0.13868
156	0.20000	1.17500	-0.04004	0.26233	0.11285	0.14690
157	0.20000	1.19000	0.07327	0.30895	0.28018	0.17872
158	0.20000	1.22500	0.63011	0.20761	0.71571	0.11696
159	0.20000	1.25000	0.81447	0.09112	0.80002	0.09993
160	0.20000	1.27500	0.79685	0.06952	0.81505	0.07785
161	0.20000	1.30000	0.78311	0.07374	0.77877	0.10604
162	0.20000	1.40000	0.76409	0.11555	0.70150	0.10733
163	0.20000	1.50000	0.81505	0.07738	0.62835	0.08584
164	0.20000	1.60000	0.83537	0.07163	0.57856	0.06153
165	0.20000	1.80000	0.86743	0.06975	0.49648	0.05801
166	0.20000	2.00000	0.88997	0.06775	0.40899	0.32198
167	0.20000	2.50000	0.91827	0.08901	0.35357	0.06517
168	0.20000	3.00000	0.94868	0.06893	0.30449	0.06494
169	0.20000	3.50000	0.96736	0.06470	0.27713	0.04051
170	1.00000	1.30000	-0.15782	0.10651	-0.01867	0.07186
171	1.00000	1.55000	0.01867	0.19998	0.07574	0.06153
172	1.00000	1.77000	1.02219	0.13621	0.43037	0.10979
173	1.00000	1.85000	1.03370	0.10615	0.47863	0.08631
174	1.00000	1.90000	1.04756	0.09887	0.47687	0.06952
175	1.20000	3.50000	1.04122	0.07233	0.23016	0.06693
176	1.20000	3.50000	1.05296	0.05801	0.27266	0.05237
177	1.20000	3.00000	1.06623	0.08044	0.31635	0.05648
178	1.20000	2.50000	1.07691	0.06940	0.35404	0.06858
179	1.20000	2.00000	1.10756	0.07233	0.42449	0.07480
180	1.20000	1.80000	0.95115	0.24847	0.35404	0.10768
181	1.20000	1.70000	0.44375	0.33502	0.16733	0.12882
182	1.20000	1.75000	0.69457	0.30519	0.26867	0.12365
183	1.20000	1.65000	0.16721	0.26468	0.10803	0.12271
184	1.20000	1.60000	0.00458	0.19082	0.06083	0.09688
185	1.20000	1.50000	-0.11238	0.13105	0.02971	0.07915
186	1.20000	1.30000	-0.15312	0.10427	0.03053	0.07621
187	1.20000	1.10000	-0.14549	0.12060	0.03957	0.08995
188	1.40000	1.10000	-0.17039	0.12752	0.05942	0.09230
189	1.40000	1.30000	-0.17931	0.13680	0.05143	0.08079
190	1.40000	1.50000	-0.15148	0.11766	0.02771	0.08173
191	1.40000	1.70000	0.11989	0.24765	0.09558	0.10968
192	1.40000	1.80000	0.55085	0.33478	0.20784	0.13340

TABLE II.- Continued.

Pt	$\frac{x}{b/2}$	$\frac{y}{b/2}$	$\frac{u}{V}$	$\frac{u'}{V}$	$\frac{v}{V}$	$\frac{v'}{V}$
193	1.40000	1.90000	1.01409	0.22464	0.34500	0.11202
194	1.40000	1.85000	0.85932	0.28828	0.28957	0.13058
195	1.40000	1.82500	0.69187	0.31717	0.23192	0.12165
196	1.40000	1.75000	0.30390	0.29979	0.12506	0.13950
197	1.40000	2.00000	1.12013	0.10956	0.36543	0.24965
198	1.40000	2.20000	1.10909	0.08854	0.38387	0.07480
199	1.40000	2.40000	1.10028	0.06987	0.36355	0.06235
200	1.40000	2.60000	1.08948	0.07316	0.35615	0.06717
201	1.40000	3.00000	1.07891	0.07222	0.31000	0.06364
202	1.40000	3.50000	1.06728	0.06036	0.27090	0.05883
203	1.60000	3.50000	1.08960	0.05989	0.25446	0.06552
204	1.60000	3.00000	1.08572	0.07457	0.30049	0.06599
205	1.60000	2.50000	1.11496	0.07468	0.33490	0.07151
206	1.60000	2.00000	1.06223	0.20009	0.33807	0.12647
207	1.60000	1.80000	0.32057	0.29979	0.11273	0.14021
208	1.60000	1.85000	0.45808	0.31318	0.16064	0.15289
209	1.60000	1.90000	0.75000	0.29603	0.19939	0.14173
210	1.60000	1.75000	0.15183	0.25176	0.12717	0.11120
211	1.60000	1.70000	0.00998	0.18671	0.06423	0.10721
212	1.60000	1.60000	-0.12036	0.14749	0.04908	0.11766
213	1.60000	1.40000	-0.16874	0.13621	0.03992	0.08079
214	1.60000	1.20000	-0.18013	0.11989	0.04568	0.10474
215	1.60000	1.00000	-0.14866	0.13727	0.02090	0.09512
216	-0.10000	1.10000	0.46219	0.10885	0.91522	0.09253
217	-0.20000	1.10000	0.36332	0.34147	0.57985	0.21689
218	0.30000	1.25000	-0.06494	0.13704	0.01585	0.08701
219	0.30000	1.27500	-0.04216	0.15712	0.04721	0.09112
220	0.30000	1.37500	0.89338	0.16287	0.72922	0.08913
221	0.20000	1.30000	0.82715	0.12189	0.81106	0.08372
222	0.25000	1.30000	0.74096	0.30308	0.74284	0.14079
223	0.35000	1.30000	-0.00341	0.15559	0.06271	0.08807
224	0.20000	1.40000	0.76667	0.13281	0.75200	0.07961
225	0.45000	1.40000	0.24401	0.23356	0.21712	0.25611
226	0.55000	1.40000	-0.01198	0.19246	0.04803	0.09418
227	0.70000	1.50000	0.13657	0.26761	0.11872	0.11390
228	1.00000	1.30000	-0.14667	0.20467	0.03546	0.08408
229*	1.00000	1.55000	-0.02466	0.18483	0.06717	0.12036
230*	1.00000	1.77000	0.98262	0.21829	0.43941	0.11508
231*	1.00000	1.90000	1.01949	0.15218	0.45209	0.08126
232	0.25000	1.02000	-0.04216	0.15524	-0.00552	0.08255
233	0.30000	1.04000	-0.05437	0.13257	-0.00305	0.08807
234*	0.40000	1.10000	-0.08173	0.13081	0.05155	0.06952
235*	0.50000	1.16000	-0.11942	0.14021	0.03088	0.08185
236	0.70000	0.87000	-0.08091	0.14385	-0.00740	0.13375
237	0.80000	0.98000	-0.11907	0.12647	0.00540	0.09324
238	0.90000	1.09000	-0.13070	0.13962	0.00399	0.13116

TABLE II.- Continued.

Pt	$\frac{x}{b/2}$	$\frac{y}{b/2}$	$\frac{u}{V}$	$\frac{u'}{V}$	$\frac{v}{V}$	$\frac{v'}{V}$
239	0.60000	0.76000	-0.05073	0.12306	-0.01515	0.09300
240	1.00000	0.57000	-0.02031	0.13269	0.00986	0.08490
241	1.05000	0.71000	-0.11132	0.13175	-0.00059	0.09159
242	1.10000	0.85000	-0.12224	0.14667	0.00986	0.10052
243	1.15000	0.99000	-0.14079	0.17720	0.01139	0.11003
244	1.20000	1.14000	-0.14443	0.14526	0.02607	0.14396
245	-0.10000	1.20000	0.32515	0.39044	0.70291	0.07457
246	-0.10000	1.30000	0.57233	0.12482	0.64056	0.07574
247	-0.10000	1.40000	0.64760	0.11437	0.61837	0.06705
248	-0.10000	1.50000	0.70056	0.11003	0.58877	0.05801
249	-0.10000	1.60000	0.74061	0.09253	0.56271	0.07762
250	-0.10000	1.70000	0.76750	0.10263	0.52865	0.06047
251	-0.10000	1.80000	0.78605	0.10193	0.47816	0.19763
252	0.90000	1.30000	-0.15806	0.13081	0.01797	0.07386
253	0.90000	1.40000	-0.12788	0.13269	0.04075	0.08032
254	0.90000	1.50000	-0.10698	0.11837	0.01773	0.09265
255	0.90000	1.60000	0.15582	0.24624	0.09899	0.12388
256	0.90000	1.70000	0.82915	0.30507	0.37189	0.16498
257	0.90000	1.80000	1.05578	0.13657	0.47816	0.15359
258	0.90000	1.90000	1.05625	0.15160	0.46712	0.11343
259	1.10000	1.90000	1.08584	0.13093	0.43906	0.11073
260	1.10000	1.80000	0.94446	0.25247	0.37553	0.11543
261	1.10000	1.70000	0.36062	0.29368	0.18847	0.13657
262	1.10000	1.60000	-0.01820	0.19446	0.06435	0.10416
263	1.10000	1.50000	-0.13809	0.14537	0.03018	0.08431
264	1.10000	1.40000	-0.12447	0.11672	0.02595	0.06952
265	1.10000	1.30000	-0.12365	0.15089	0.04251	0.10110
266	1.90000	1.60000	-0.11790	0.15841	0.02630	0.09030
267	1.90000	1.70000	-0.08654	0.17215	0.04345	0.11473
268	1.90000	1.80000	0.05554	0.24636	0.04591	0.13821
269	1.90000	1.90000	0.32797	0.31822	0.08114	0.16956
270	1.90000	2.00000	0.64549	0.33396	0.17884	0.13387
271	1.90000	2.10000	0.99683	0.25270	0.27125	0.12447
272	1.90000	2.20000	1.14526	0.14162	0.32386	0.11343
273	1.90000	2.30000	1.13316	0.11144	0.34359	0.08243
274	1.80000	2.30000	1.11719	0.19000	0.33807	0.17156
275	1.80000	2.20000	1.12224	0.11496	0.34007	0.13046
276	1.80000	2.10000	1.05355	0.18330	0.30801	0.17614
277	1.80000	2.00000	0.79944	0.30965	0.22299	0.15101
278	1.80000	1.90000	0.39338	0.33995	0.12271	0.14843
279	1.80000	1.80000	0.08795	0.26644	0.06552	0.12165
280	1.80000	1.70000	-0.10251	0.20244	0.05225	0.11649
281	1.80000	1.60000	-0.10627	0.16381	0.04004	0.09652
282	1.00000	1.20000	-0.14667	0.15453	0.01339	0.08443
283*	0.0	1.50000	0.78593	0.09382	0.61519	0.08572
284*	0.0	2.00000	0.88692	0.08173	0.44927	0.06318

TABLE II.- Continued.

Pt	$\frac{x}{b/2}$	$\frac{y}{b/2}$	$\frac{u}{\bar{V}}$	$\frac{u'}{\bar{V}}$	$\frac{v}{\bar{V}}$	$\frac{v'}{\bar{V}}$
285*	0.0	1.80000	0.84429	0.13070	0.49706	0.07809
286*	0.0	1.70000	0.81235	0.21595	0.52149	0.12705
287*	0.0	1.60000	0.77607	0.21923	0.54122	0.16733
288*	0.0	1.50000	0.64209	0.39854	0.45702	0.40207
289*	0.0	1.40000	0.51667	0.51339	0.49648	0.36555
290*	0.0	1.30000	0.07715	0.72287	0.06141	0.57222
291*	0.50000	1.15700	-0.09230	0.10392	0.01080	0.09840
292*	0.40000	1.10000	-0.08466	0.10662	0.01292	0.09758
293	0.30000	1.04000	-0.06940	0.09382	-0.00270	0.10568
294	0.25000	1.02000	-0.05895	0.10216	0.00705	0.09547
295	0.90000	1.10000	-0.12811	0.11332	0.00364	0.09042
296	0.80000	0.98200	-0.12694	0.11919	0.01186	0.08596
297	0.70000	0.87000	-0.08314	0.11578	-0.00540	0.08889
298	0.60000	0.75600	-0.05096	0.10110	-0.01057	0.08091
299	0.50000	0.64000	-0.00845	0.10733	-0.02360	0.08666
300	0.70000	0.50000	0.01832	0.10510	-0.01562	0.08690
301	0.80000	0.70000	-0.04861	0.11813	-0.00810	0.08654
302	0.95000	0.90000	-0.10897	0.12729	0.02090	0.08924
303	1.20000	1.13600	-0.14667	0.13351	0.02724	0.08842
304	1.15000	0.99300	-0.14068	0.14584	0.02395	0.07961
305	1.10000	0.85000	-0.12729	0.12412	0.02959	0.08854
306	1.05000	0.70700	-0.10322	0.13903	0.01773	0.09993
307	1.01000	0.61800	-0.08008	0.13046	0.00388	0.08748
308	1.00000	0.56500	-0.05636	0.12823	-0.01597	0.09018
309	0.95000	0.40000	-0.04122	0.29556	0.06318	0.37271
310	1.20000	0.50000	-0.03581	0.13950	0.00963	0.08924
311	1.40000	0.50000	-0.07633	0.12999	0.03523	0.09629
312	1.60000	0.50000	-0.08396	0.13809	0.03581	0.08995
313	2.00000	0.50000	-0.11813	0.14162	0.03699	0.08502
314	1.80000	0.50000	-0.10498	0.14549	0.04497	0.08701
315	2.00000	0.40000	-0.08055	0.14667	0.03828	0.08149
316	2.00000	0.30000	-0.06881	0.14138	0.03687	0.48697
317	2.00000	0.60000	-0.12565	0.14890	0.03264	0.09253
318	2.00000	0.70000	-0.12612	0.15876	0.04650	0.09347
319	2.00000	0.80000	-0.16076	0.13821	0.05155	0.09206
320	2.00000	1.00000	-0.18647	0.13727	0.04721	0.10157
321	2.00000	1.20000	-0.18037	0.14302	0.05695	0.09324
322	2.00000	1.30000	-0.16968	0.16616	0.05108	0.09523
323	0.30000	0.80000	-0.02208	0.10651	-0.01233	0.07222
324	0.60000	1.00000	-0.08549	0.11907	0.00975	0.08490
325	1.40000	0.80000	-0.14537	0.14537	0.04544	0.09805
326	1.40000	1.10000	-0.16534	0.13175	0.02924	0.08596
327	1.60000	1.10000	-0.15418	0.14302	0.02184	0.08325
328	1.60000	0.80000	-0.14819	0.15019	0.02689	0.09359
329	1.80000	0.80000	-0.15066	0.14995	0.05613	0.10709
330	1.80000	1.10000	-0.16252	0.14831	0.04744	0.09065

TABLE II.- Continued.

Pt	$\frac{x}{b/2}$	$\frac{y}{b/2}$	$\frac{u}{V}$	$\frac{u'}{V}$	$\frac{v}{V}$	$\frac{v'}{V}$
331	-0.30000	1.30000	0.58936	0.12259	0.51996	0.16498
332	-0.30000	1.10000	0.43037	0.22158	0.51667	0.23520
333	-0.30000	.00000	0.35686	0.22957	0.48744	0.25188
334	-0.40000	0.80000	0.18812	0.44105	0.34758	0.25975
335	-0.40000	0.60000	0.20937	0.28758	0.27266	0.29779
336	-0.40000	0.40000	0.16193	0.31188	0.15899	0.30824
337	-0.40000	0.20000	-0.06799	0.53605	0.12341	0.19551
338	-0.40000	0.0	-0.06705	0.51691	0.03793	0.25470
339	-0.40000	-0.20000	-0.05308	0.51092	0.09981	0.42449
340	-0.40000	-0.40000	-0.00423	0.48051	-0.15500	0.06717
341	-0.60000	-0.40000	0.26163	0.35345	-0.09429	0.21477
342	-0.60000	-0.20000	0.33619	0.12142	-0.00012	0.27337
343	-0.60000	0.0	0.30437	0.11473	0.02971	0.23133
344	-0.60000	0.20000	0.30719	0.15442	0.14514	0.34277
345	-0.60000	0.40000	0.33055	0.13551	0.17027	0.24824
346	-0.60000	0.60000	0.37142	0.10698	0.24084	0.15171
347	-0.60000	0.80000	0.41839	0.08725	0.29885	0.15054
348	-0.60000	1.00000	0.49096	0.07703	0.35157	0.09429
349	-0.60000	1.20000	0.56552	0.05589	0.38715	0.18729
350	-0.60000	1.40000	0.65529	0.06505	0.39596	0.16851
351	-0.60000	1.60000	0.72123	0.06224	0.40395	0.08255
352	-0.60000	1.60000	0.71360	0.07046	0.39021	0.17649
353	-0.60000	2.00000	0.80672	0.09570	0.36543	0.11743
354	-1.00000	2.00000	0.80061	0.07410	0.29380	0.16240
355	-1.00000	1.50000	0.69481	0.10791	0.29756	0.07868
356	-1.00000	1.00000	0.56470	0.12083	0.24542	0.10592
357	-1.00000	0.80000	0.50611	0.22722	0.21653	0.09406
358	-1.00000	0.60000	0.36449	0.35733	0.17532	0.10110
359	-1.00000	0.40000	0.23462	0.52184	0.13269	0.24977
360	-1.00000	0.20000	0.43988	0.23192	0.09101	0.30167
361	-1.00000	0.0	0.46818	0.10698	0.02924	0.20949
362	-1.00000	-0.20000	0.47757	0.11519	-0.02161	0.19798
363	-1.00000	-0.40000	0.45291	0.24295	-0.04920	0.31341
364	-1.00000	-0.60000	0.44634	0.33384	-0.04380	0.40254
365	-2.00000	-0.60000	0.71442	0.09512	-0.06470	0.06294
366	-2.00000	-0.40000	0.71395	0.06376	-0.05002	0.06952
367	-2.00000	-0.20000	0.70021	0.08713	-0.01902	0.06881
368	-2.00000	0.0	0.70197	0.06975	-0.01116	0.07950
369	-2.00000	0.20000	0.70409	0.06846	0.03311	0.06928
370	-2.00000	0.40000	0.70103	0.09641	0.05026	0.08455
371	-2.00000	0.60000	0.70362	0.08302	0.07457	0.09312
372	-2.00000	0.80000	0.71841	0.08419	0.10193	0.08008

TABLE II.- Concluded.

Pt	$\frac{x}{b/2}$	$\frac{y}{b/2}$	$\frac{u}{\bar{V}}$	$\frac{u'}{\bar{V}}$	$\frac{v}{\bar{V}}$	$\frac{v'}{\bar{V}}$
373	-2.00000	1.00000	0.74378	0.07410	0.12588	0.07586
374	-2.00000	1.20000	0.74871	0.07363	0.13727	0.06928
375	-2.00000	1.40000	0.76198	0.07139	0.15571	0.07057
376	-2.00000	1.60000	0.78452	0.08960	0.16428	0.07363
377	-2.00000	2.00000	0.83055	0.07163	0.18906	0.08666
378	-2.00000	2.50000	0.87459	0.06764	0.17755	0.08091
379	-1.80000	0.0	0.66040	0.10322	0.00481	0.07492
380	-1.60000	0.0	-0.63492	0.72863	-0.00153	0.09558
381	-1.20000	0.0	-0.14267	0.56999	0.01292	0.19129
382	-0.80000	0.0	0.39432	0.18471	0.01080	0.20632
383	-0.60000	0.0	0.21383	0.38856	0.01785	0.12318

TABLE III.- VELOCITY DATA FOR SHARP EDGE MODEL
$M = 0.5$, $Re = .15 \cdot 10^6$

(*indicates points dropped from analysis)

Pt	$\frac{x}{b/2}$	$\frac{y}{b/2}$	$\frac{u}{V}$	$\frac{u'}{V}$	$\frac{v}{V}$	$\frac{v'}{V}$
384	0.20000	1.00000	-0.07122	0.05893	0.00346	0.06101
385	0.20000	1.10000	-0.08639	0.06627	0.00101	0.05624
386	0.20000	1.15000	-0.08776	0.07290	-0.00179	0.05409
387	0.20000	1.17500	-0.05015	0.10233	0.05576	0.07445
388	0.20000	1.20000	0.08657	0.16263	0.26955	0.13773
389	0.20000	1.22500	0.36913	0.20549	0.60549	0.13618
390	0.20000	1.25000	0.65881	0.16131	0.80227	0.11493
391	0.20000	1.27500	0.77307	0.11701	0.88997	0.09015
392	0.20000	1.30000	0.85469	0.05200	0.88961	0.07606
393	0.20000	1.35000	0.80776	0.05725	0.87642	0.06896
394	0.20000	1.40000	0.74597	0.10036	0.82609	0.07701
395	0.20000	1.50000	0.82734	0.08543	0.69743	0.05779
396	0.20000	1.60000	0.80561	0.22699	0.62418	0.13893
397	0.20000	1.70000	0.88287	0.07964	0.58406	0.10973
398	0.20000	1.80000	0.88364	0.08931	0.56406	0.07469
399	2.00000	2.40000	1.23397	0.06293	0.36227	0.05678
400	2.00000	2.30000	1.23940	0.07594	0.36173	0.05851
401	2.00000	2.20000	1.21552	0.14036	0.34454	0.05860
402	2.00000	2.10000	1.08955	0.25773	0.31373	0.08436
403	2.00000	2.00000	0.70466	0.32824	0.28125	0.11570
404	2.00000	1.90000	0.37576	0.32472	0.15773	0.13303
405	2.00000	1.92500	0.43887	0.32860	0.19379	0.13212
406	2.00000	1.95000	0.52281	0.33504	0.21439	0.12173
407	2.00000	1.85000	0.20131	0.29015	0.11612	0.11779
408	2.00000	1.80000	0.10304	0.26800	0.08436	0.13707
409	2.00000	1.75000	-0.00197	0.23027	0.06257	0.11875
410	2.00000	1.70000	-0.06436	0.19528	0.04919	0.12776
411	2.00000	1.60000	-0.15475	0.14907	0.05152	0.09558
412	2.00000	1.50000	-0.17958	0.13815	0.04054	0.11015
413	2.00000	1.40000	-0.18901	0.14000	0.05582	0.09397
414	2.00000	1.30000	-0.19845	0.14048	0.03803	0.08627
415	2.00000	1.20000	-0.20866	0.13319	0.04961	0.08633
416	2.00000	1.00000	-0.19821	0.14967	0.05940	0.08949
417	2.00000	0.80000	-0.18764	0.14293	0.05069	0.08591
418	2.00000	0.70000	-0.17606	0.14012	0.05087	0.07946
419	2.00000	0.60000	-0.13946	0.14215	0.05582	0.08030
420	2.00000	0.50000	-0.12358	0.13660	0.04185	0.07737
421*	2.00000	0.40000	-0.09242	0.14436	0.00764	0.14167
422	2.00000	0.40000	-0.07152	0.14173	0.05248	0.24890
423	1.90000	1.40000	-0.18460	0.12621	0.04722	0.07934
424	1.90000	1.50000	-0.18710	0.13182	0.06113	0.09964
425	1.90000	1.60000	-0.15093	0.16155	0.04878	0.09504

TABLE III.- Continued.

Pt	$\frac{x}{b/2}$	$\frac{y}{b/2}$	$\frac{u}{V}$	$\frac{u'}{V}$	$\frac{v}{V}$	$\frac{v'}{V}$
426	1.90000	1.70000	-0.04012	0.18245	0.05057	0.11206
427	1.90000	1.80000	0.18788	0.28304	0.12836	0.10609
428	1.90000	1.90000	0.49003	0.33528	0.18525	0.12018
429	1.90000	2.00000	0.78919	0.36000	0.33242	0.10716
430	1.90000	2.10000	1.14913	0.21916	0.32096	0.05296
431	1.90000	2.20000	1.26525	0.06776	0.29642	0.19361
432	1.20000	1.13600	-0.16919	0.14346	0.00663	0.07033
433	1.20000	1.20000	-0.19672	0.10925	0.04758	0.06543
434	1.20000	1.30000	-0.17564	0.13463	0.03493	0.06597
435	1.20000	1.40000	-0.19140	0.11964	0.01421	0.06018
436	1.20000	1.50000	-0.14776	0.12448	0.01558	0.07003
437	1.20000	1.60000	0.00764	0.20645	0.04597	0.09003
438	1.20000	1.70000	0.37785	0.29487	0.20866	0.11487
439	1.20000	1.65000	0.15606	0.25015	0.11564	0.09373
440	1.20000	1.75000	0.69851	0.30746	0.32328	0.11976
441	1.20000	1.80000	0.89696	0.29182	0.41164	0.10764
442	1.20000	2.00000	1.20746	0.06275	0.34537	0.23612
443*	2.00000	2.05000	0.77636	0.36782	0.33576	0.12253
444*	2.00000	2.15000	1.19600	0.10728	0.16478	0.25158
445*	2.00000	2.05000	0.80358	0.30797	0.22478	0.20340
446	0.0	1.50000	0.68498	0.05542	0.57479	0.05101
447	0.0	1.80000	0.79482	0.04017	0.47872	0.04070
448	0.0	1.70000	0.76734	0.04255	0.50989	0.04380
449	0.0	1.60000	0.73528	0.04535	0.53665	0.04487
450	0.0	1.40000	0.62479	0.04672	0.60751	0.04797
451	0.0	1.30000	0.52670	0.04869	0.66824	0.05423
452	0.0	1.20000	0.42652	0.07271	0.74184	0.07706
453	0.0	1.10000	0.21400	0.07223	0.81567	0.09815
454	0.0	1.05000	0.02729	0.21633	0.73391	0.11526
455	0.10000	1.05000	-0.05912	0.05447	0.02342	0.04964
456	0.10000	1.10000	-0.06448	0.06097	0.04708	0.06508
457	0.10000	1.20000	0.57986	0.23856	0.83617	0.26031
458	0.10000	1.30000	0.59625	0.10703	0.77616	0.05364
459	0.10000	1.15000	0.30095	0.19607	0.38951	0.30554
460*	0.10000	1.20000	0.65334	0.06645	0.94225	0.07759
461	0.10000	1.40000	0.64726	0.09410	0.66502	0.09297
462	0.10000	1.50000	0.74178	0.06913	0.61824	0.05119
463	0.10000	1.60000	0.77980	0.05852	0.57515	0.04660
464	0.10000	1.70000	0.81305	0.05513	0.53456	0.04309
465	0.10000	1.80000	0.83004	0.05441	0.50387	0.04052
466*	0.20000	1.80000	0.86841	0.05906	0.51853	0.04261
467*	0.20000	1.70000	0.82962	0.11603	0.54762	0.06281
468*	0.20000	1.60000	0.83045	0.06764	0.59595	0.04952
469*	0.20000	1.50000	0.76931	0.07324	0.65572	0.04696
470*	0.20000	1.40000	0.72741	0.08701	0.75864	0.05226

TABLE III.- Continued.

Pt	$\frac{x}{b/2}$	$\frac{y}{b/2}$	$\frac{u}{V}$	$\frac{u'}{V}$	$\frac{v}{V}$	$\frac{v'}{V}$
471*	0.20000	1.30000	0.86311	0.06907	0.82110	0.04684
472*	0.20000	1.27500	0.02271	0.14154	0.17300	0.08772
473*	0.20000	1.25000	0.45346	0.19869	0.56251	0.10250
474*	0.20000	1.27500	0.60423	0.12133	0.71293	0.25834
475*	0.20000	1.22500	0.22181	0.19392	0.34023	0.12288
476*	0.20000	1.10000	-0.07586	0.05930	-0.00232	0.05715
477	0.25000	1.01500	-0.06311	0.05834	-0.01663	0.06943
478	0.30000	1.10000	-0.08486	0.06907	-0.00435	0.06103
479	0.30000	1.20000	-0.10048	0.07187	-0.00757	0.05221
480	0.30000	1.30000	0.16281	0.18272	0.26836	0.10578
481	0.30000	1.25000	-0.06436	0.08534	0.02199	0.05012
482	0.30000	1.35000	0.64607	0.14964	0.69559	0.09482
483	0.30000	1.32500	0.45375	0.20369	0.52908	0.12354
484	0.30000	1.37500	0.82980	0.09333	0.76097	0.05727
485	0.30000	1.40000	0.97640	0.05203	0.74791	0.05340
486	0.30000	1.50000	0.83397	0.06430	0.72497	0.05560
487	0.30000	1.60000	0.86031	0.07521	0.62932	0.03850
488	0.30000	1.70000	0.89607	0.06818	0.58749	0.04231
489	0.30000	1.80000	0.90942	0.06454	0.54392	0.04225
490	0.40000	1.80000	0.93892	0.08933	0.55661	0.04273
491	0.40000	1.70000	0.93319	0.07277	0.60870	0.04362
492	0.40000	0.60000	0.90614	0.06669	0.67569	0.05209
493	0.40000	1.50000	0.99172	0.04756	0.70542	0.04452
494	0.40000	1.40000	0.52980	0.19785	0.54064	0.08474
495	0.40000	1.45000	0.94958	0.12104	0.68105	0.08731
496	0.40000	1.42500	0.69893	0.24762	0.67318	0.10006
497	0.40000	1.37500	0.33915	0.24476	0.38570	0.11198
498	0.40000	1.35000	0.13611	0.19136	0.19541	0.07688
499	0.40000	1.30000	-0.08856	0.08999	0.00328	0.05602
500	0.40000	1.20000	-0.09672	0.08135	-0.01162	0.05113
501	0.40000	1.10000	-0.09934	0.08147	-0.00656	0.05763
502	0.40000	1.00000	-0.06871	0.07902	-0.00793	0.05662
503	0.50000	1.00000	-0.07962	0.08409	-0.01383	0.04923
504	0.50000	1.10000	-0.09917	0.07849	-0.01263	0.05662
505	0.50000	1.20000	-0.09487	0.08802	-0.00697	0.05578
506	0.50000	1.30000	-0.12157	0.08671	0.00072	0.05846
507	0.50000	1.40000	0.09678	0.18021	0.15977	0.07908
508	0.50000	1.50000	0.87223	0.20375	0.64505	0.07652
509	0.50000	1.60000	0.99774	0.04636	0.64893	0.04803
510	0.50000	1.42500	0.33015	0.21472	0.31156	0.07974
511	0.50000	1.45000	0.50125	0.21824	0.43701	0.08886
512	0.50000	1.47500	0.72390	0.24547	0.53892	0.10524
513	0.50000	1.55000	1.06067	0.05292	0.62265	0.03611
514	0.50000	1.70000	0.95560	0.07342	0.62980	0.05048
515	0.50000	1.80000	0.98689	0.06788	0.56663	0.04452

TABLE III.- Continued.

Pt	$\frac{x}{b/2}$	$\frac{y}{b/2}$	$\frac{u}{V}$	$\frac{u'}{V}$	$\frac{v}{V}$	$\frac{v'}{V}$
516	0.50000	2.00000	0.99231	0.06889	0.50334	0.04511
517	0.60000	1.80000	0.9[illegible]851	0.08123	0.57950	0.05060
518	0.60000	1.70000	1.02020	0.05083	0.60828	0.05280
519	0.60000	1.60000	1.08903	0.05393	0.59452	0.03564
520	0.60000	1.55000	0.84309	0.18844	0.58611	0.08170
521	0.60000	1.50000	0.47426	0.24934	0.38099	0.10453
522	0.60000	1.45000	0.12187	0.21257	0.14374	0.08874
523	0.60000	1.52500	0.65453	0.23057	0.49410	0.09249
524	0.60000	1.47500	0.32807	0.22700	0.26990	0.07294
525	0.60000	1.40000	-0.05936	0.11734	0.01168	0.05536
526	0.60000	1.30000	-0.14148	0.10089	-0.01037	0.04589
527	0.60000	1.20000	-0.12986	0.08492	0.01466	0.06818
528	0.60000	1.10000	-0.11091	0.08921	-0.02044	0.07551
529	0.90000	1.10000	-0.16031	0.09672	-0.01520	0.06967
530	0.90000	1.20000	-0.14696	0.10703	0.00054	0.05238
531	0.90000	1.30000	-0.16365	0.09928	0.01150	0.05703
532	0.90000	1.40000	-0.16901	0.09547	0.00781	0.05191
533	0.90000	1.50000	-0.08540	0.13105	0.02205	0.07163
534	0.90000	1.60000	0.27843	0.26031	0.18099	0.08737
535	0.90000	1.50000	-0.07175	0.14017	0.02223	0.06985
536	0.90000	1.55000	0.03826	0.18600	0.07408	0.07723
537	0.90000	1.65000	0.60346	0.26335	0.34410	0.10215
538	0.90000	1.62500	0.45113	0.26853	0.27199	0.09601
539	0.90000	1.67500	0.72163	0.24821	0.44398	0.08897
540	0.90000	1.70000	0.90060	0.23021	0.50393	0.09285
541	0.90000	1.80000	1.13218	0.04875	0.54464	0.03737
542	0.90000	1.90000	1.10840	0.04791	0.55268	0.04273
543	0.90000	2.00000	1.08093	0.06824	0.53957	0.05054
544	1.00000	2.00000	1.11466	0.05298	0.52819	0.04636
545	1.00000	1.90000	1.140[illegible]	0.04958	0.52938	0.04541
546	1.00000	1.80000	1.15876	0.07229	0.54833	0.06001
547	1.00000	1.70000	0.64207	0.30036	0.36996	0.07574
548	1.00000	1.60000	0.10530	0.21621	0.10942	0.06871
549	1.00000	1.75000	0.90173	0.22539	0.44779	0.07247
550	1.00000	1.65000	0.35840	0.27092	0.21466	0.08141
551	1.00000	1.50000	-0.13862	0.11395	0.02586	0.06913
552	1.00000	1.40000	-0.15608	0.09952	0.00441	0.06359
553*	1.00000	1.30000	-0.17139	0.10441	-0.00733	0.05238
554	1.00000	1.20000	-0.16347	0.10942	0.02962	0.08254
555	1.00000	1.10000	-0.13838	0.11251	0.01561	0.06317
556	1.10000	1.10000	-0.16591	0.12294	0.00632	0.07539
557	1.10000	1.20000	-0.15590	0.13159	-0.00656	0.08719
558	1.10000	1.30000	-0.16770	0.11895	0.01412	0.07229
559	1.10000	1.40000	-0.16377	0.11180	0.02312	0.06764
560	1.10000	1.50000	-0.15894	0.11359	0.01681	0.05882
561	1.10000	1.60000	-0.02777	0.15375	0.03880	0.09064

TABLE III.- Concluded.

Pt	$\frac{x}{b/2}$	$\frac{u}{b/2}$	$\frac{u}{V}$	$\frac{u'}{V}$	$\frac{v}{V}$	$\frac{v'}{V}$
562	1.10000	1.70000	0.34297	0.26853	0.19172	0.08969
563	1.10000	1.65000	0.12473	0.24207	0.08576	0.08796
564	1.10000	1.75000	0.60197	0.27521	0.34994	0.08576
565	1.10000	1.80000	0.94416	0.26818	0.46400	0.07223
566	1.10000	1.85000	1.16210	0.10465	0.52938	0.05471
567	1.10000	1.90000	1.17741	0.05375	0.50846	0.04565
568	1.10000	2.00000	1.16323	0.04660	0.51925	0.04976
569	1.10000	2.10000	1.13498	0.05590	0.52986	0.04166
570	1.10000	2.20000	1.13796	0.04899	0.48653	0.04762
571	0.30000	1.04300	-0.05763	0.06728	0.02068	0.05471
572	0.50000	1.15700	-0.11079	0.08665	-0.01156	0.05417
573	0.80000	0.98200	-0.12670	0.11901	-0.04750	0.06246
574	0.70000	0.87000	-0.09476	0.11329	-0.00167	0.09333
575	0.60000	0.75600	-0.02998	0.08784	-0.00799	0.09184
576*	1.20000	1.13600	-0.16740	0.11502	0.04708	0.07342
577	1.15000	0.99300	-0.15173	0.11663	-0.00703	0.07330
578	1.10000	0.85000	-0.11955	0.12521	0.01162	0.09422
579	1.05000	0.70700	-0.08206	0.11955	-0.02247	0.07628
580	1.01000	0.61800	-0.04881	0.10667	-0.02092	0.07580
581	1.00000	0.56500	-0.01645	0.12098	-0.05131	0.10638
582	0.98000	0.50000	0.02878	0.10173	-0.01818	0.05787
583	1.20000	0.50000	0.00471	0.12139	-0.08838	0.05310
584	1.40000	0.50000	-0.03647	0.11758	0.03850	0.08868
585	1.60000	0.50000	-0.06645	0.13880	0.03605	0.05167
586	1.80000	0.50000	-0.06275	0.13820	0.01907	0.08826
587*	2.00000	0.50000	-0.09720	0.12628	0.02068	0.03713
588*	2.00000	0.80000	-0.18814	0.12700	0.05656	0.05435
589	2.00000	1.10000	-0.20703	0.10679	0.07086	0.05012
590	1.80000	1.10000	-0.19362	0.13981	0.01871	0.04184
591	1.80000	0.80000	-0.16901	0.13558	0.02884	0.06180
592	1.60000	0.80000	-0.17116	0.11669	0.06532	0.10936
593	1.60000	1.10000	-0.18707	0.15197	0.03331	0.08212
594	1.40000	1.10000	-0.15793	0.13075	0.03820	0.06055
595	1.40000	0.80000	-0.15185	0.12765	0.03355	0.09368
596	0.80000	0.70000	-0.05012	0.10083	-0.02908	0.06132
597	0.95000	0.90000	-0.10101	0.11204	-0.04136	0.08862
598	0.40000	0.80000	-0.10602	0.08582	-0.03111	0.07604
599	0.40000	0.80000	-0.02098	0.07306	-0.03641	0.10447
600	-0.50000	1.00000	0.45483	0.05143	0.08570	0.24839
601	-0.50000	1.20000	0.52402	0.03123	0.32437	0.05727
602	-0.50000	1.40000	0.60423	0.03153	0.37944	0.08147
603	-0.50000	1.60000	0.67723	0.03337	0.35650	0.04899
604	-0.50000	2.00000	0.78886	0.03528	0.36144	0.06406
605	-0.10000	2.00000	0.84595	0.04231	0.37128	0.14315
606	-0.10000	1.80000	0.78415	0.04052	0.48319	0.05602
607	-0.10000	1.60000	0.70584	0.04219	0.38486	0.13147
608	-0.10000	1.40000	0.58516	0.04541	0.12128	0.25495

TABLE IV.- VELOCITY DATA FOR ROUND EDGE MODEL
M = .25, Re = .25 × 10^6

(*indicates points dropped from analysis)

Pt	$\frac{x}{b/2}$	$\frac{y}{b/2}$	$\frac{u}{\bar{V}}$	$\frac{u'}{\bar{V}}$	$\frac{v}{\bar{V}}$	$\frac{v'}{\bar{V}}$
609*	-0.20000	1.50000	0.79641	0.14136	0.54216	0.08172
610	-0.20000	2.00000	0.90470	0.09223	0.41344	0.14820
611	-0.20000	1.80000	0.88002	0.08963	0.45879	0.07121
612	-0.20000	1.70000	0.89655	0.08160	0.48370	0.08101
613	-0.20000	1.60000	0.83656	0.10109	0.51464	0.06967
614	-0.20000	1.40000	0.77161	0.10900	0.58526	0.07900
615	-0.20000	1.30000	0.70666	0.17100	0.62459	0.08314
616	-0.20000	1.20000	0.63699	0.12600	0.67336	0.07074
617*	-0.10000	1.20000	0.66675	0.18812	0.75508	0.06601
618	-0.10000	1.25000	0.71977	0.10097	0.72024	0.06743
619	-0.10000	1.30000	0.76299	0.08184	0.65753	0.07003
620*	-0.10000	1.30000	0.76075	0.08148	0.66308	0.06826
621	-0.10000	1.40000	0.80231	0.07652	0.61313	0.06590
622	-0.10000	1.50000	0.83396	0.07251	0.55716	0.08207
623	-0.10000	1.60000	0.85569	0.06743	0.52728	0.06944
624	-0.10000	1.70000	0.87541	0.06247	0.49114	0.06294
625	-0.10000	1.80000	0.89254	0.06519	0.46800	0.05940
626	-0.10000	2.00000	0.91863	0.06294	0.40966	0.12577
627	0.0	2.00000	0.94284	0.10687	0.42773	0.06306
628	0.0	1.80000	0.92194	0.07806	0.48512	0.06448
629	0.0	1.70000	0.90931	0.06637	0.51323	0.06365
630	0.0	1.60000	0.89549	0.06814	0.55113	0.05964
631	0.0	1.50000	0.87624	0.07204	0.58243	0.05952
632	0.0	1.40000	0.85439	0.07676	0.63840	0.06637
633	0.0	1.30000	0.78602	0.10735	0.72237	0.06448
634	0.0	1.25000	0.76405	0.11254	0.77893	0.07546
635	0.0	1.20000	0.81613	0.07333	0.81944	0.07570
636	0.0	1.15000	0.86738	0.06554	0.83184	0.06424
637	0.10000	1.15000	0.07192	0.16970	0.15942	0.10723
638	0.10000	1.20000	0.74244	0.24740	0.60227	0.10191
639	0.10000	1.30000	0.90364	0.06802	0.74693	0.07381
640	0.10000	1.17500	0.38179	0.23016	0.48878	0.11325
641	0.10000	1.40000	0.88309	0.09884	0.67796	0.06542
642	0.10000	1.50000	0.91675	0.10109	0.61290	0.05538
643	0.10000	1.60000	0.93481	0.07180	0.56519	0.06802
644	0.10000	1.70000	0.94580	0.06684	0.52811	0.06743
645	0.10000	1.80000	0.95914	0.08066	0.50390	0.07310
646	0.20000	1.80000	0.98299	0.08928	0.50709	0.06353
647	0.20000	1.70000	0.98170	0.09188	0.53826	0.06719
648	0.20000	1.60000	0.97520	0.10711	0.57806	0.06117
649	0.20000	1.50000	0.95607	0.08030	0.61762	0.06412

TABLE IV.- Continued.

Pt	$\frac{x}{b/2}$	$\frac{y}{b/2}$	$\frac{u}{V}$	$\frac{u'}{V}$	$\frac{v}{V}$	$\frac{v'}{V}$
650	0.20000	1.40000	0.95477	0.07841	0.69249	0.07333
651	0.20000	1.30000	1.01630	0.10274	0.65612	0.08278
652	0.20000	1.20000	0.02197	0.15624	0.11195	0.07381
653	0.20000	1.25000	0.47095	0.24740	0.75472	0.12470
654*	0.20000	1.25000	0.40624	0.23902	0.37600	0.16308
655	0.20000	1.27500	0.79334	0.24055	0.53779	0.31660
656	0.20000	1.10000	-0.08892	0.08668	0.03236	0.07558
657	0.10000	1.05000	-0.09967	0.07558	0.00803	0.07286
658	0.10000	1.10000	-0.10900	0.07853	0.02846	0.07983
659	0.0	1.10000	0.14561	0.22662	0.00945	0.55550
660	-0.05000	1.10000	0.79570	0.07865	0.01878	0.37931
661	-0.10000	1.10000	0.60286	0.13923	0.23040	0.52610
662	-0.15000	1.10000	0.54263	0.13510	0.24067	0.55621
663	-0.20000	1.10000	0.52586	0.09436	0.00756	0.27114
664	-0.20000	1.15000	0.57050	0.09684	0.34223	0.57204
665	-0.15000	1.15000	0.59258	0.11266	0.54263	0.59447
666	-0.10000	1.15000	0.65092	0.11868	0.28590	0.50661
667	-0.05000	1.15000	0.72166	0.11384	0.30231	0.65683
668*	0.0	1.15000	0.86644	0.07794	0.81767	0.10038
669	0.18000	0.97000	-0.05834	0.07711	0.05102	0.16958
670	0.25000	1.01500	-0.07747	0.08503	-0.00650	0.07688
671	0.30000	1.04300	-0.09223	0.08975	0.00791	0.06920
672	0.30000	1.10000	-0.11101	0.10487	0.03000	0.08680
673	0.30000	1.20000	-0.11101	0.08396	0.00579	0.06873
674	0.30000	1.30000	0.38026	0.24705	0.30940	0.10250
675	0.30000	1.40000	1.04889	0.07156	0.65600	0.07239
676	0.30000	1.35000	1.05031	0.12411	0.61632	0.08739
677	0.30000	1.32500	0.79299	0.26464	0.55125	0.11160
678	0.30000	1.25000	0.01122	0.16533	0.08668	0.10050
679	0.30000	1.27500	0.12530	0.18682	0.15139	0.10345
680	0.30000	1.31000	0.46032	0.25697	0.38321	0.22048
681	0.30000	1.50000	1.00331	0.08373	0.63769	0.07133
682	0.30000	1.60000	1.01370	0.11278	0.58007	0.06861
683	0.30000	1.70000	1.01913	0.08314	0.57062	0.07097
684	0.30000	1.80000	1.02409	0.11762	0.51760	0.08231
685	0.30000	2.00000	1.01889	0.12104	0.44202	0.08928
686	0.40000	2.00000	1.04889	0.10569	0.44934	0.14301
687	0.40000	1.80000	1.04051	0.09046	0.52220	0.07121
688	0.40000	1.70000	1.03791	0.15316	0.54440	0.06991
689*	0.40000	1.70000	1.04405	0.09967	0.54535	0.06696
690*	0.40000	1.60000	1.00685	0.09152	0.55090	0.09660
691*	0.40000	1.70000	1.04936	0.07806	0.51075	0.10061
692	0.40000	1.60000	1.05042	0.08928	0.54074	0.12990
693	0.40000	1.50000	1.07003	0.08833	0.57452	0.06601
694	0.40000	1.40000	0.93470	0.26783	0.50945	0.18375

TABLE IV.- Continued.

Pt	$\frac{x}{b/2}$	$\frac{y}{b/2}$	$\frac{u}{V}$	$\frac{u'}{V}$	$\frac{v}{V}$	$\frac{v'}{V}$
695	0.40000	1.35000	0.36774	0.25012	0.26760	0.10522
696	0.40000	1.30000	0.02515	0.16863	0.09223	0.08987
697	0.40000	1.32500	0.14820	0.22603	0.15328	0.09648
698	0.40000	1.37500	0.52374	0.27350	0.37081	0.15517
699	0.40000	1.20000	-0.11349	0.10014	0.01618	0.06755
700	0.40000	1.10000	-0.11845	0.08680	0.01382	0.06838
701	0.40000	1.00000	-0.10853	0.09471	-0.00154	0.08184
702	0.40000	0.90000	-0.07487	0.09211	0.00496	0.07794
703	0.40000	0.80000	-0.04771	0.08857	0.00059	0.07357
704	0.50000	1.00000	-0.07877	0.10239	0.00744	0.07735
705	0.50000	1.10000	-0.11632	0.11195	0.02409	0.07487
706	0.50000	1.20000	-0.12128	0.10711	0.00945	0.07475
707	0.50000	1.30000	-0.07404	0.10900	0.03637	0.08503
708	0.50000	1.40000	0.33940	0.26500	0.25626	0.11431
709	0.50000	1.50000	1.10805	0.11313	0.54901	0.07912
710	0.50000	1.45000	0.90777	0.27055	0.47012	0.09447
711	0.50000	1.42500	0.59849	0.30739	0.38911	0.10274
712	0.50000	1.60000	1.09589	0.06932	0.53082	0.06613
713	0.50000	1.70000	1.07747	0.08042	0.52445	0.06684
714	0.50000	1.80000	1.08302	0.07239	0.48772	0.05574
715	0.50000	2.00000	1.07936	0.06259	0.45146	0.05975
716	0.60000	2.00000	1.09991	0.06778	0.43552	0.05786
717	0.60000	1.80000	1.10723	0.06908	0.49043	0.05940
718	0.60000	1.70000	1.12329	0.07274	0.50201	0.06306
719	0.60000	1.60000	1.13533	0.07239	0.51937	0.06188
720	0.60000	1.50000	0.97095	0.26606	0.45158	0.09943
721	0.60000	1.45000	0.46906	0.30043	0.28885	0.11762
722	0.60000	1.47500	0.70489	0.32676	0.35923	0.11998
723	0.60000	1.42500	0.25413	0.26783	0.19792	0.10923
724	0.60000	1.40000	0.14041	0.23465	0.12766	0.11443
725	0.60000	1.30000	-0.12093	0.11963	0.02870	0.09176
726	0.60000	1.20000	-0.11833	0.10569	0.01145	0.07109
727	0.60000	1.10000	-0.11585	0.10711	0.00803	0.06755
728	0.60000	1.00000	-0.11750	0.11797	0.01488	0.09412
729	0.60000	0.75600	-0.07168	0.11691	-0.00354	0.17974
730	0.70000	0.87000	-0.06708	0.13096	0.01063	0.08514
731	0.80000	0.98200	-0.11502	0.11974	0.01016	0.10168
732	0.80000	0.60000	-0.04263	0.13722	-0.01016	0.10239
733	0.90000	0.86000	-0.10191	0.12825	0.02374	0.08538
734	0.90000	1.00000	-0.13061	0.14147	0.02633	0.09152
735	0.90000	1.10000	-0.15328	0.11514	0.04452	0.08857
736	0.90000	1.20000	-0.14667	0.13262	0.01358	0.07605
737	0.90000	1.30000	-0.16852	0.15340	0.04665	0.09034
738	0.90000	1.40000	-0.11845	0.13805	0.01653	0.10616
739	0.90000	1.50000	0.12305	0.25366	0.10687	0.14313
740	0.90000	1.52500	0.16639	0.25520	0.11242	0.12907

TABLE IV.- Continued.

Pt	$\frac{x}{b/2}$	$\frac{y}{b/2}$	$\frac{u}{V}$	$\frac{u'}{V}$	$\frac{v}{V}$	$\frac{v'}{V}$
741	0.90000	1.55000	0.30940	0.31282	0.19532	0.14277
742	0.90000	1.57500	0.44296	0.30491	0.22095	0.13888
743	0.90000	1.60000	0.63250	0.34247	0.29393	0.09790
744	0.90000	1.65000	1.03649	0.25378	0.37565	0.10321
745	0.90000	1.70000	1.17478	0.13214	0.44367	0.10002
746	1.63000	1.62500	0.90352	0.33951	0.36124	0.11951
747	0.90000	1.80000	1.15376	0.12423	0.43989	0.12104
748	0.90000	1.90000	1.14702	0.18340	0.43363	0.08432
749	0.90000	2.00000	1.14608	0.13840	0.42159	0.06897
750	1.00000	2.00000	1.14891	0.16356	0.38439	0.28047
751	1.00000	1.90000	1.18009	0.08810	0.41875	0.09376
752	1.00000	1.80000	1.16226	0.16096	0.41120	0.06944
753	1.00000	1.70000	1.10416	0.23725	0.40198	0.10250
754	1.00000	1.60000	0.42147	0.33751	0.19910	0.13037
755	1.00000	1.50000	0.05031	0.21847	0.06897	0.11101
756	1.00000	1.65000	0.81885	0.33999	0.29263	0.13273
757	1.00000	1.55000	0.18292	0.26275	0.14608	0.13144
758	1.00000	1.40000	-0.12045	0.14643	0.02740	0.10841
759	1.00000	1.30000	-0.12907	0.13462	0.02657	0.09235
760	1.00000	1.20000	-0.16757	0.10593	0.06046	0.17737
761	1.00000	1.10000	-0.17336	0.12459	0.02681	0.11290
762	1.00000	0.56500	-0.03991	0.29535	0.01417	0.09837
763	1.01000	0.61800	-0.11030	0.13935	-0.01630	0.09672
764	1.05000	0.70700	-0.07440	0.15057	0.00213	0.14159
765	1.10000	0.85000	-0.13167	0.14714	0.02126	0.08077
766	1.15000	0.99300	-0.13262	0.13982	0.01252	0.09943
767	1.20000	1.13600	-0.17796	0.13699	0.02893	0.08739
768	1.20000	1.20000	-0.19568	0.12435	0.04003	0.09530
769	1.20000	1.30000	-0.15163	0.14195	0.05231	0.06554
770	1.20000	1.40000	-0.13085	0.13262	0.03531	0.08385
771	1.20000	1.50000	-0.06436	0.17100	0.04322	0.10156
772*	-0.20000	1.50000	0.82322	0.13651	0.54239	0.07971
773*	-0.20000	1.50000	0.78708	0.13557	0.51641	0.07853
774	-0.20000	1.50000	0.78909	0.13793	0.52940	0.08054
775.	0.10000	1.25000	0.92985	0.13510	0.72485	0.07511
776*	0.10000	1.15000	0.09506	0.20241	0.19025	0.12175
777	0.20000	1.15000	-0.08514	0.14195	0.00933	0.07794
778	0.20000	1.35000	0.94910	0.16521	0.65612	0.07723
779	0.40000	1.45000	1.04960	0.14336	0.57310	0.07829
780	0.40000	1.25000	-0.08066	0.13604	0.01205	0.06448
781	0.60000	1.35000	-0.03673	0.18139	0.04027	0.08739
782	0.60000	1.55000	1.09471	0.14419	0.50520	0.08184
783	0.90000	1.45000	0.03070	0.19627	0.06802	0.11939
784	0.90000	1.75000	1.10664	0.19450	0.43847	0.08290
785	1.00000	1.75000	1.12884	0.15340	0.41580	0.09695
786	1.00000	1.45000	-0.03059	0.19839	0.02563	0.09471
787	1.20000	1.60000	0.27480	0.28496	0.12140	0.13675

TABLE IV.- Continued.

Pt	x/(b/2)	y/(b/2)	u/V	u'/V	v/V	v'/V
788	1.20000	1.70000	0.80515	0.33089	0.26559	0.13344
789	1.20000	1.65000	0.54086	0.34211	0.18387	0.13876
790	1.20000	1.75000	1.05692	0.24563	0.33810	0.11880
791	1.20000	1.80000	1.12671	0.18529	0.37104	0.09105
792	1.20000	1.85000	1.13640	0.21127	0.39159	0.11963
793	1.20000	1.90000	1.14324	0.16474	0.40057	0.08113
794	1.20000	2.00000	1.14242	0.15683	0.39183	0.08278
795	1.10000	2.00000	1.12293	0.19095	0.40187	0.07286
796	1.10000	1.90000	1.15210	0.11490	0.42265	0.07239
797	1.10000	1.80000	1.14702	0.16273	0.42324	0.08243
798	1.10000	1.75000	1.12683	0.17596	0.39738	0.10522
799	1.10000	1.70000	0.99339	0.29086	0.33987	0.26559
800	1.10000	1.65000	0.70099	0.36597	0.27267	0.14419
801	1.10000	1.60000	0.39513	0.30125	0.20324	0.13191
802	1.10000	1.55000	0.16143	0.27350	0.11620	0.13415
803	1.10000	1.50000	-0.01299	0.20583	0.04192	0.10770
804	1.10000	1.40000	-0.13474	0.17135	0.03177	0.09991
805	1.10000	1.30000	-0.16249	0.13120	0.03023	0.08869
806	1.10000	1.20000	-0.17052	0.12589	0.04051	0.09613
807	1.10000	1.10000	-0.16285	0.13108	0.03035	0.08940
808	1.20000	0.50000	-0.08786	0.21221	0.02598	0.09176
809	1.40000	0.50000	-0.08361	0.13829	0.02681	0.09069
810	1.60000	0.50000	-0.11384	0.14336	0.03271	0.08727
811	1.80000	0.50000	-0.13581	0.15246	0.03484	0.07617
812	2.00000	0.50000	-0.13026	0.16745	0.04027	0.07971
813	2.20000	0.50000	-0.16521	0.15706	0.03342	0.09223
814	2.40000	0.50000	-0.18847	0.17419	0.04145	0.07912
815	2.55000	0.50000	-0.21871	0.15163	0.02988	0.09400
816	2.55000	0.40000	-0.16615	0.16899	0.04381	0.07759
817	2.55000	0.60000	-0.18883	0.17442	0.01464	0.09376
818	2.55000	0.70000	-0.16781	0.15990	0.05090	0.07511
819	2.55000	0.80000	-0.21693	0.20820	0.05668	0.09400
820	2.55000	1.00000	-0.17985	0.18080	0.04771	0.10333
821	2.55000	1.20000	-0.19851	0.19273	0.06212	0.10534
822	2.55000	1.40000	-0.17749	0.18009	0.05810	0.11467
823	2.55000	1.60000	-0.10912	0.22426	0.06873	0.14124
824	2.55000	1.80000	0.13805	0.28625	0.10581	0.16651
825	2.55000	1.90000	0.40990	0.35983	0.10227	0.18103
826	2.55000	2.00000	0.65494	0.36372	0.12789	0.16651
827	2.55000	2.10000	0.96871	0.30243	0.16167	0.13321
828	2.55000	2.20000	1.13167	0.22721	0.21044	0.13640
829	2.55000	2.30000	1.19650	0.17560	0.24020	0.11538
830	2.55000	2.40000	1.21020	0.15801	0.27208	0.09046
831	2.00000	2.40000	1.18706	0.11148	0.29948	0.06342
832	2.00000	2.20000	1.20135	0.11986	0.30704	0.09495
833	2.00000	2.00000	1.07298	0.25803	0.25106	0.12081

TABLE IV.- Continued.

Pt	$\frac{x}{b/2}$	$\frac{y}{b/2}$	$\frac{u}{V}$	$\frac{u'}{V}$	$\frac{v}{V}$	$\frac{v'}{V}$
834	2.00000	1.90000	0.75661	0.34306	0.17820	0.13829
835	2.00000	1.80000	0.36538	0.34754	0.11502	0.17289
836	2.00000	1.70000	0.12258	0.29039	0.06944	0.18446
837	2.00000	1.95000	0.88368	0.35026	0.20737	0.13569
838	2.00000	1.85000	0.53094	0.38769	0.14372	0.15293
839	2.00000	1.75000	0.23229	0.31790	0.10298	0.17430
840	2.00000	1.60000	-0.05810	0.20076	0.05078	0.14372
841	2.00000	1.50000	-0.13309	0.18800	0.06070	0.09778
842	2.00000	1.40000	-0.14750	0.24315	0.05857	0.17938
843	2.00000	1.30000	-0.17938	0.21316	0.05043	0.12010
844	2.00000	1.20000	-0.19591	0.20158	0.03602	0.14348
845	2.00000	1.10000	-0.18788	0.18304	0.05739	0.13510
846	2.00000	1.00000	-0.20642	0.18706	0.03519	0.12624
847	2.00000	0.90000	-0.19166	0.25378	0.02220	0.14006
848	2.00000	0.80000	-0.18718	0.19391	0.04936	0.12530
849	2.00000	0.70000	-0.15966	0.20383	0.00791	0.13569
850	2.00000	0.60000	-0.15104	0.21717	0.03779	0.12506
851*	2.00000	0.50000	-0.15128	0.23559	0.02881	0.10699
852	2.40000	0.80000	-0.20796	0.21575	0.03165	0.12872
853	2.40000	1.10000	-0.20725	0.20394	0.08597	0.17064
854	1.80000	1.10000	-0.18529	0.17974	0.04936	0.12258
855	1.80000	0.80000	-0.15635	0.19190	0.05716	0.11183
1001	1.90000	2.40000	1.11656	0.29854	0.28897	0.14206
1002	1.90000	2.20000	1.12872	0.34825	0.29476	0.23051
1003	1.90000	2.00000	1.07806	0.27645	0.27858	0.14620
1004	1.90000	1.90000	0.81330	0.36290	0.19391	0.15257
1005	1.90000	1.80000	0.40919	0.37778	0.14632	0.18044
1006	1.90000	1.85000	0.60794	0.37045	0.14053	0.20513
1007*	1.90000	1.95000	0.86101	0.40919	0.20973	0.14726
1008	1.90000	1.75000	0.26453	0.36112	0.08869	0.21079
1009	1.90000	1.95000	0.98359	0.32652	0.20572	0.16120
1010	1.90000	1.70000	0.12246	0.31212	0.07782	0.21422
1011	1.90000	1.65000	0.04535	0.25555	0.02811	0.18139
1012	1.90000	1.60000	-0.03932	0.26724	0.06330	0.16710
1013	1.90000	1.50000	-0.12978	0.21823	0.04924	0.12093
1014	1.90000	1.40000	-0.13368	0.18269	0.05338	0.11195
1015	1.60000	0.60000	-0.12825	0.26453	0.05302	0.09943
1016	1.60000	0.70000	-0.14950	0.22048	0.04606	0.15092
1017	1.60000	0.80000	-0.11514	0.18387	0.03224	0.17017
1018	1.60000	0.90000	-0.12116	0.17241	0.05102	0.12057
1019	1.60000	1.00000	-0.14206	0.18470	0.02362	0.14112
1020	1.60000	1.10000	-0.17383	0.19957	0.03200	0.13746
1021	1.60000	1.20000	-0.18481	0.20949	0.07097	0.08963
1022	1.60000	1.30000	-0.17702	0.16828	0.03283	0.14714
1023	1.60000	1.40000	-0.14183	0.20406	0.05680	0.22130
1024	1.60000	1.50000	-0.13037	0.23181	0.05125	0.11691

TABLE IV.- Continued.

Pt	$\frac{x}{b/2}$	$\frac{y}{b/2}$	$\frac{u}{\bar{V}}$	$\frac{u'}{\bar{V}}$	$\frac{v}{\bar{V}}$	$\frac{v'}{\bar{V}}$
1025	1.60000	1.60000	0.00142	0.25366	0.03188	0.14868
1026	1.60000	1.70000	0.25213	0.34695	0.10675	0.25709
1027	1.60000	1.80000	0.66875	0.42501	0.19544	0.17962
1028	1.60000	1.90000	1.00579	0.44202	0.30834	0.19662
1029	1.60000	2.00000	1.09589	0.38167	0.30279	0.31590
1030	1.60000	2.10000	1.04724	0.45642	0.29523	0.30338
1031	1.60000	2.20000	1.04735	0.48843	0.33644	0.20442
1032	1.60000	1.85000	0.91993	0.41911	0.17537	0.30668
1033	1.60000	1.75000	0.45087	0.37093	0.13781	0.13439
1034	1.40000	1.10000	-0.20335	0.29547	0.03909	0.22874
1035	1.40000	0.80000	-0.19119	0.31684	0.02385	0.18245
1036	-0.70000	0.0	0.32050	0.12612	0.10038	0.43859
1037	-0.70000	-0.10000	0.26157	0.29358	-0.02067	0.32700
1038	-0.70000	-0.20000	0.28980	0.25342	-0.05775	0.34861
1039	-0.70000	0.10000	0.26075	0.23855	0.06330	0.44580
1040	-0.70000	0.20000	0.24315	0.31412	0.10298	0.40116
1041	-0.70000	0.40000	0.17855	0.42903	0.16852	0.38805
1042	-0.70000	0.60000	0.38699	0.11408	0.16403	0.29700
1043	-0.70000	0.80000	0.41190	0.18375	0.23441	0.31944
1044	-0.70000	0.90000	0.48205	0.11963	0.29110	0.33632
1045	-0.70000	1.00000	0.50638	0.16108	0.33880	0.34341
1046	-0.70000	1.10000	0.56129	0.16120	0.34365	0.27397
1047	-0.70000	1.20000	0.58880	0.23536	0.28696	0.30302
1048	-0.70000	1.40000	0.69119	0.09991	0.36549	0.20111
1049	-0.70000	1.60000	0.69780	0.31318	0.32546	0.27043
1050	-0.60000	1.10000	0.49717	0.25968	0.38462	0.34719
1051	-0.60000	0.94000	0.45276	0.17997	0.34459	0.23713
1052	-0.60000	0.80000	0.29830	0.27468	0.19367	0.32629
1053	-0.60000	0.60000	0.34695	0.10994	0.19898	0.25272
1054	-0.50000	1.10000	0.54251	0.11939	0.42855	0.29924
1055	-0.40000	1.10000	0.50272	0.17277	0.48051	0.24374
1056	-0.30000	1.10000	0.46032	0.14844	0.50118	0.31519
1057*	-0.25000	1.10000	-0.37837	0.64384	0.52563	0.24410
1058	-0.50000	0.94000	0.37707	0.32664	0.44296	0.07924
1059	-0.40000	0.94000	-0.12541	0.64395	0.52858	0.08467
1060*	-0.20000	1.50000	0.78519	0.12140	0.53224	0.06011
1061	-0.25000	1.10000	0.51547	0.06826	0.35935	0.45784
1062*	-0.25000	1.10000	0.51464	0.07050	0.33137	0.49669
1063*	-0.50000	1.10000	0.34034	0.05857	0.40706	0.24622
1064	-0.50000	0.60000	0.25272	0.05668	0.32641	0.11703
1065	-0.40000	0.60000	-0.50815	0.58066	0.34707	0.20501
1066	-0.40000	0.80000	-0.45194	0.50295	0.46682	0.20123
1067*	-0.10000	1.10000	0.68517	0.08160	0.37671	0.5[illegible]05
1068	-0.10000	1.12500	0.66202	0.10321	0.57546	0.43540
1069*	-0.10000	1.15000	0.67962	0.10628	0.77244	0.06849
1070	-0.10000	1.17500	0.68163	0.11490	0.76724	0.06956

TABLE IV.- Concluded.

Pt	$\frac{x}{b/2}$	$\frac{y}{b/2}$	$\frac{u}{V}$	$\frac{u'}{V}$	$\frac{v}{V}$	$\frac{v'}{V}$
1071	-0.10000	1.20000	0.70205	0.08219	0.73252	0.06838
1072*	-0.30000	1.10000	0.47426	0.27586	0.62459	0.07581
1073	-0.30000	0.94000	-0.24598	0.29157	0.63155	0.09471
1074	-0.35000	0.94000	-1.17123	0.62931	0.60522	0.08196
1075	-0.35000	0.80000	-1.07015	0.73323	0.55066	0.08951
1076	-0.30000	0.80000	-0.94131	0.79180	0.60380	0.07263
1077	-0.28000	0.80000	-1.07286	0.78543	0.65411	0.05220
1078	-0.25000	0.94000	-1.02409	0.80905	0.29169	0.42052
1079	-0.10000	1.07500	0.62518	0.35522	0.02338	0.42241
1080	-0.10000	1.05000	0.70631	0.15435	0.21351	0.62907
1081	-0.10000	1.02500	0.75685	0.07097	0.11538	0.60002
1082	0.0	1.02500	-0.11065	0.11538	0.03212	0.09058
1083	0.10000	1.02500	-0.08644	0.09849	0.02362	0.17419
1084	0.10000	1.00000	-0.07877	0.08514	0.02208	0.18080
1085	0.10000	0.97500	-0.06129	0.11042	0.01216	0.09872
1086	0.10000	0.95000	-0.07475	0.11207	0.02681	0.15978
1087	0.15000	0.95000	-0.06885	0.12683	0.01240	0.09719
1088	0.20000	0.95000	-0.08231	0.12140	0.04818	0.15340
1089	0.20000	0.90000	-0.05255	0.10829	0.01287	0.10605
1090	0.20000	0.85000	-0.04251	0.15057	0.00047	0.10782
1091	0.20000	0.80000	-0.01641	0.08455	-0.00508	0.11148
1092	0.25000	0.80000	-0.02622	0.07688	-0.00071	0.11538
1093	0.30000	0.80000	-0.05220	0.08467	0.01807	0.10652

TABLE V.- VELOCITY DATA FOR ROUND EDGE MODEL
$M = 0.5$, $Re = .15 \cdot 10^6$

(*indicates points dropped from analysis)

Pt	$\frac{x}{b/2}$	$\frac{y}{b/2}$	$\frac{u}{V}$	$\frac{u'}{V}$	$\frac{v}{V}$	$\frac{v'}{V}$
1094	-0.20000	1.50000	0.78678	0.06268	0.49396	0.05096
1095	-0.20000	1.40000	0.74827	0.06764	0.53451	0.05048
1096	-0.20000	1.30000	0.69492	0.07428	0.57476	0.05574
1097	0.60000	1.00000	-0.11956	0.10305	0.00060	0.06094
1098	0.60000	1.10000	-0.13313	0.10006	0.00233	0.06023
1099	0.60000	1.20000	-0.13152	0.09085	0.00377	0.05371
1100	0.60000	0.75600	-0.07506	0.09551	-0.01011	0.06914
1101	0.60000	1.30000	-0.08738	0.12033	0.01232	0.05748
1102	0.60000	1.40000	0.30676	0.23331	0.17075	0.08092
1103	0.60000	1.50000	0.99037	0.21884	0.45544	0.06585
1104	0.60000	1.60000	1.11794	0.04109	0.47667	0.04121
1105	0.60000	1.70000	1.10245	0.05102	0.47279	0.04701
1106	0.60000	1.80000	1.07667	0.06639	0.44001	0.04468
1107	0.60000	1.90000	1.08074	0.06358	0.41394	0.04043
1108	0.60000	1.35000	0.02865	0.18636	0.06142	0.09677
1109	0.60000	1.45000	0.58935	0.24982	0.30012	0.08822
1110	0.60000	1.37500	0.15646	0.22069	0.10383	0.07548
1111	0.60000	1.42500	0.42321	0.24593	0.21740	0.10849
1112	0.60000	1.47500	0.72566	0.24719	0.38547	0.08074
1113	0.60000	1.49000	0.83684	0.22249	0.43433	0.07452
1114	-0.20000	1.50000	0.77177	0.05293	0.50694	0.04217
1115	-0.20000	1.40000	0.73074	0.06328	0.55054	0.04743
1116	-0.20000	1.30000	0.66208	0.11376	0.57392	0.05221
1117	-0.20000	1.20000	0.53301	0.09522	0.58699	0.07835
1118*	-0.20000	1.10000	0.43236	0.04635	-0.13959	0.35843
1119	-0.20000	1.05000	-0.05825	0.35341	0.06764	0.25574
1120	-0.20000	1.07500	0.39892	0.05126	0.12536	0.27578
1121	-0.20000	1.06000	0.37787	0.04707	0.15891	0.27022
1122	-0.10000	1.05000	0.58379	0.15825	0.14408	0.22650
1123*	-0.10000	1.10000	0.61178	0.06495	-1.69246	0.44528
1124*	-0.10000	1.15000	0.49073	0.09408	-1.91088	0.42961
1125	-0.10000	1.20000	0.57087	0.06962	0.71645	0.04199
1126	-0.10000	1.30000	0.64234	0.04097	0.60335	0.15090
1127	-0.10000	1.40000	0.72793	0.04785	0.58110	0.04880
1128	-0.10000	1.50000	0.75167	0.03606	0.53517	0.03337
1129	-0.10000	1.60000	0.76687	0.03230	0.50197	0.05987
1130	-0.10000	1.70000	0.80048	0.02949	0.47159	0.03577
1131	-0.10000	1.80000	0.81633	0.02949	0.45012	0.03750
1132	0.0	1.80000	0.83415	0.01980	0.45203	0.04432
1133	0.0	1.70000	4.19438	0.00084	-2.92638	0.07781
1134	0.0	1.70000	0.89868	0.04611	0.48840	0.04850

TABLE V.- Continued.

Pt	$\frac{x}{b/2}$	$\frac{y}{b/2}$	$\frac{u}{V}$	$\frac{u'}{V}$	$\frac{v}{V}$	$\frac{v'}{V}$
1135	0.0	1.60000	0.88170	0.05030	0.52859	0.04850
1136	0.0	1.50000	0.86238	0.05598	0.56782	0.04605
1137	0.0	1.40000	0.83313	0.06256	0.62165	0.06124
1138	0.0	1.30000	0.72291	0.08493	0.69151	0.06633
1139	0.0	1.20000	0.80138	0.05281	0.78852	0.06693
1140	0.0	1.80000	0.91238	0.04163	0.46555	0.04360
1141	0.0	2.00000	0.93385	0.04097	0.41812	0.03947
1142	-0.10000	2.00000	0.90879	0.03756	0.40849	0.04342
1143	-0.10000	1.80000	0.88134	0.04103	0.45496	0.04294
1144	-0.10000	1.60000	0.84450	0.04516	0.50072	0.07913
1145	-0.10000	1.40000	0.77679	0.05449	0.58929	0.05897
1146	-0.10000	1.30000	0.71639	0.06364	0.65263	0.05173
1147	-0.10000	1.20000	0.55341	0.15239	0.62500	0.26878
1148	-0.10000	1.10000	0.56435	0.07751	0.14797	0.21896
1149	-0.20000	1.10000	0.42410	0.04946	0.14151	0.28636
1150	-0.20000	1.20000	0.56489	0.05467	0.64713	0.06669
1151	-0.20000	1.30000	0.66609	0.05036	0.60927	0.04252
1152	-0.20000	1.40000	0.71591	0.05006	0.55389	0.05616
1153	-0.20000	1.50000	0.76519	0.04300	0.52608	0.04055
1154	-0.20000	1.60000	0.79976	0.04749	0.49330	0.04862
1155	-0.20000	1.80000	0.85293	0.03750	0.44222	0.04157
1156	-0.20000	2.00000	0.88415	0.03600	0.40383	0.03349
1157	0.10000	2.00000	0.95772	0.04043	0.43050	0.03517
1158	0.10000	1.80000	0.94300	0.04157	0.47398	0.03553
1159	0.10000	1.60000	0.92195	0.05000	0.54850	0.03816
1160	0.10000	1.50000	0.89791	0.05951	0.59623	0.03977
1161	0.10000	1.40000	0.81394	0.09653	0.65520	0.04557
1162	0.10000	1.30000	0.88146	0.03194	0.73457	0.03882
1163	0.10000	1.20000	0.67476	0.01884	0.53977	0.12536
1164	0.10000	1.10000	-0.10425	0.06047	0.01675	0.06394
1165*	0.10000	1.00000	0.96609	0.88032	0.04007	0.05251
1166	0.10000	1.15000	-0.01657	0.14294	0.09504	0.06077
1167	0.10000	1.17500	0.22201	0.15981	0.23054	0.08266
1168	0.10000	1.25000	0.80072	0.09563	0.65484	0.14839
1169	0.20000	1.25000	0.28810	0.21980	0.34504	0.09545
1170	0.20000	1.30000	0.81549	0.14874	0.61208	0.09450
1171	0.20000	1.40000	0.92566	0.05837	0.65467	0.04516
1172	0.20000	1.35000	0.98122	0.03146	0.65060	0.04324
1173	0.20000	1.27500	0.73164	0.16561	0.55903	0.09426
1174	0.20000	1.50000	0.90604	0.09246	0.60658	0.04862
1175	0.40000	1.50000	1.04127	0.03642	0.56537	0.04019
1176	0.40000	1.40000	0.75084	0.19211	0.52243	0.06980
1177	0.40000	1.30000	0.11094	0.20598	0.11465	0.07333
1178	0.40000	1.35000	0.43164	0.21932	0.28355	0.07877
1179	0.40000	1.45000	1.07488	0.08457	0.56848	0.05096
1180	0.40000	1.25000	-0.10556	0.09384	0.00353	0.06693

TABLE V.- Concluded.

Pt	$\frac{x}{b/2}$	$\frac{y}{b/2}$	$\frac{u}{V}$	$\frac{u'}{V}$	$\frac{v}{V}$	$\frac{v'}{V}$
1181	0.40000	1.20000	-0.10598	0.08666	-0.00233	0.05700
1182	0.40000	1.10000	-0.11663	0.07201	-0.00042	0.05622
1183	-0.70000	1.10000	0.53080	0.03104	0.36806	0.04354
1184	-0.60000	1.10000	0.52010	0.03164	0.40957	0.04342
1185	-0.50000	1.10000	0.50150	0.03696	0.44844	0.08331
1186	-0.40000	1.10000	0.48266	0.04031	0.48134	0.14635
1187	-0.30000	1.10000	0.43529	0.04599	0.37231	0.28600
1188	-0.40000	0.94000	0.36938	0.03062	0.48499	0.09001
1189	-0.50000	0.94000	0.40377	0.03266	0.41770	0.06603
1190	-0.60000	0.94000	0.43834	0.03307	0.37237	0.04372
1191	-0.70000	0.94000	0.46328	0.03020	0.33720	0.04109
1192	-0.70000	0.80000	0.40927	0.03122	0.30801	0.03056
1193	-0.60000	0.80000	0.36998	0.03708	0.35341	0.03248
1194	-0.50000	0.80000	0.32249	0.03272	0.36782	0.08349
1195	-0.40000	0.80000	0.25239	0.03092	0.17410	0.26059
1196	-0.40000	0.60000	0.17261	0.04240	0.15144	0.30090
1197	-0.50000	0.60000	0.24743	0.03834	0.29504	0.04480
1198	-0.60000	0.60000	0.30353	0.03343	0.26238	0.03559
1199	-0.70000	0.60000	0.35562	0.03224	0.22476	0.13977
1200	1.00000	0.60000	-0.09432	0.11693	-0.00472	0.06555
1201	1.00000	0.80000	-0.11316	0.12279	0.02984	0.06292
1202	1.00000	1.00000	-0.13600	0.12099	0.03260	0.06310
1203	1.00000	1.20000	-0.22482	0.10843	0.00108	0.07249
1204	1.00000	1.40000	-0.14856	0.09312	-0.00825	0.06746
1205	1.00000	1.60000	0.49856	0.23170	0.22327	0.09438
1206	1.00000	1.80000	1.16005	0.04821	0.41477	0.04749
1207	1.00000	1.50000	0.08876	0.17051	0.08612	0.07787
1208	1.00000	1.47500	-0.00263	0.19169	0.04677	0.08403
1209	1.00000	1.70000	1.05149	0.20395	0.38774	0.06172
1210	1.00000	1.90000	1.15006	0.04498	0.41286	0.04557
1211	0.60000	1.55000	1.06142	0.10395	0.50197	0.04868

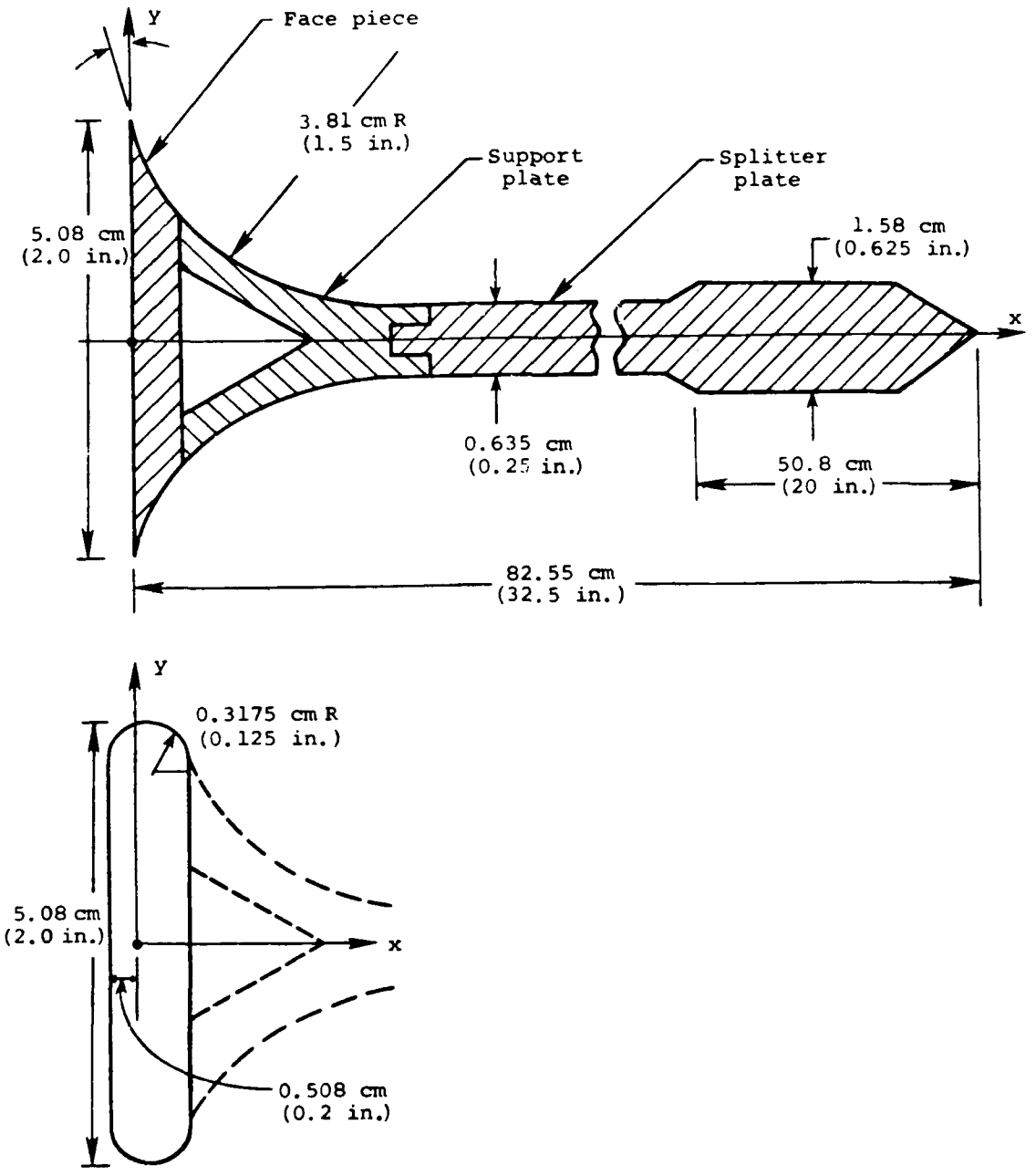

(a) Model configurations.

Figure 1.- Test apparatus.

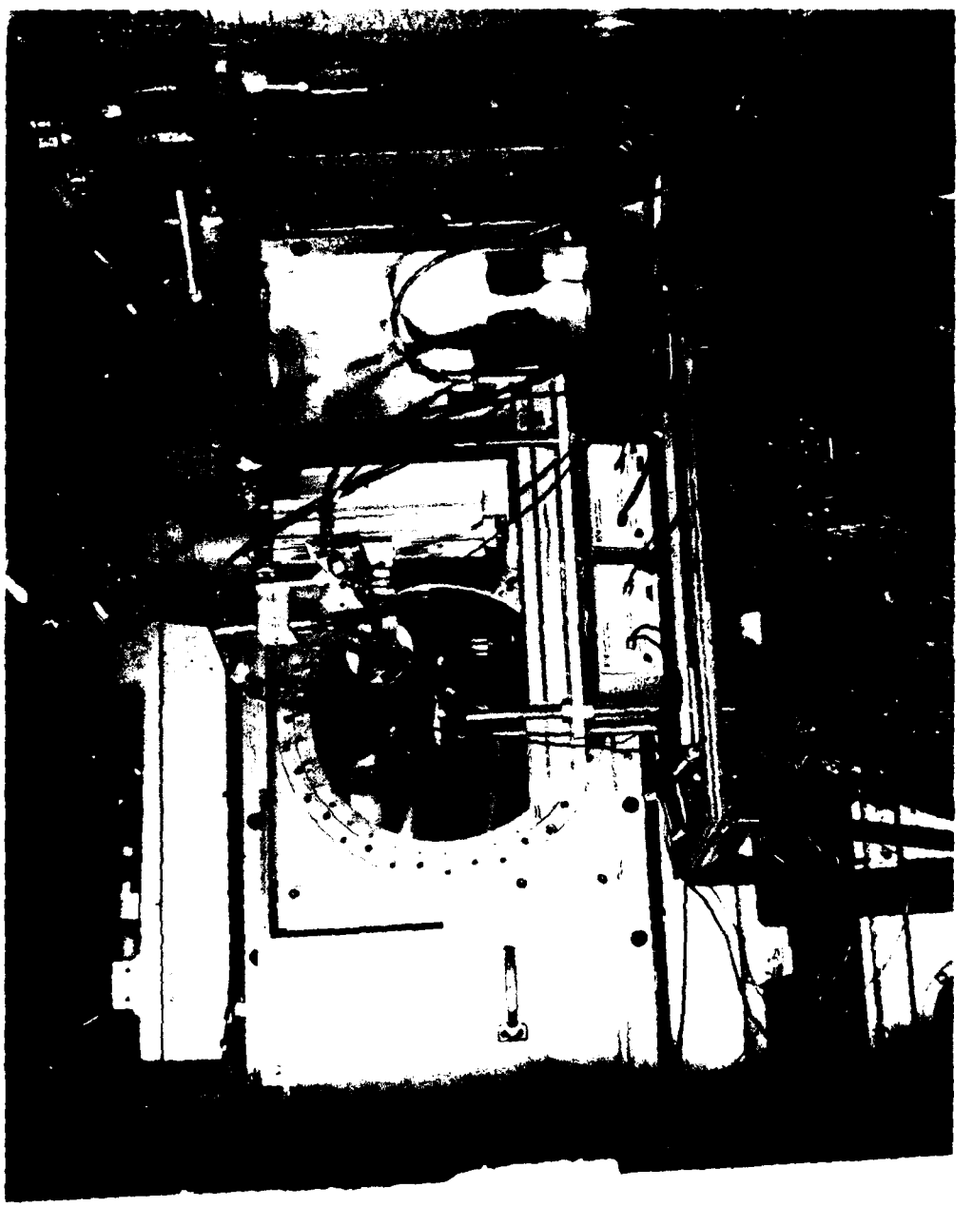

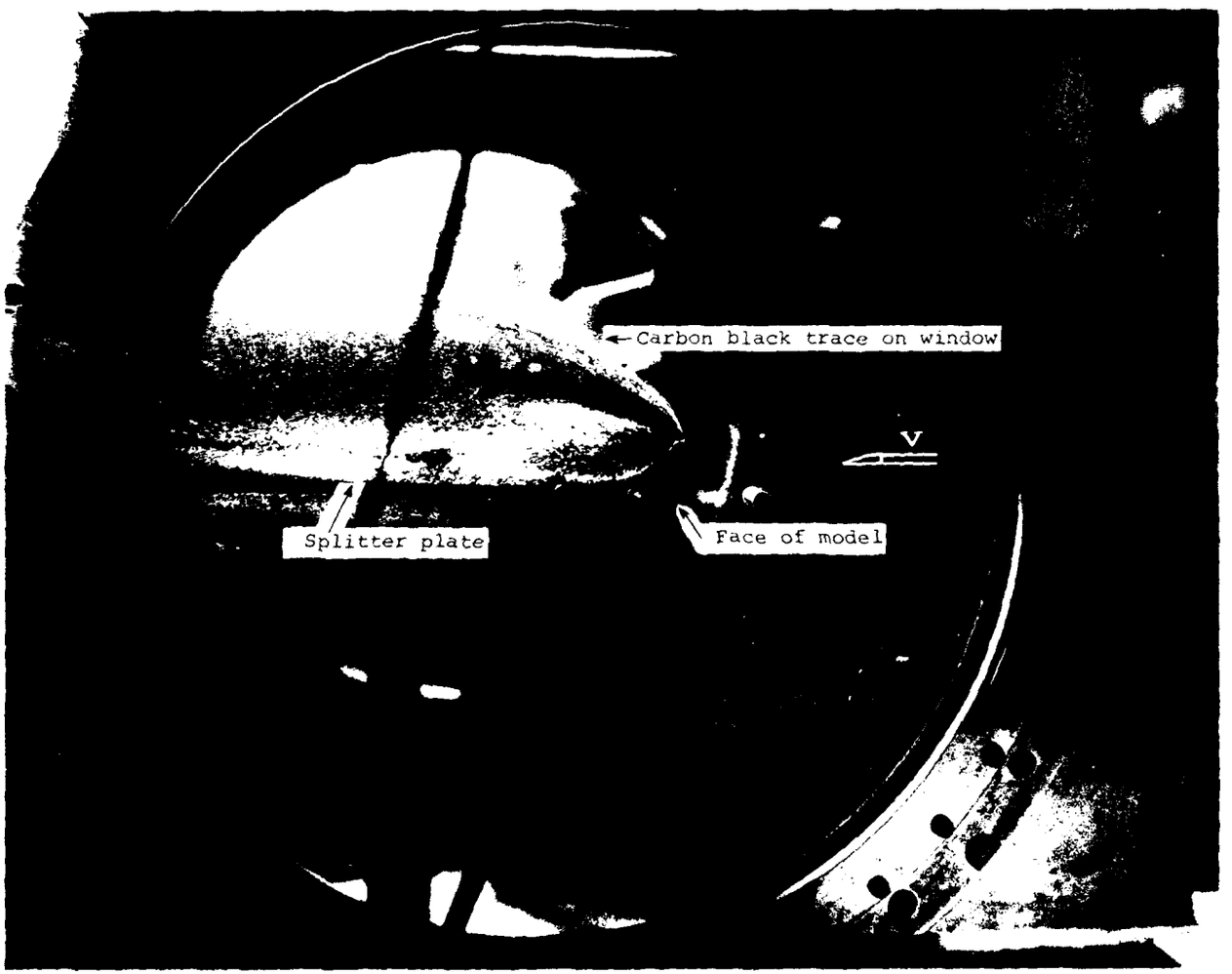

(c) Close view of model and window.

Figure 1.- Concluded.

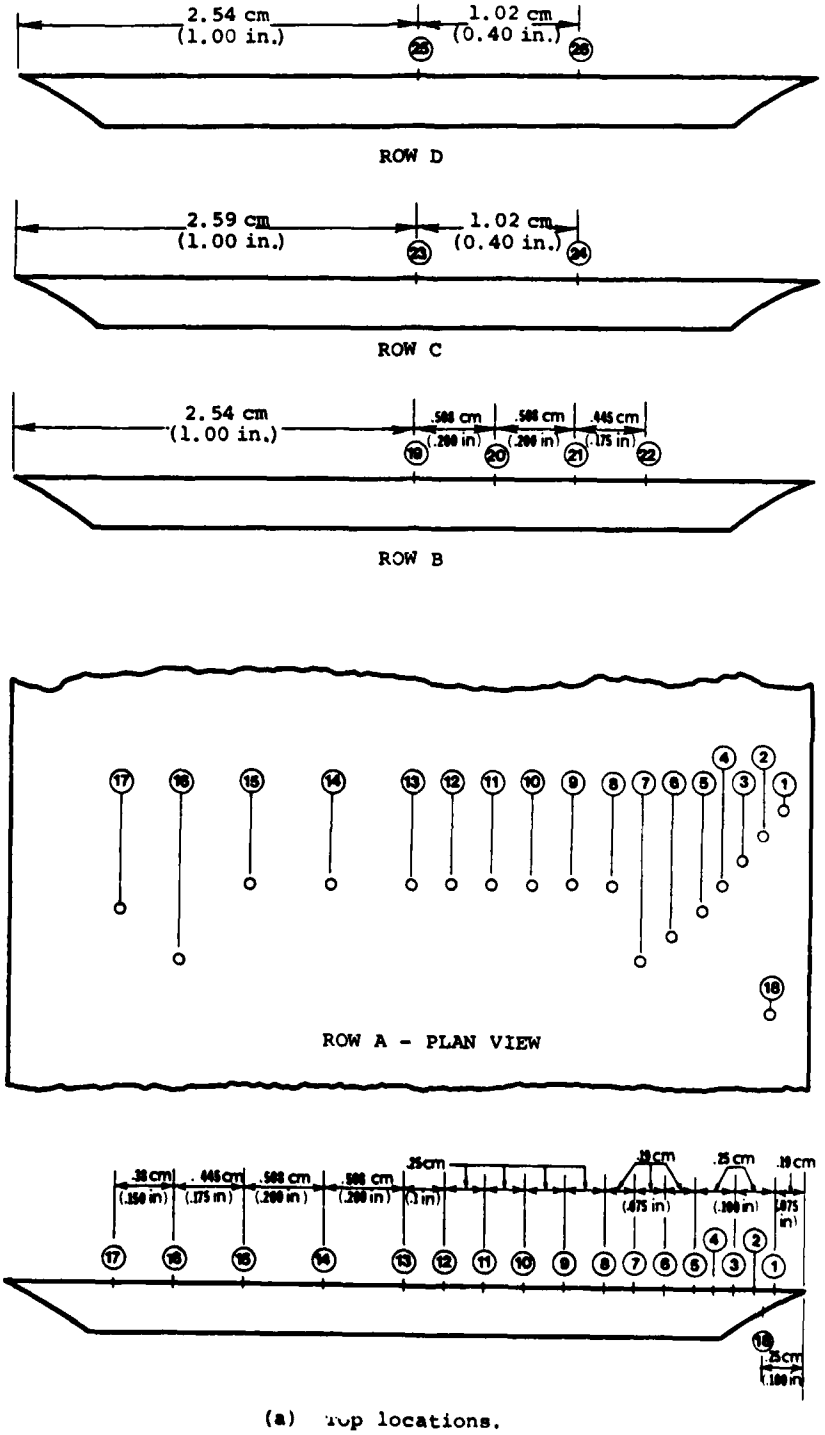

(a) Top locations.

Figure 2.- Pressure tap locations - sharp-edged face.

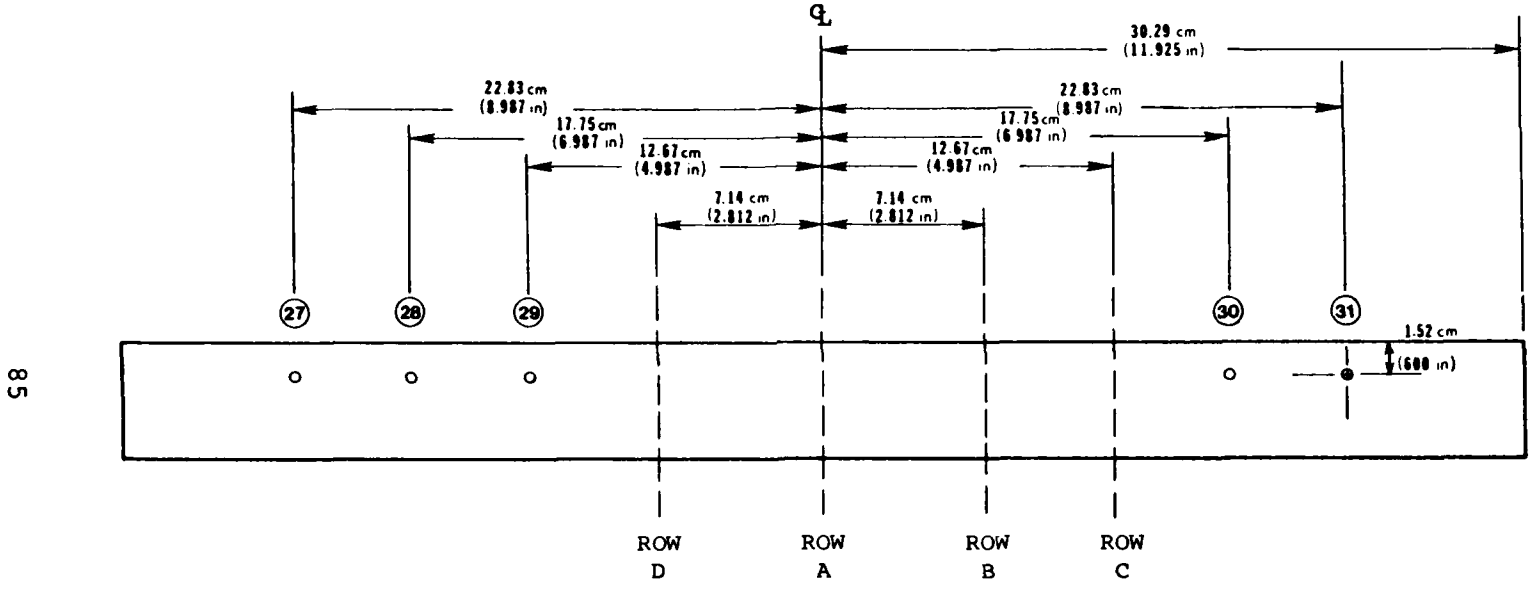

(b) Row locations.

Figure 2.- Concluded.

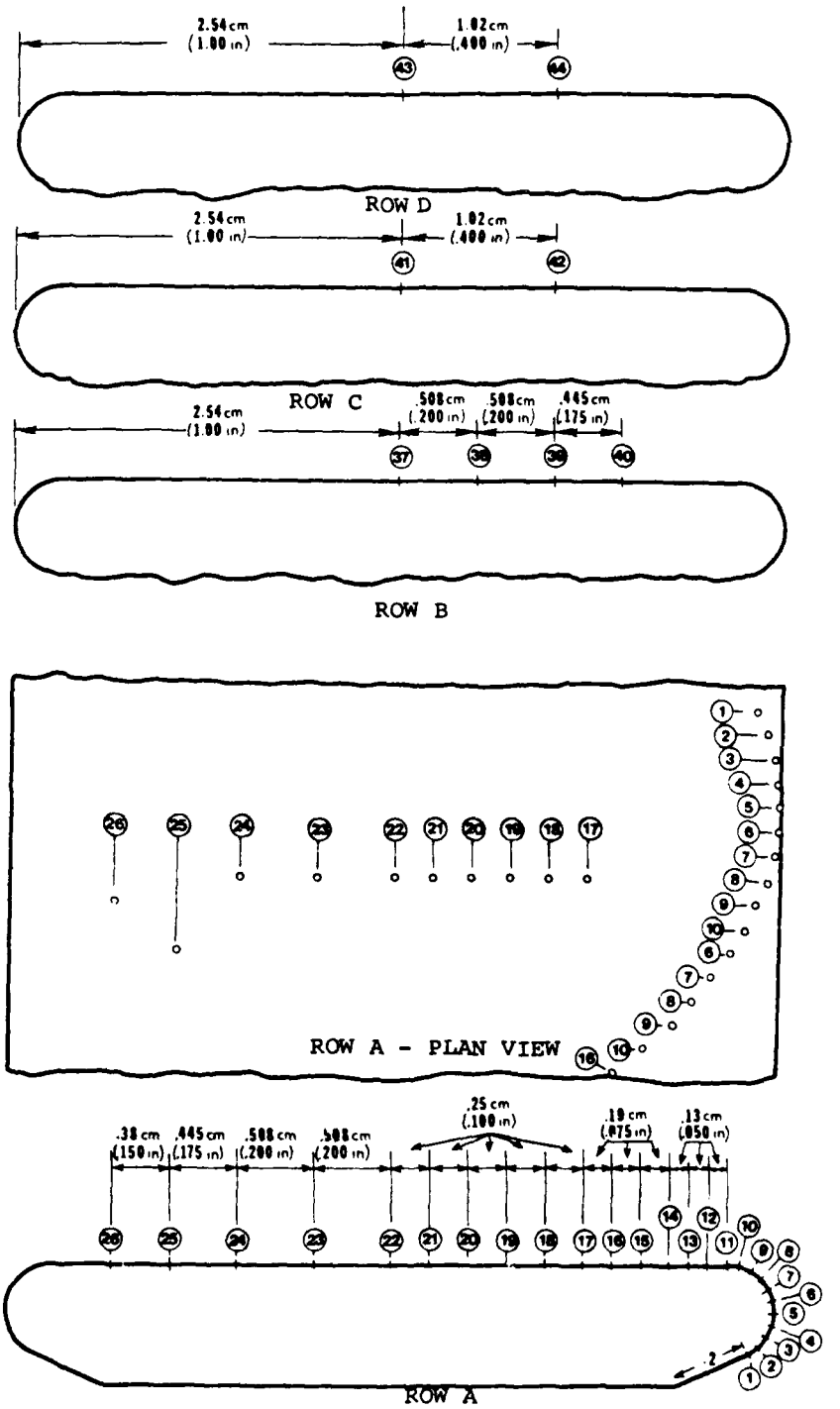

(a) Tap locations

Figure 3.- Pressure tap locations - round-edged plate.

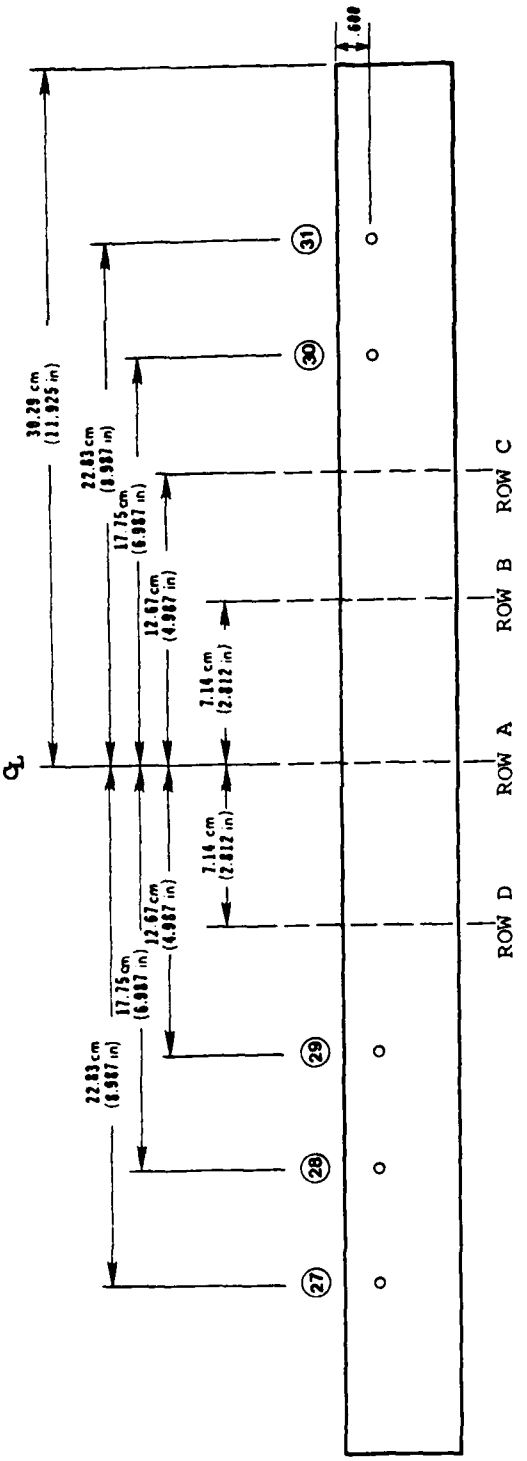

(b) Row locations

Figure 3.- Concluded.

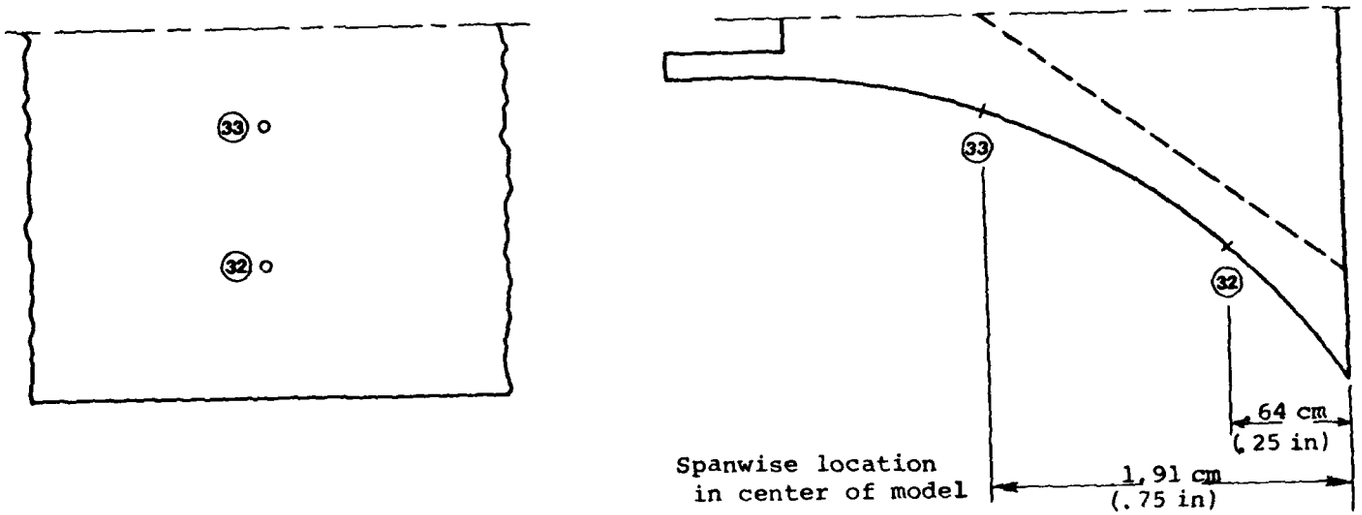

Figure 4.- Pressure tap locations on support plate.

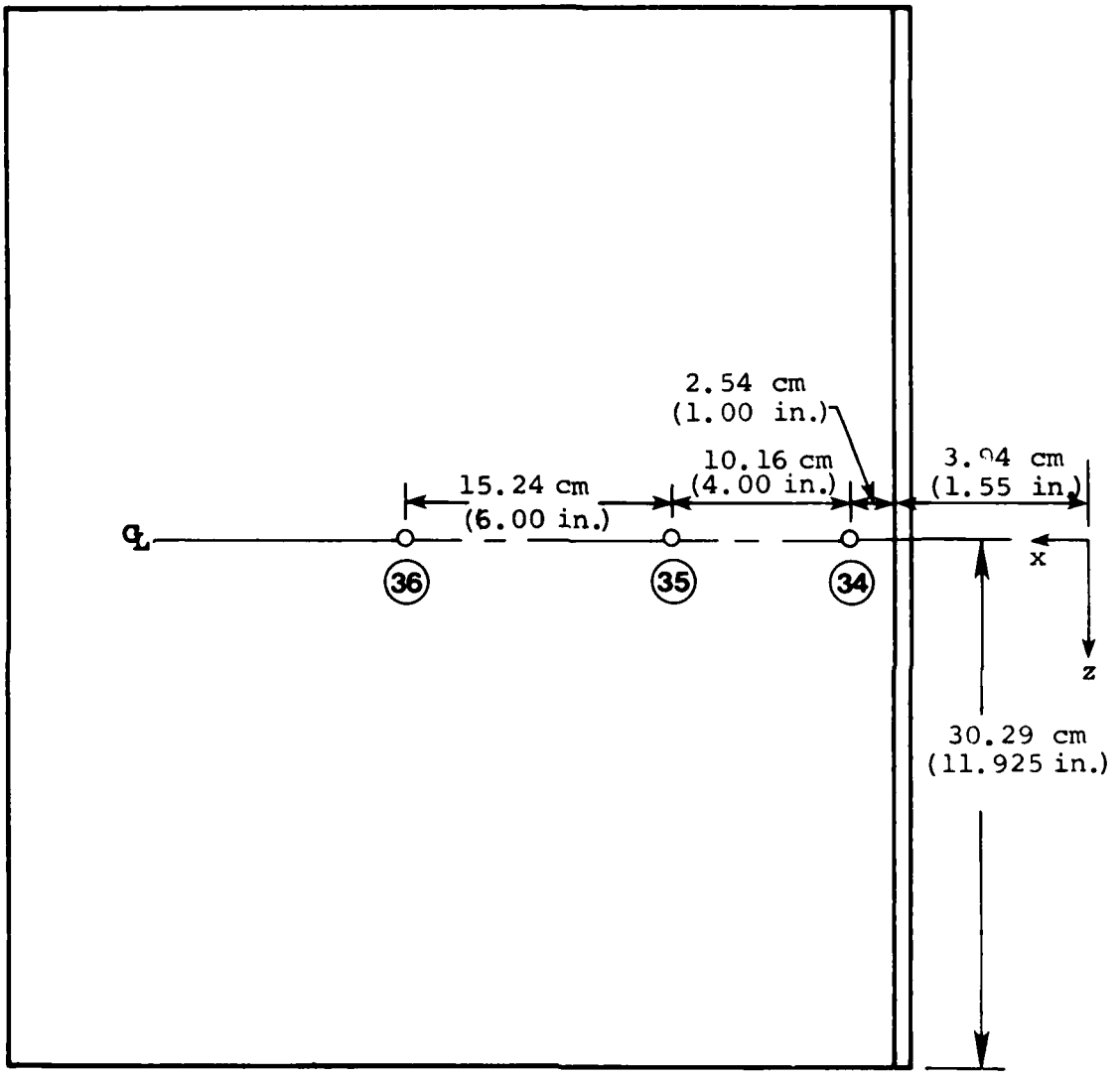

Figure 5.- Pressure tap location on splitter plate.

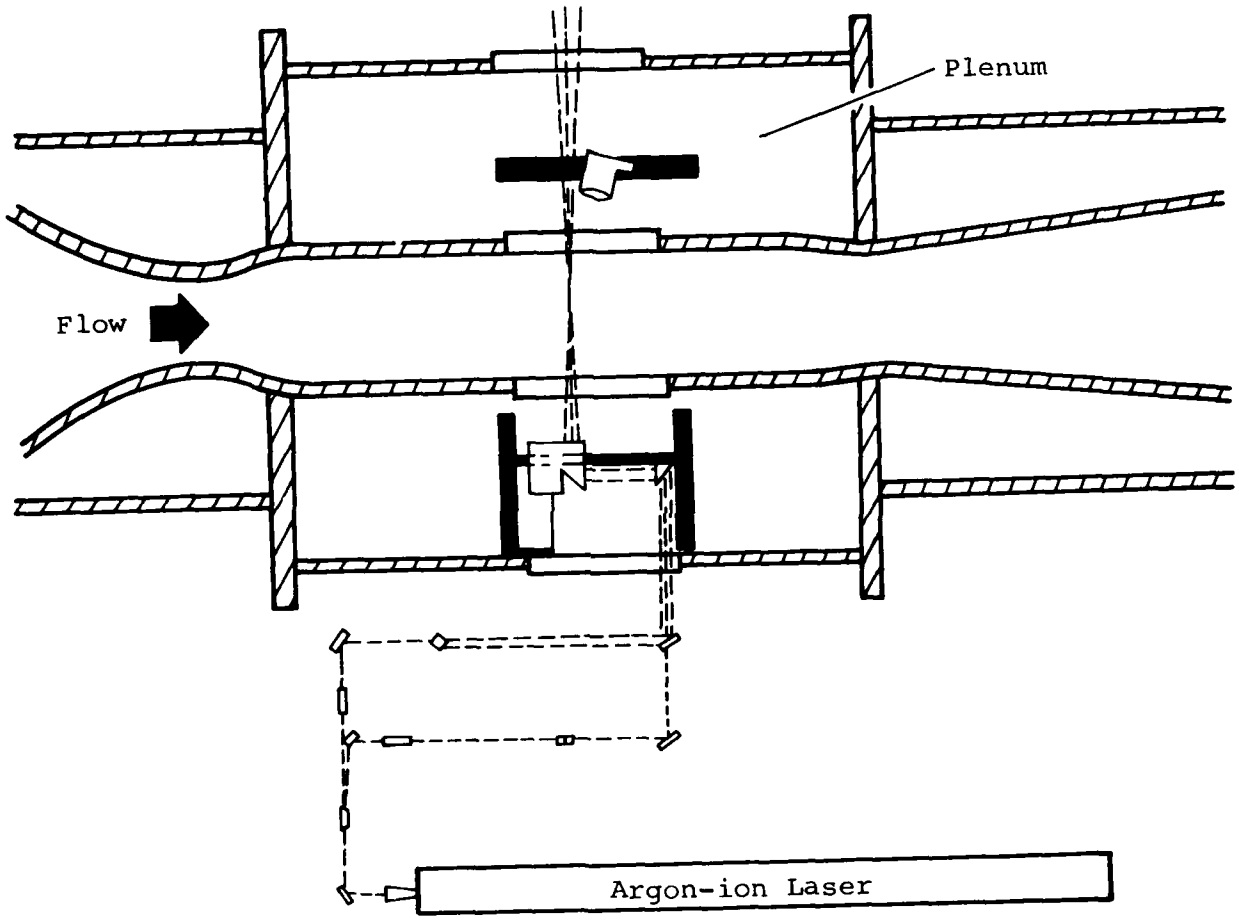

Figure 6.- Laser velocimeter installation
NASA/Ames 2- by 2-foot TWT.

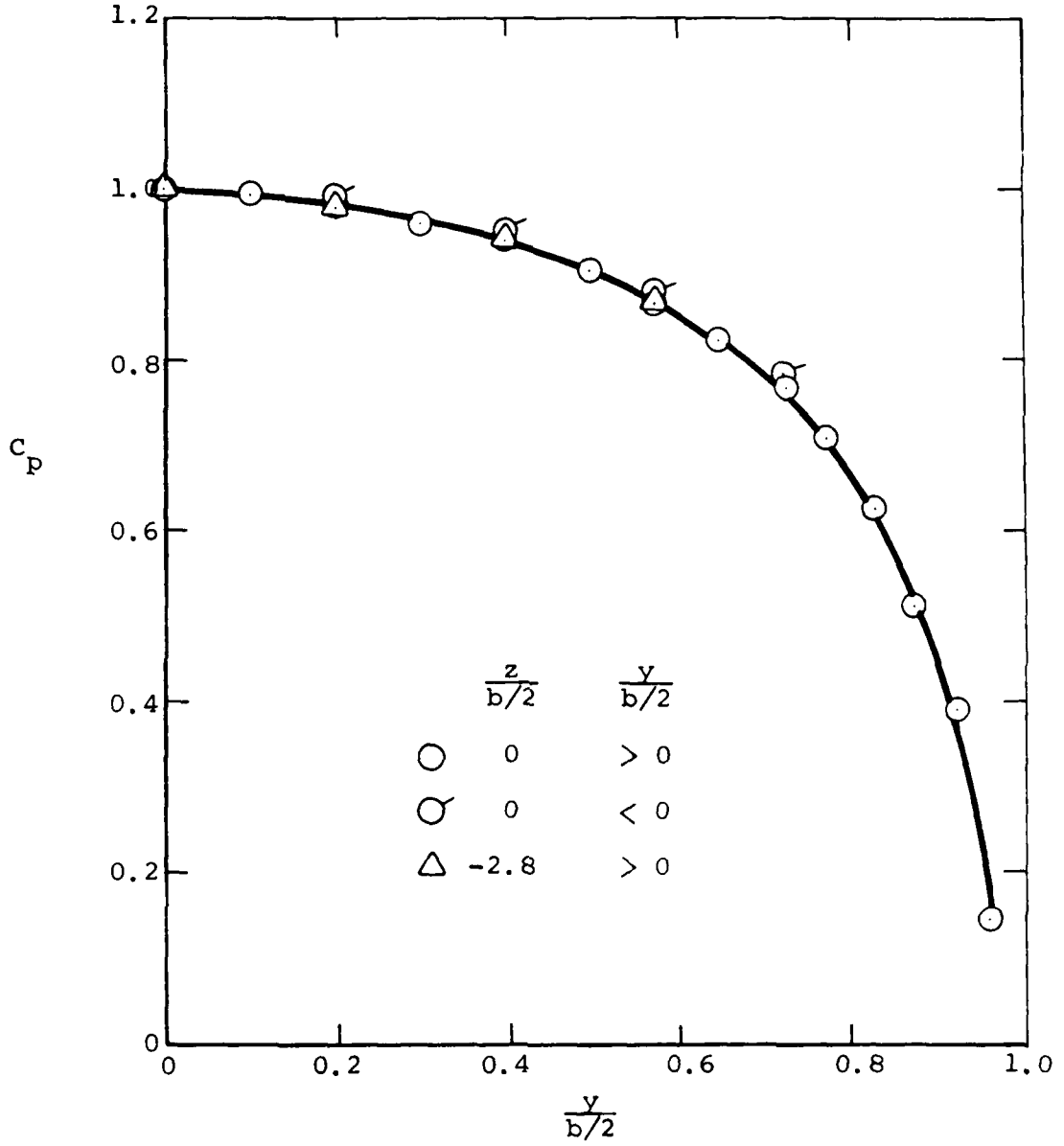

(a) Sharp edge model, M = 0.25, Re = 0.063×10^6

Figure 7.- Variation of static pressure on the model face with distance from centerline.

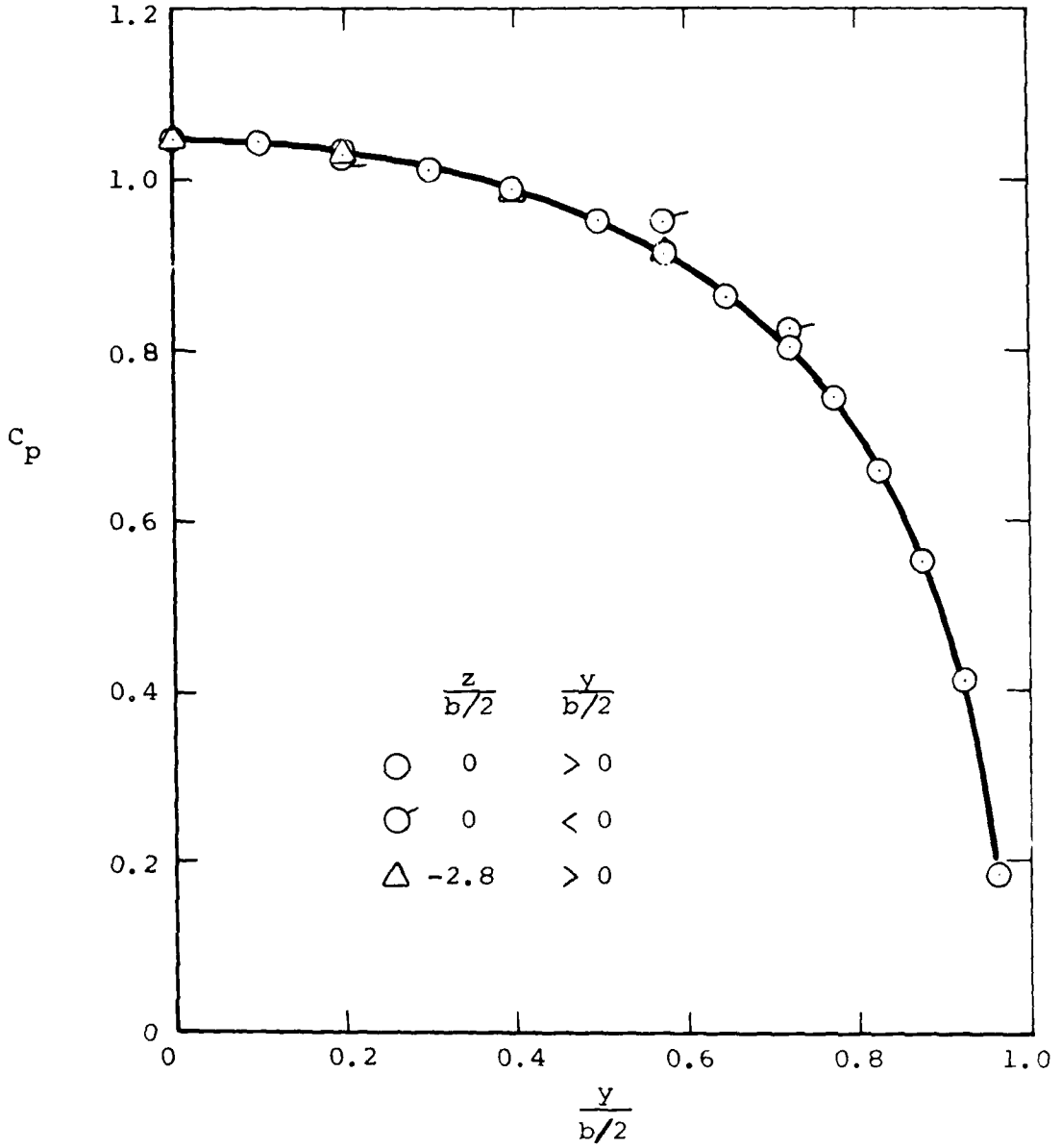

(b) Sharp edge model, M = 0.25, Re = 0.25×10^6

Figure 7.- Continued.

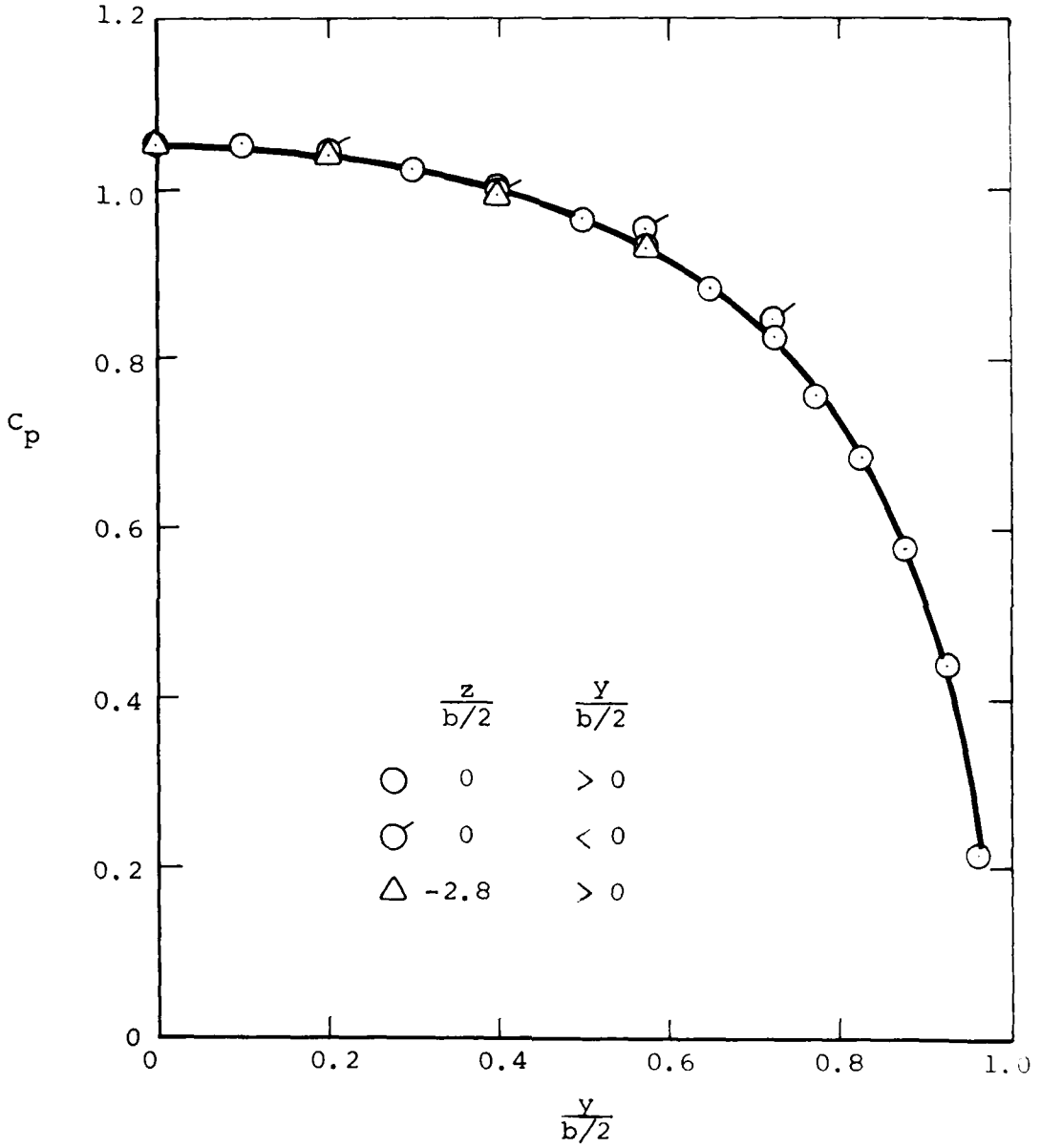

(c) Sharp edge model, M = 0.5, Re = 0.15×10^6

Figure 7.- Continued.

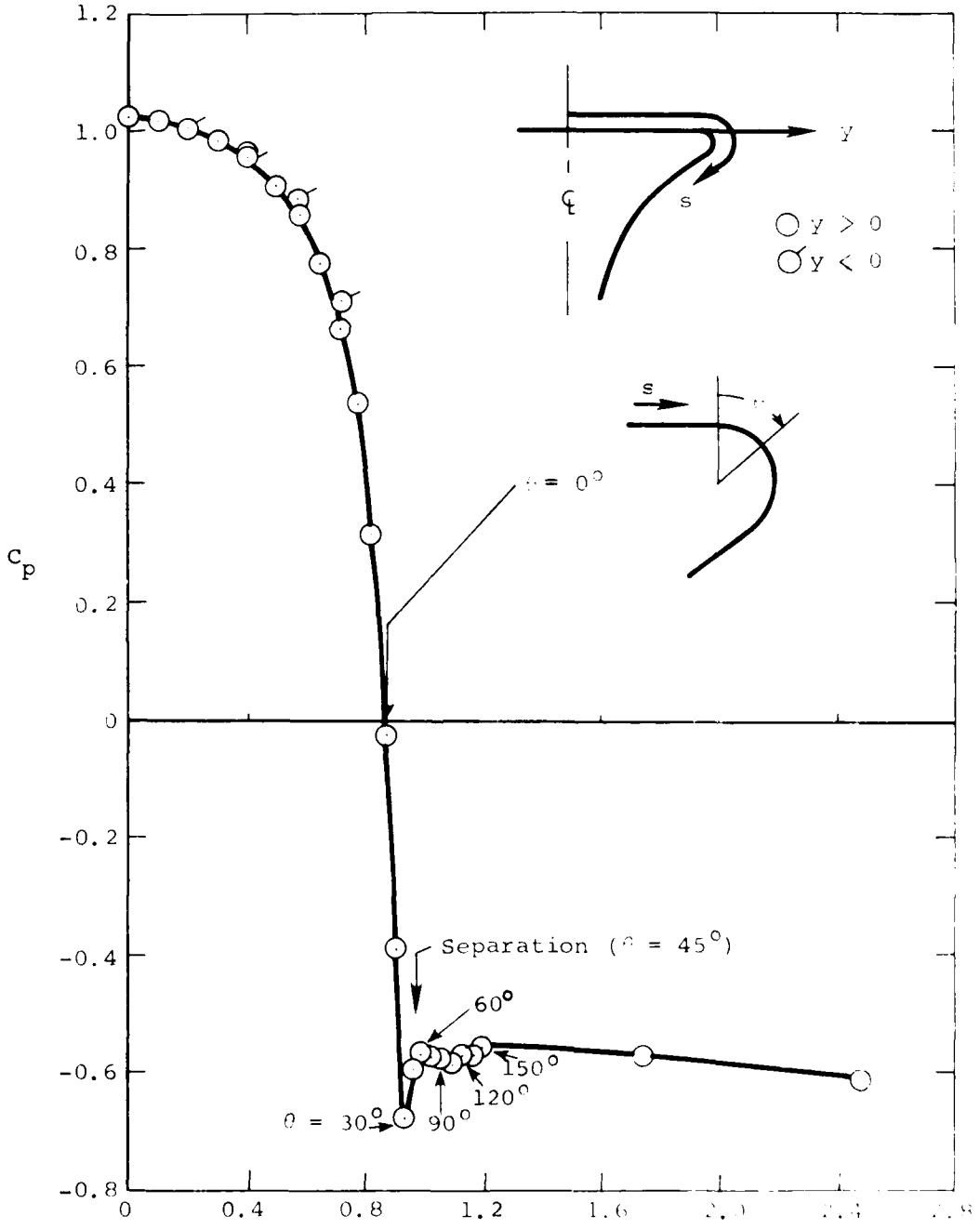

(d) Round edge model, M = 0.25, Re = 0.25×10⁶

Figure 7.- Concluded.

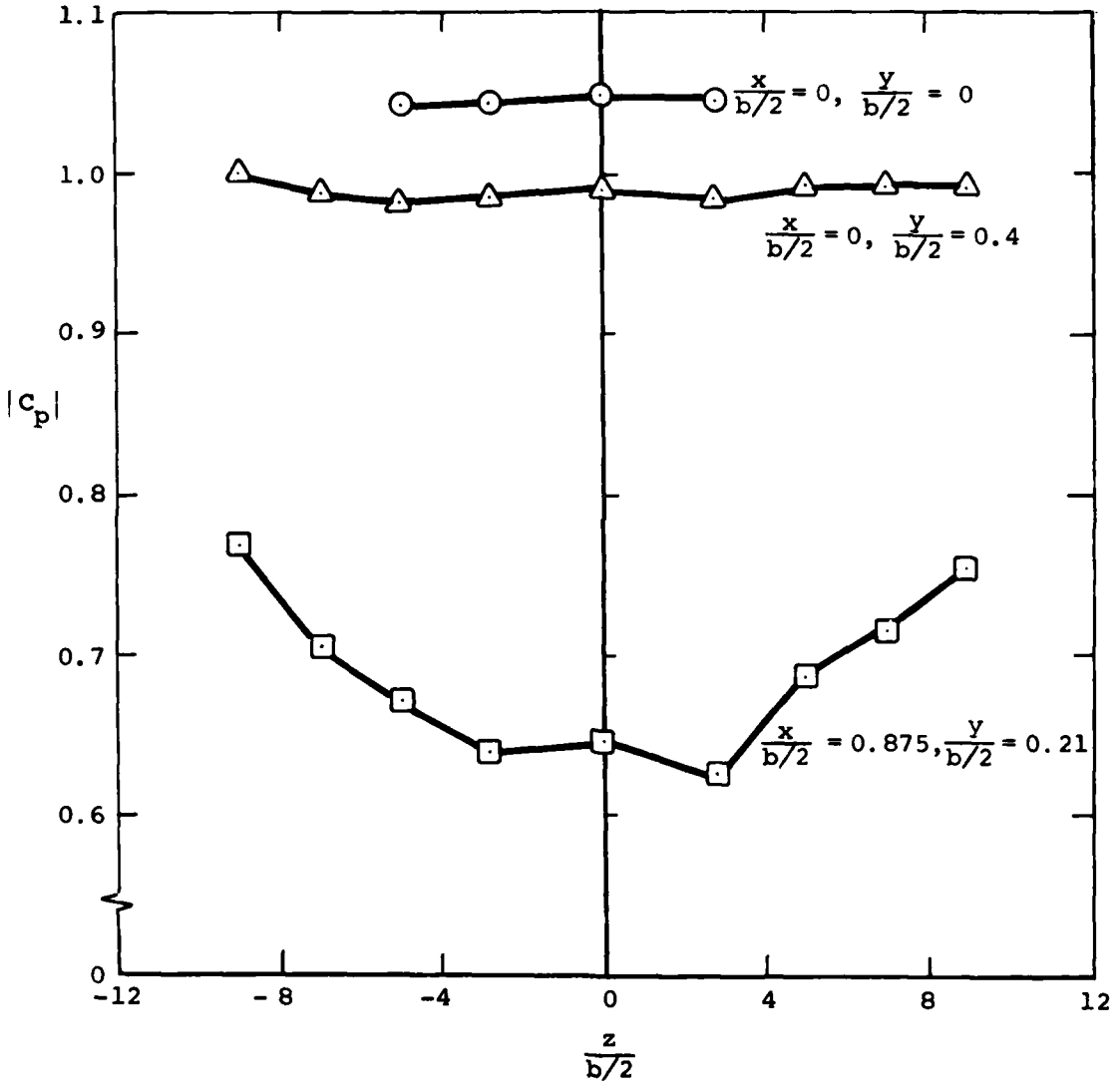

(a) Sharp edge model, M = 0.25, Re = 0.25×10^6

Figure 8.- Spanwise variation of magnitude of front and rear surfaces static pressure.

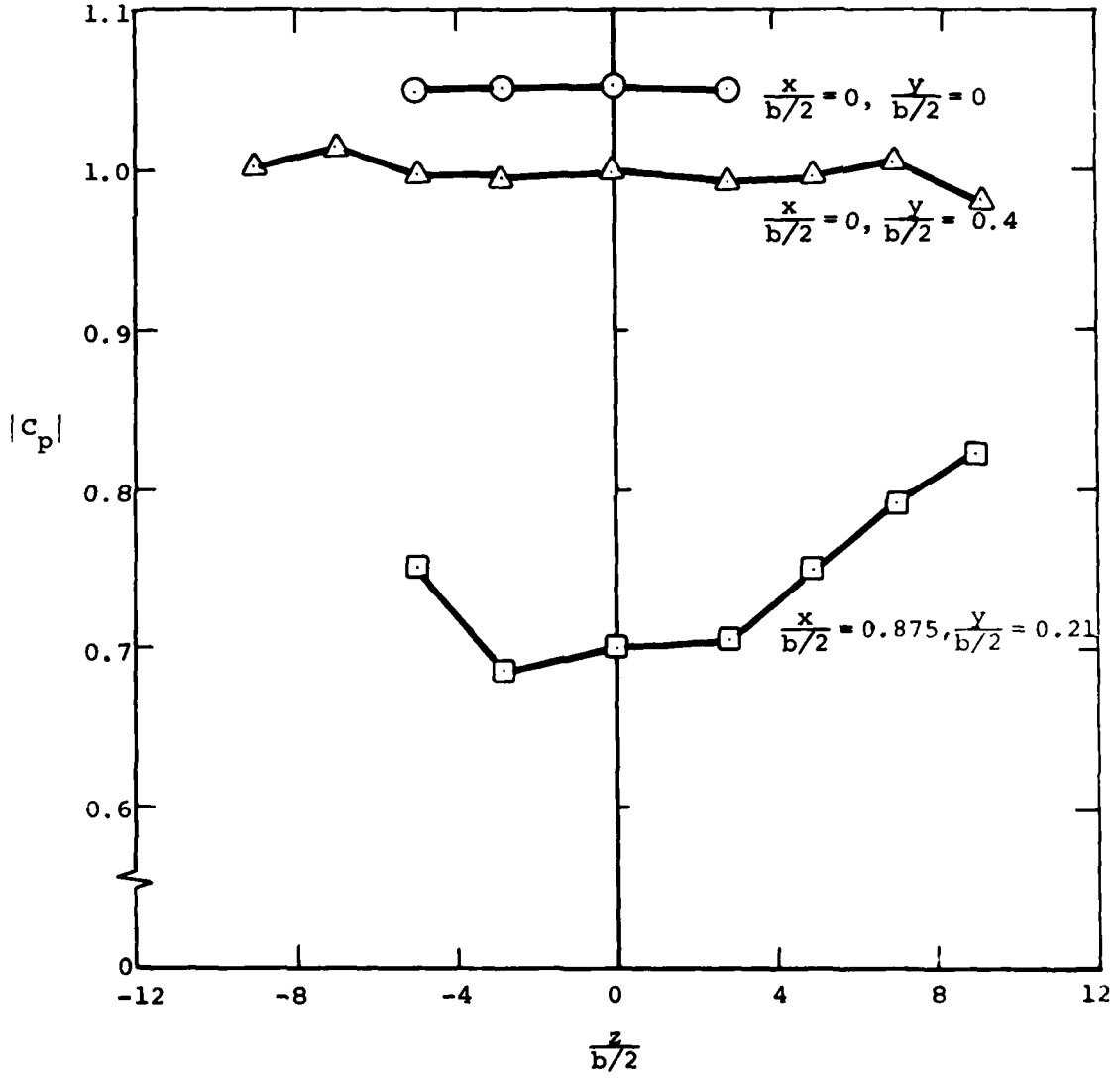

(b) Sharp edge model, M = 0.5, Re = 0.15×10^6

Figure 8.- Continued.

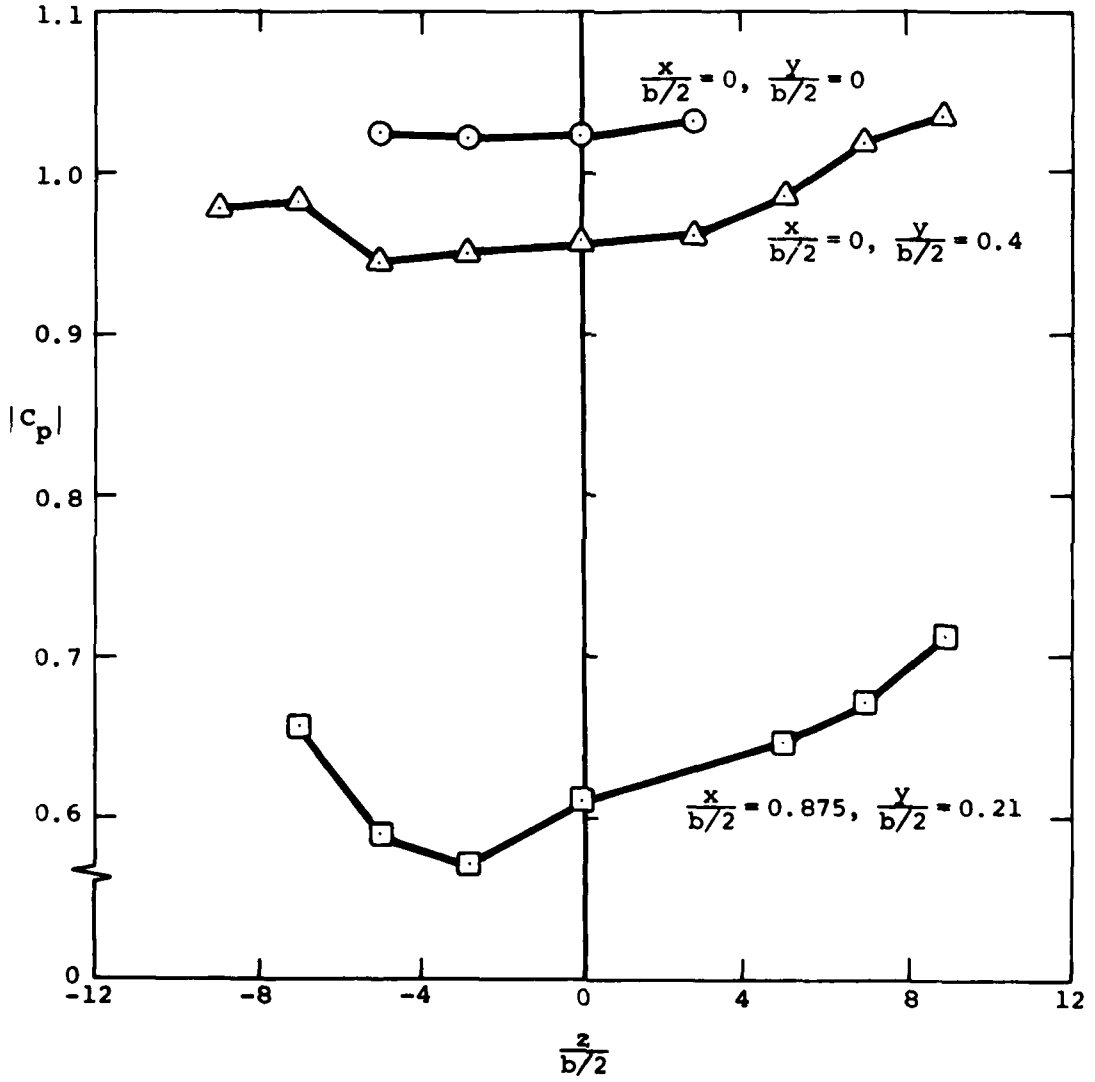

(c) Round edge model, M = 0.25, Re = 0.25×10^6

Figure 8.- Concluded.

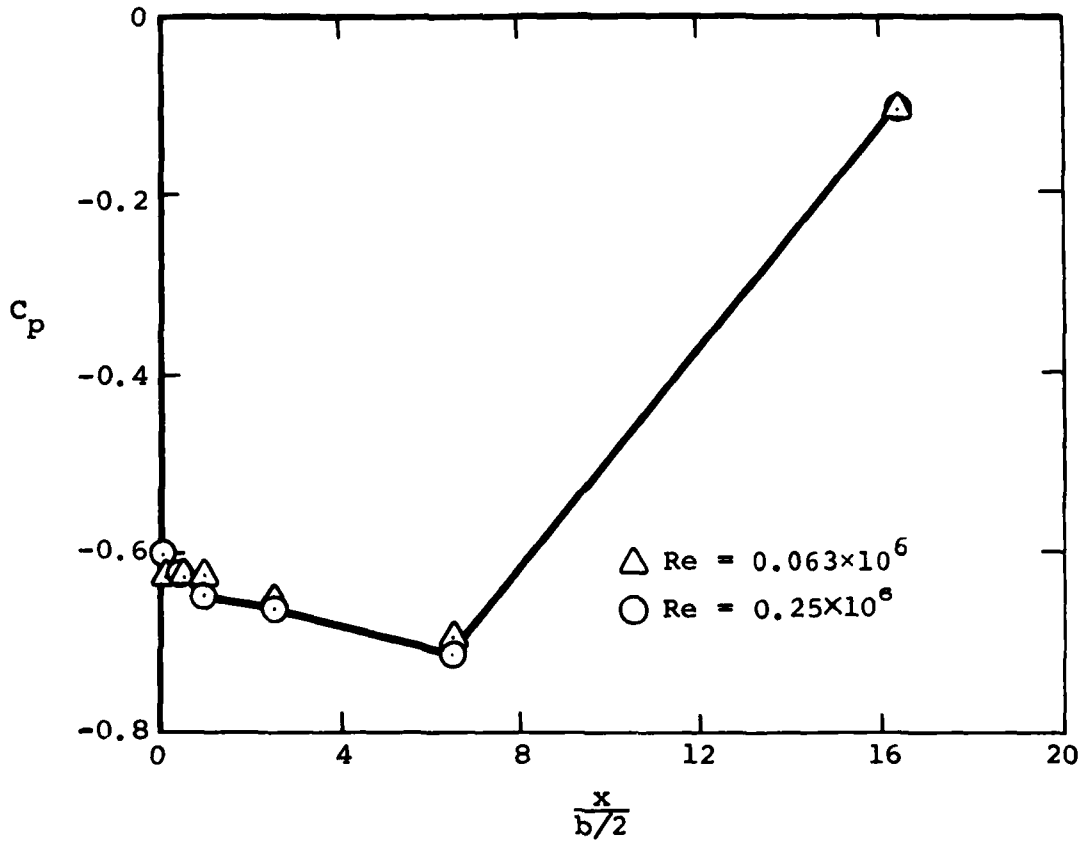

(a) Sharp edge model, M = 0.25

Figure 9.- Streamwise variation of static pressure in separated region at z = 0.

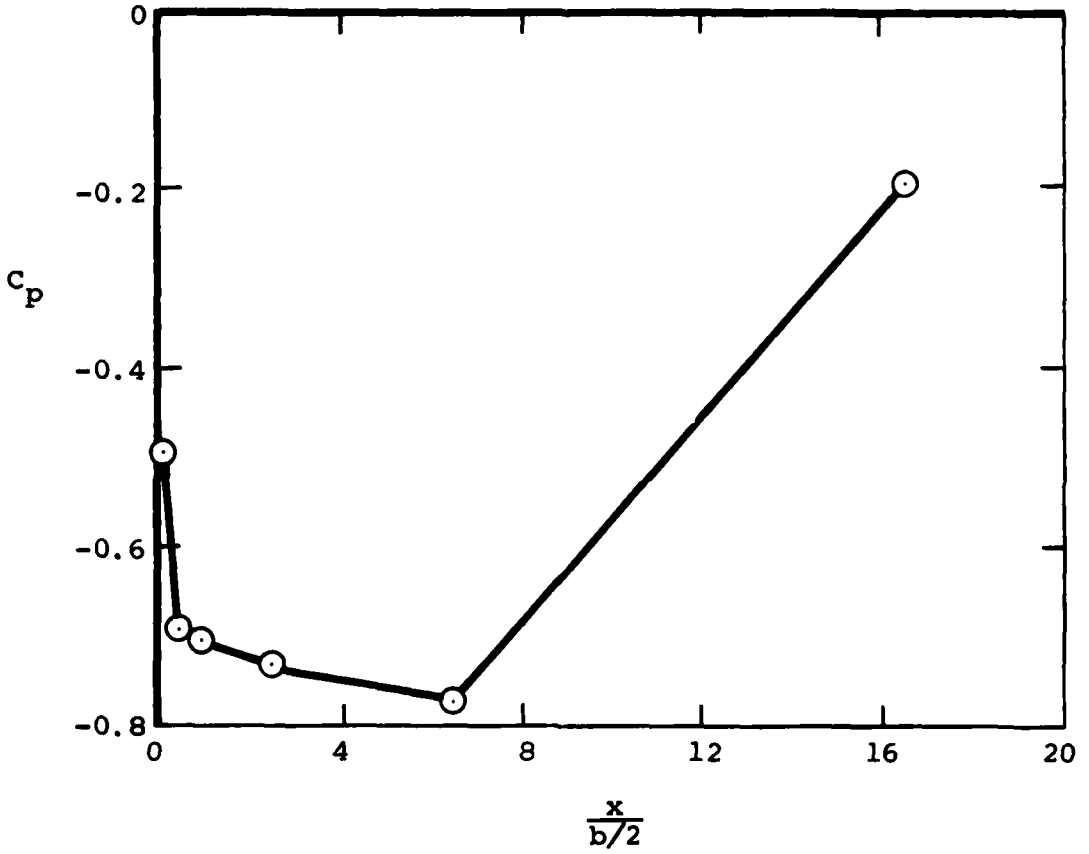

(b) Sharp edge model, M = 0.5, Re = 0.15×10^6

Figure 9.- Continued.

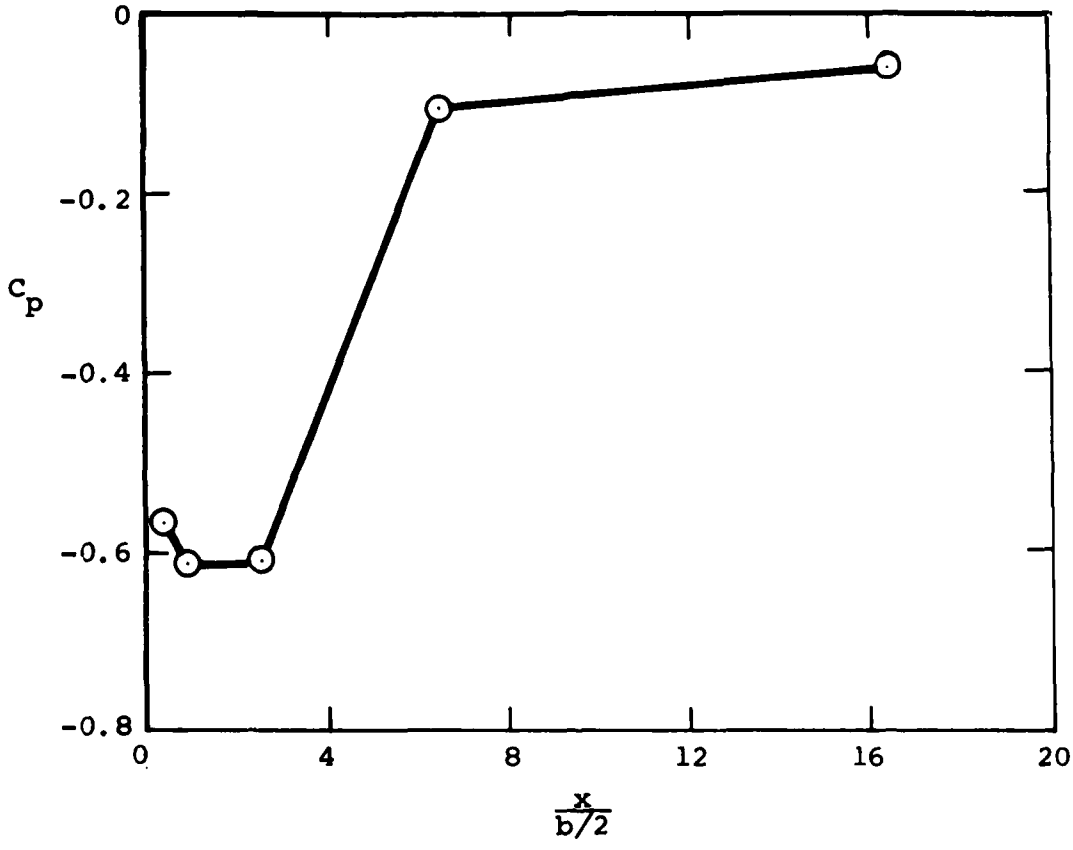

(c) Round edge model, M = 0.25, Re = 0.25×10^6

Figure 9.- Concluded.

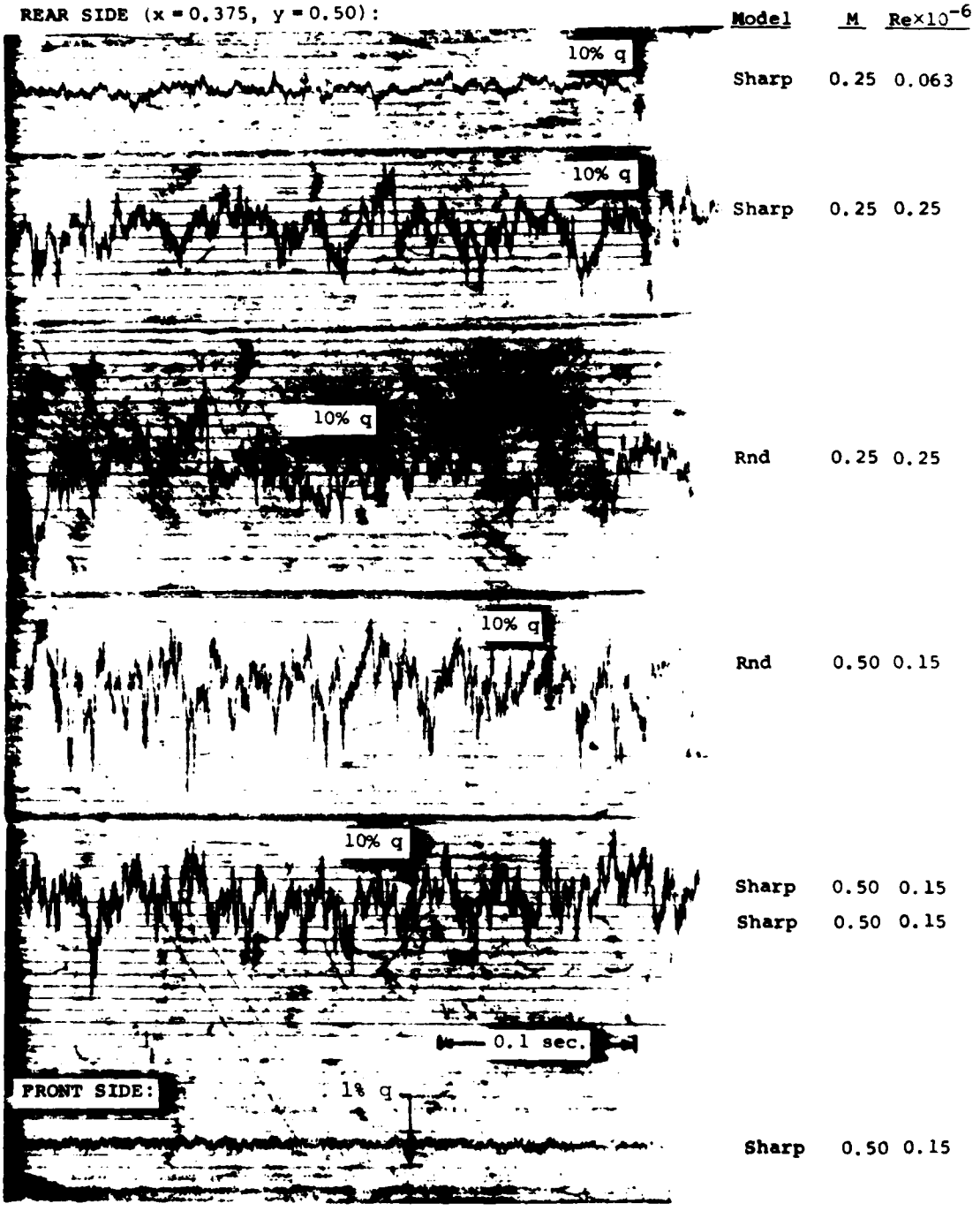

Figure 10.- Unsteady pressure traces.

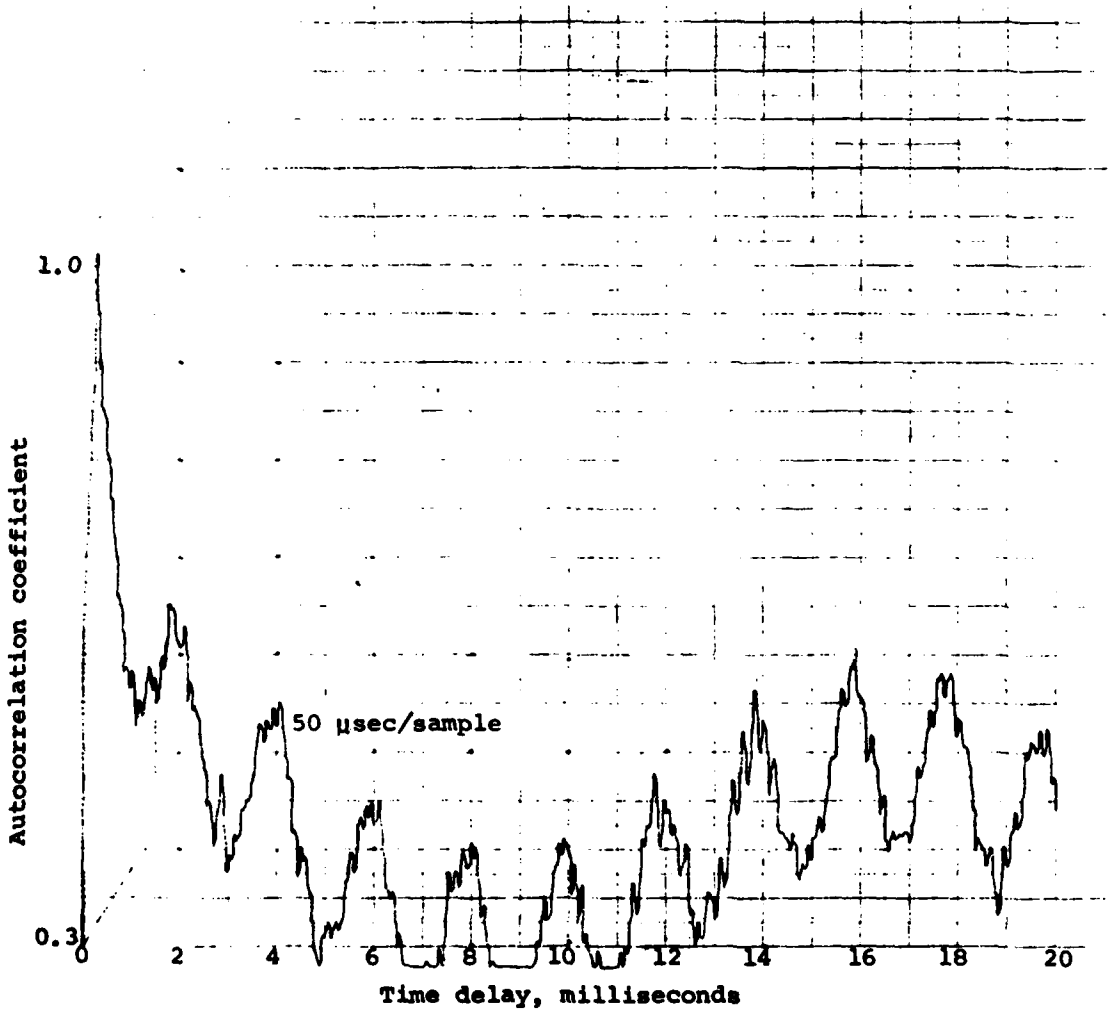

(a) Front face transducer.

Figure 11.- Autocorrelation results for the sharp edge model at M = 0.25, Re = 0.063×10^6.

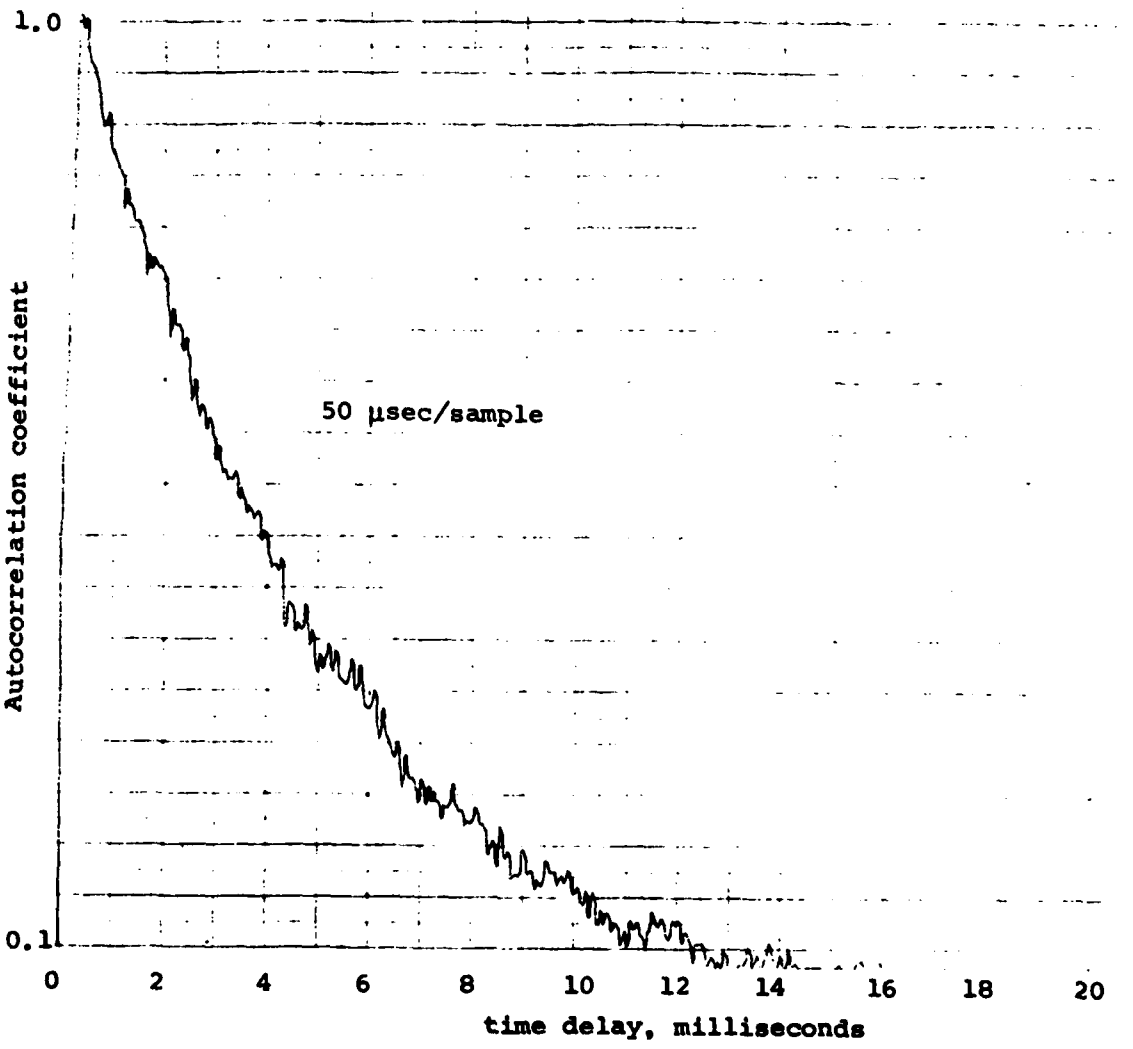

(b) Support plate transducer

Figure 11.- Concluded.

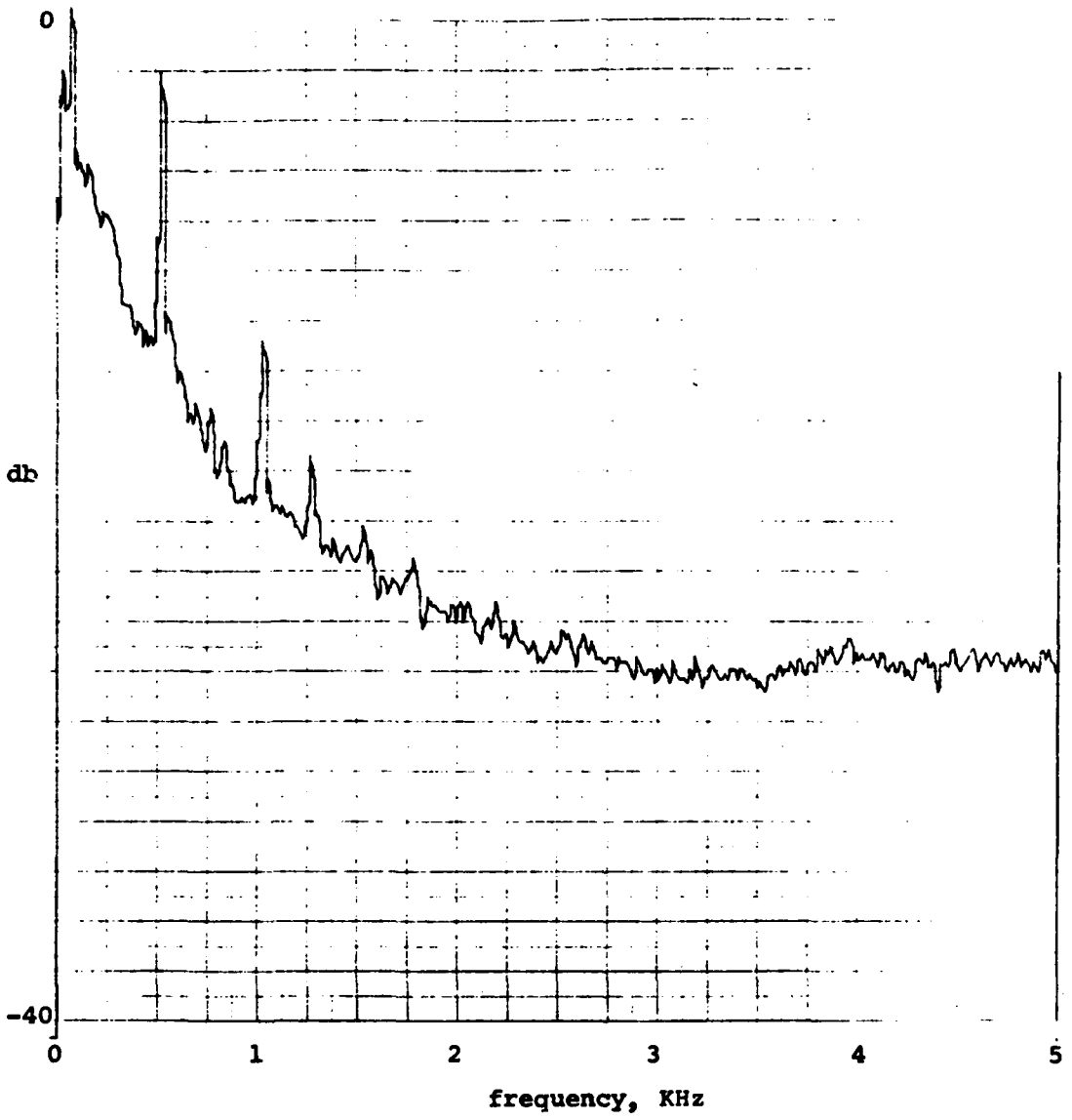

(a) Front face transducer.

Figure 12.- Power spectral density results for sharp edge model at M = 0.25, Re = 0.063×10^6.

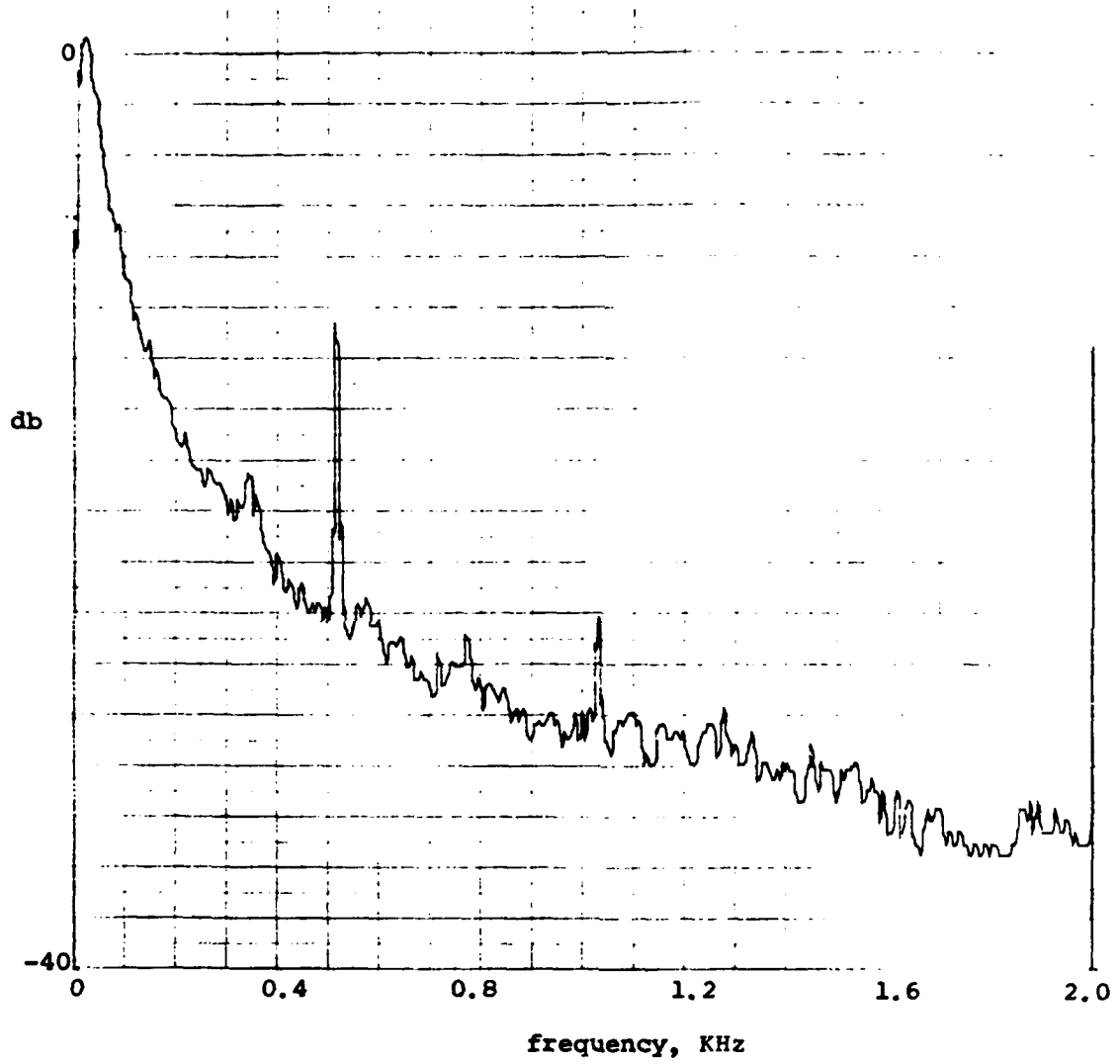

(b) Support plate transducer.

Figure 12.- Concluded.

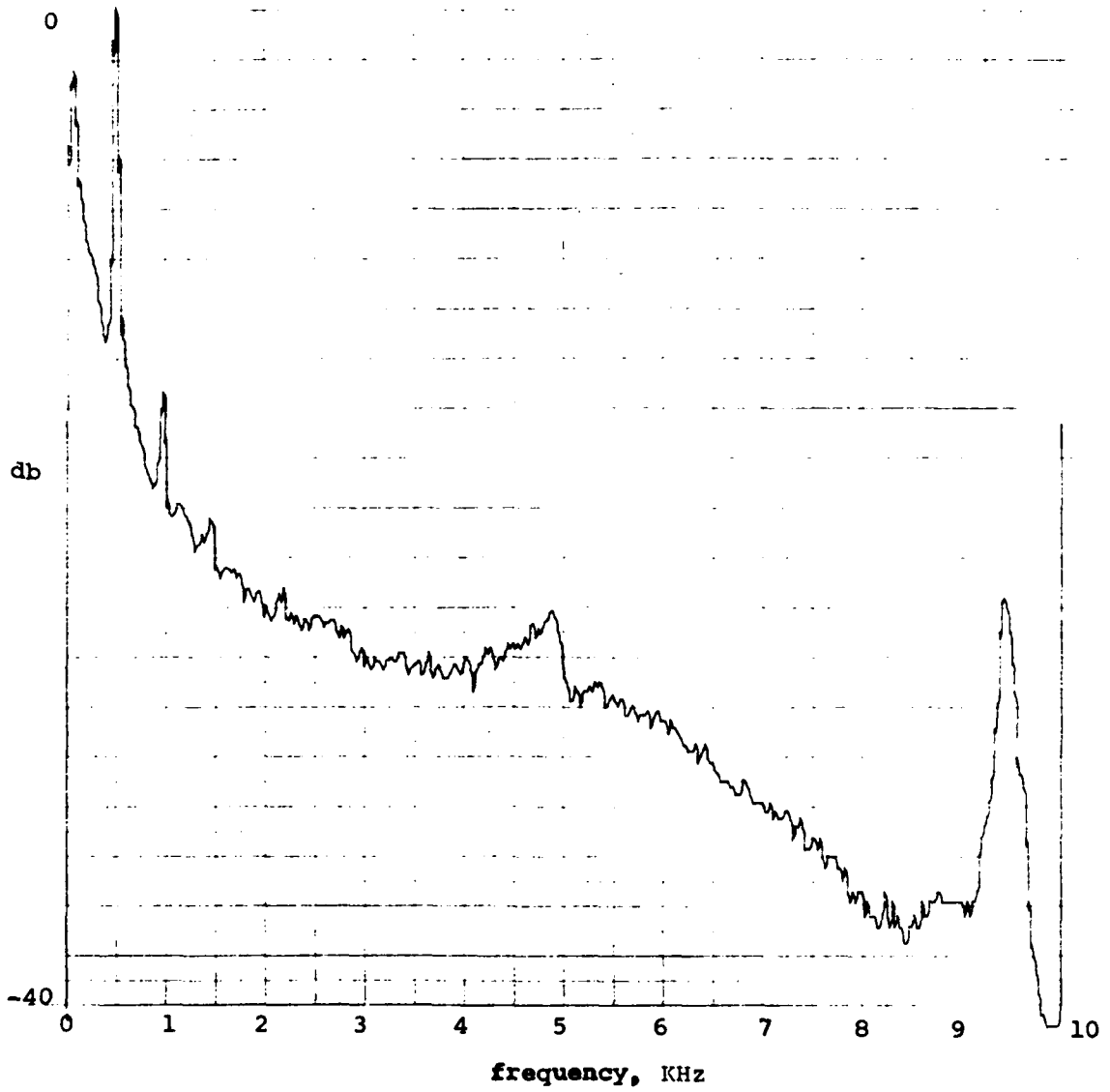

Figure 13.- Power spectral density results for front face transducer on round edge model at M = 0.25, Re = 0.25×10^6.

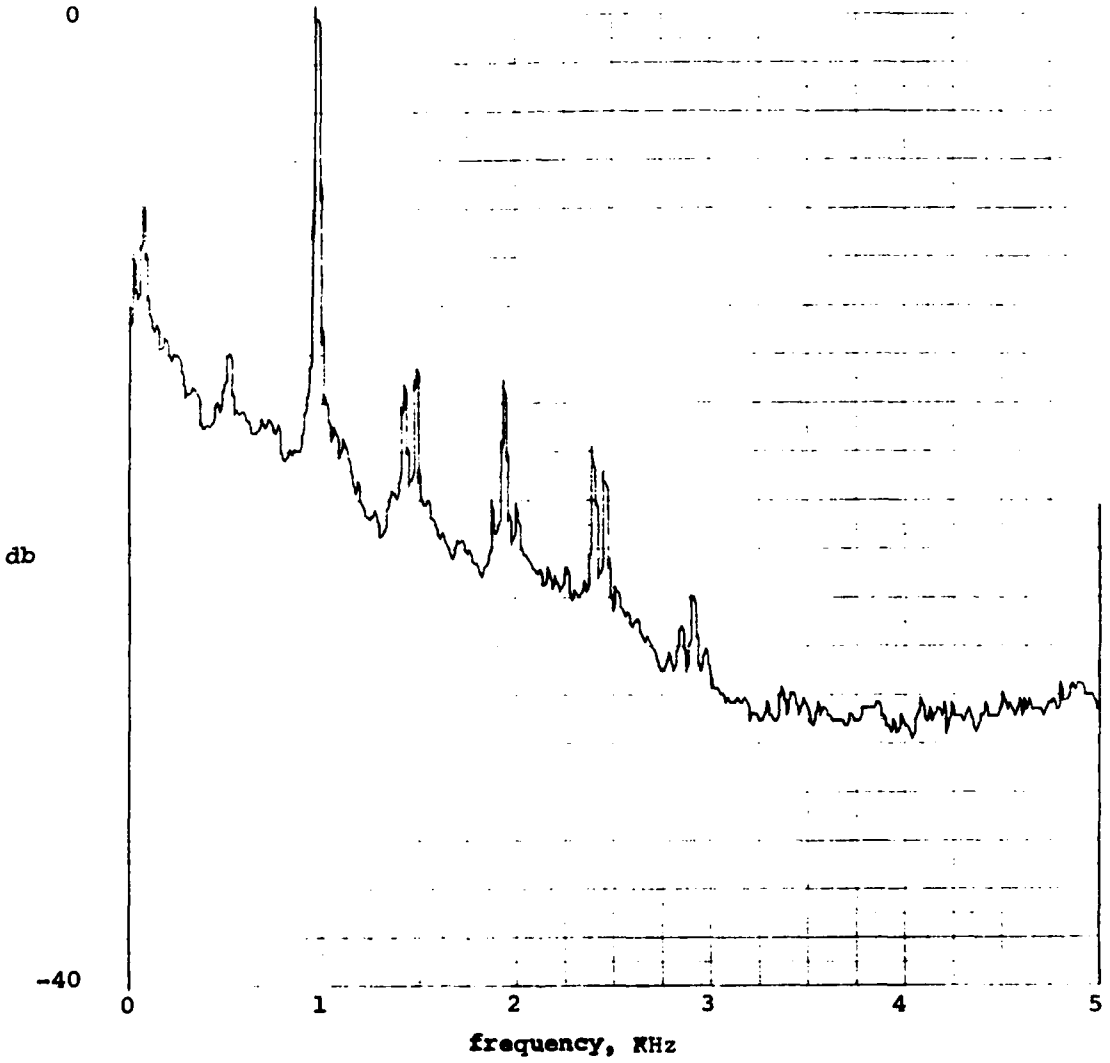

Figure 14.- Power spectral density results for front face transducer on sharp edge model at M = 0.5 and Re = 0.15×10^{6}/ft.

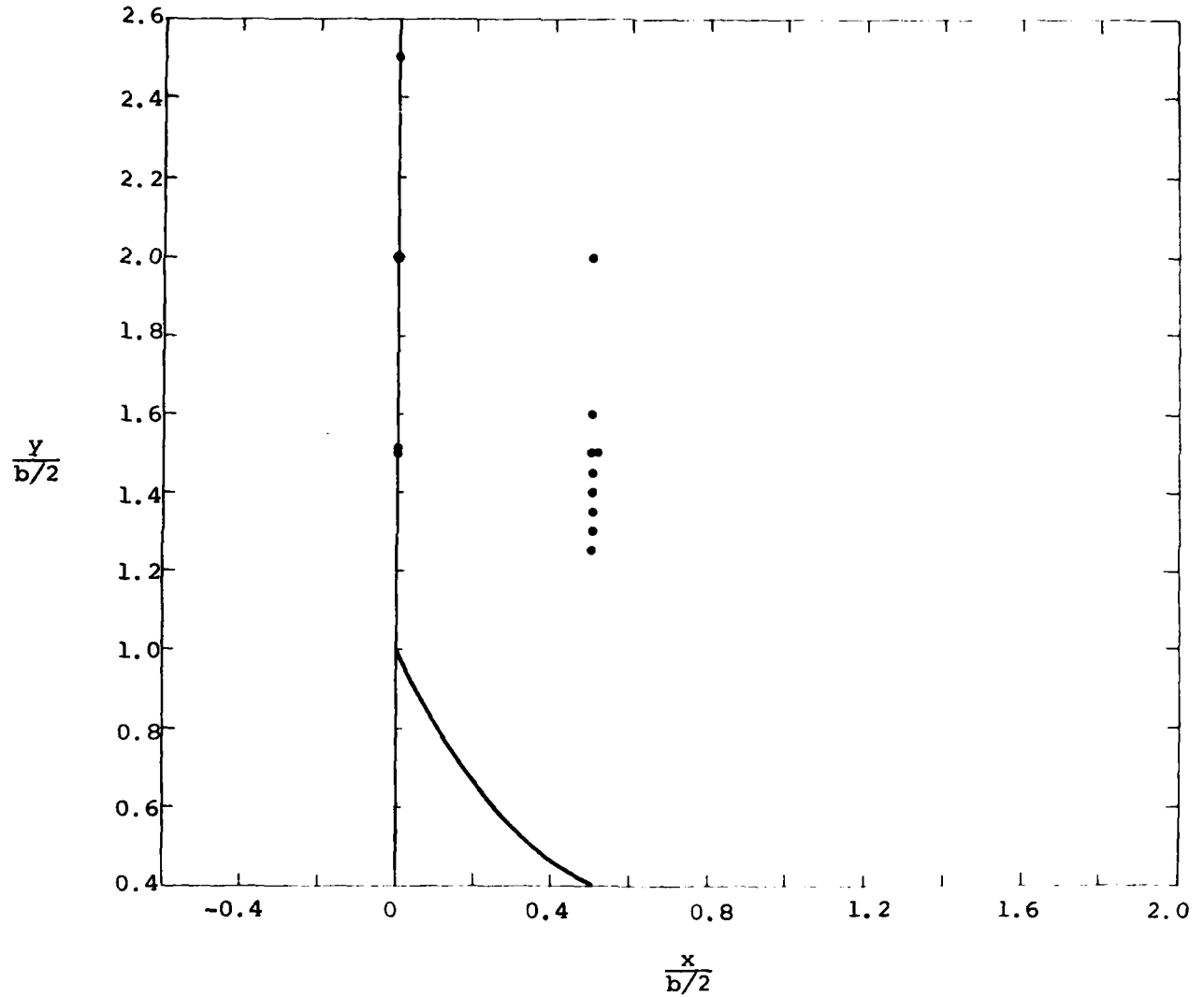

(a) Sharp edge model at $M = 0.25$ and $Re = 0.063 \times 10^6$ (points 1-13).

Figure 15.- Positions of velocity measurements.

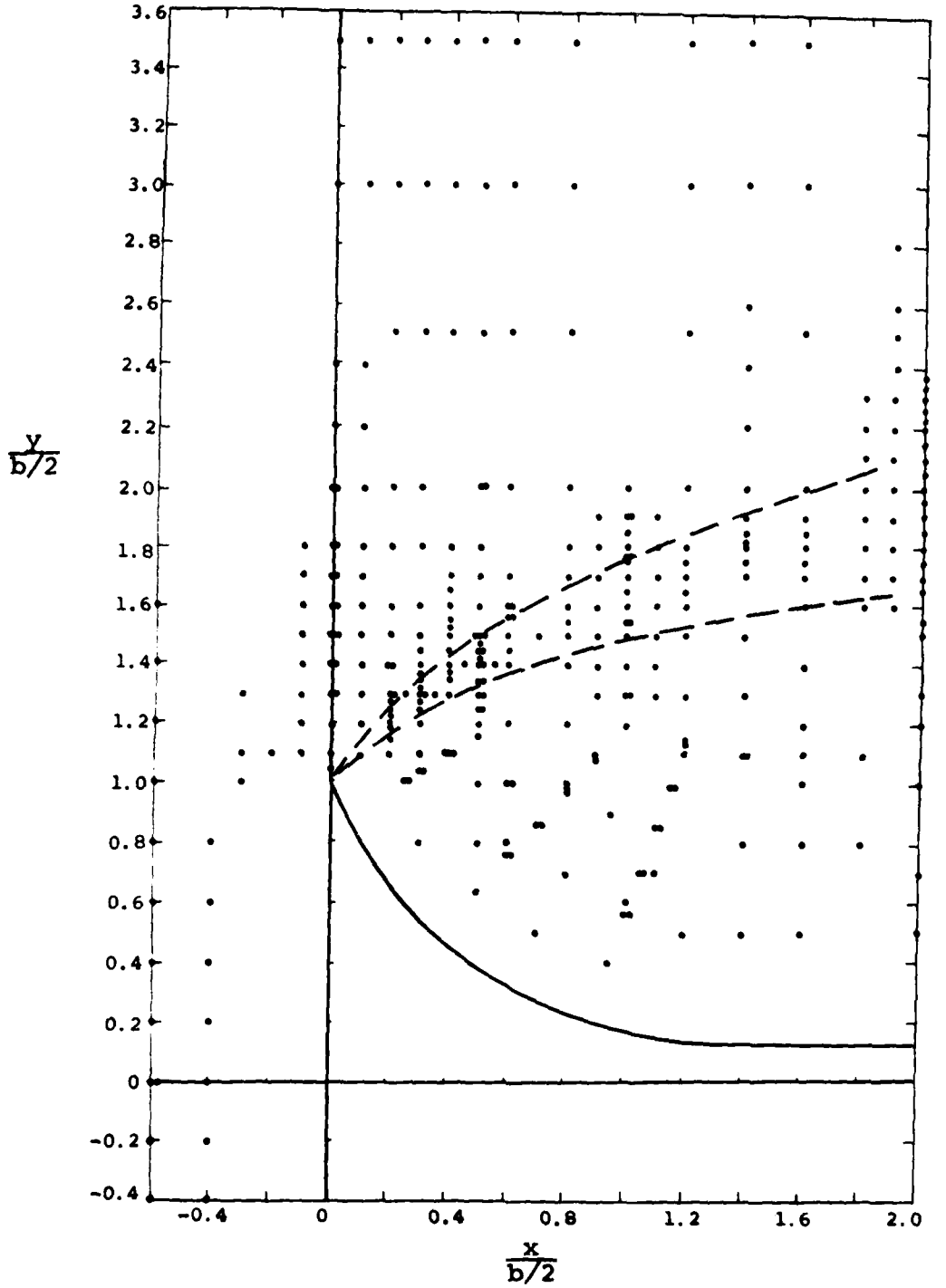

(b) Sharp edge model at $M = 0.25$ and $Re = 0.25 \times 10^6$ (points 14-383).

Figure 15.- Continued.

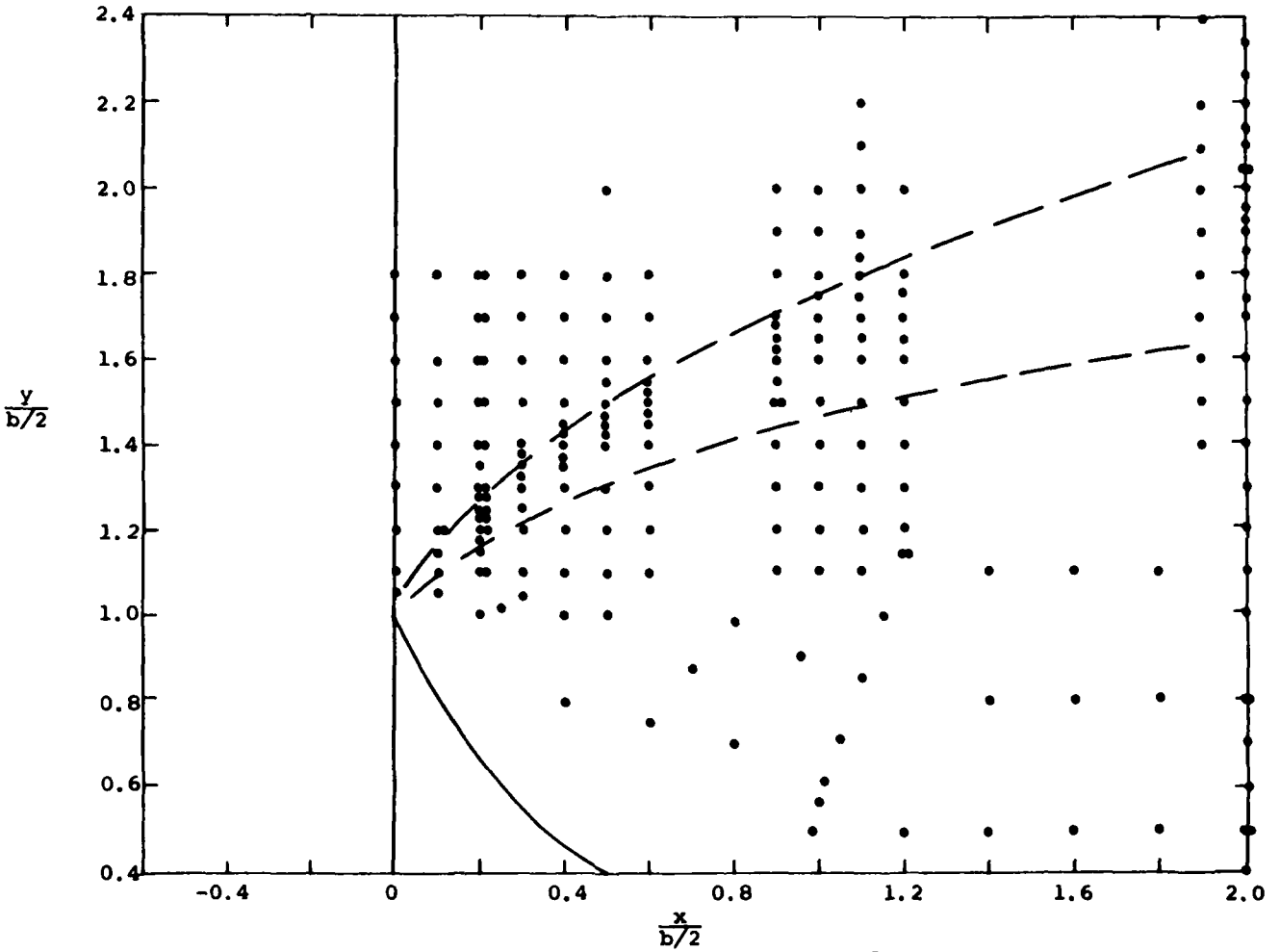

(c) Sharp edge model at $M = 0.5$ and $Re = 0.15 \times 10^6$ (points 384-608).

Figure 15.- Continued.

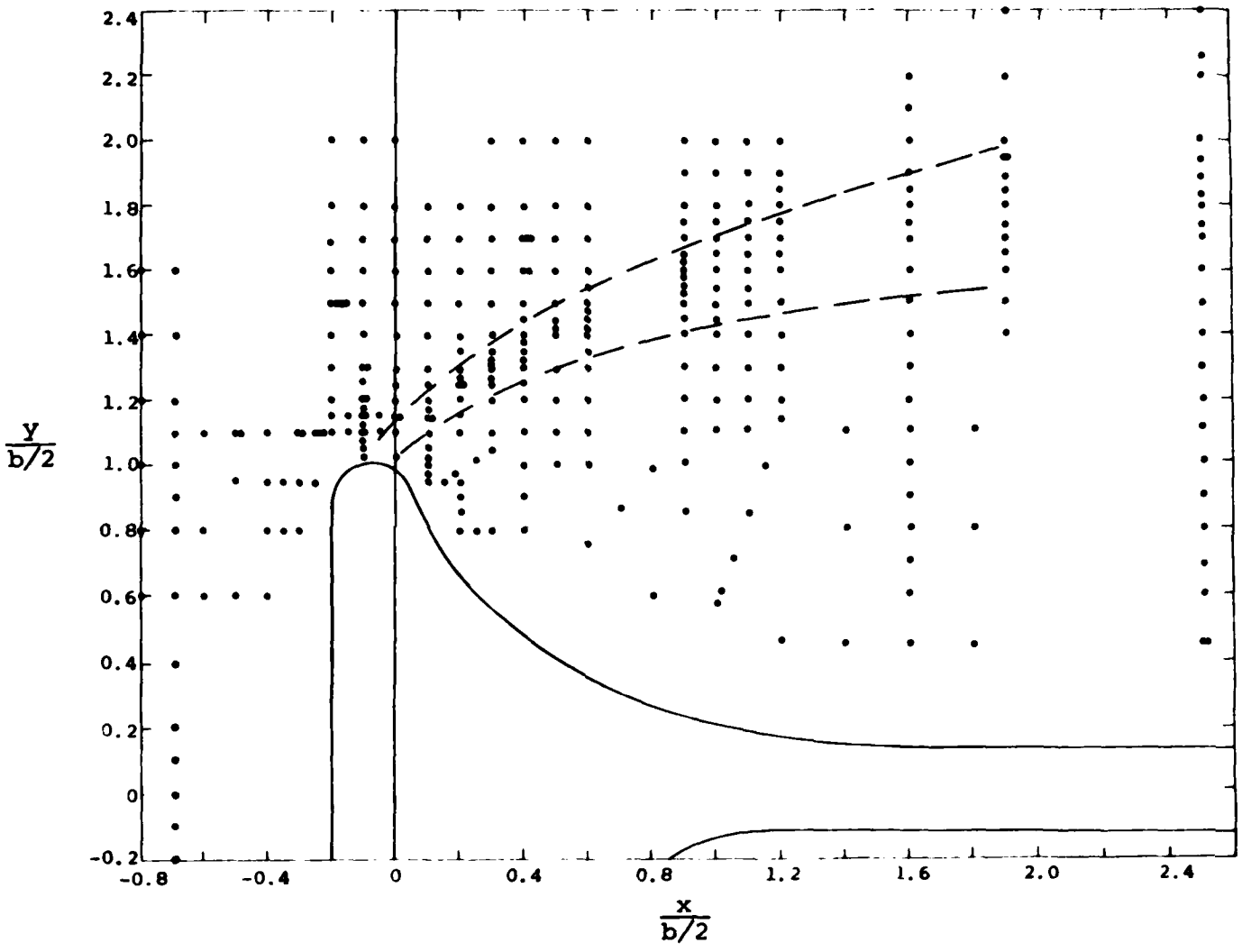

(d) Round edge model at $M = 0.25$ and $Re = 0.25 \times 10^6$ (points 609-1093).

Figure 15.- Continued.

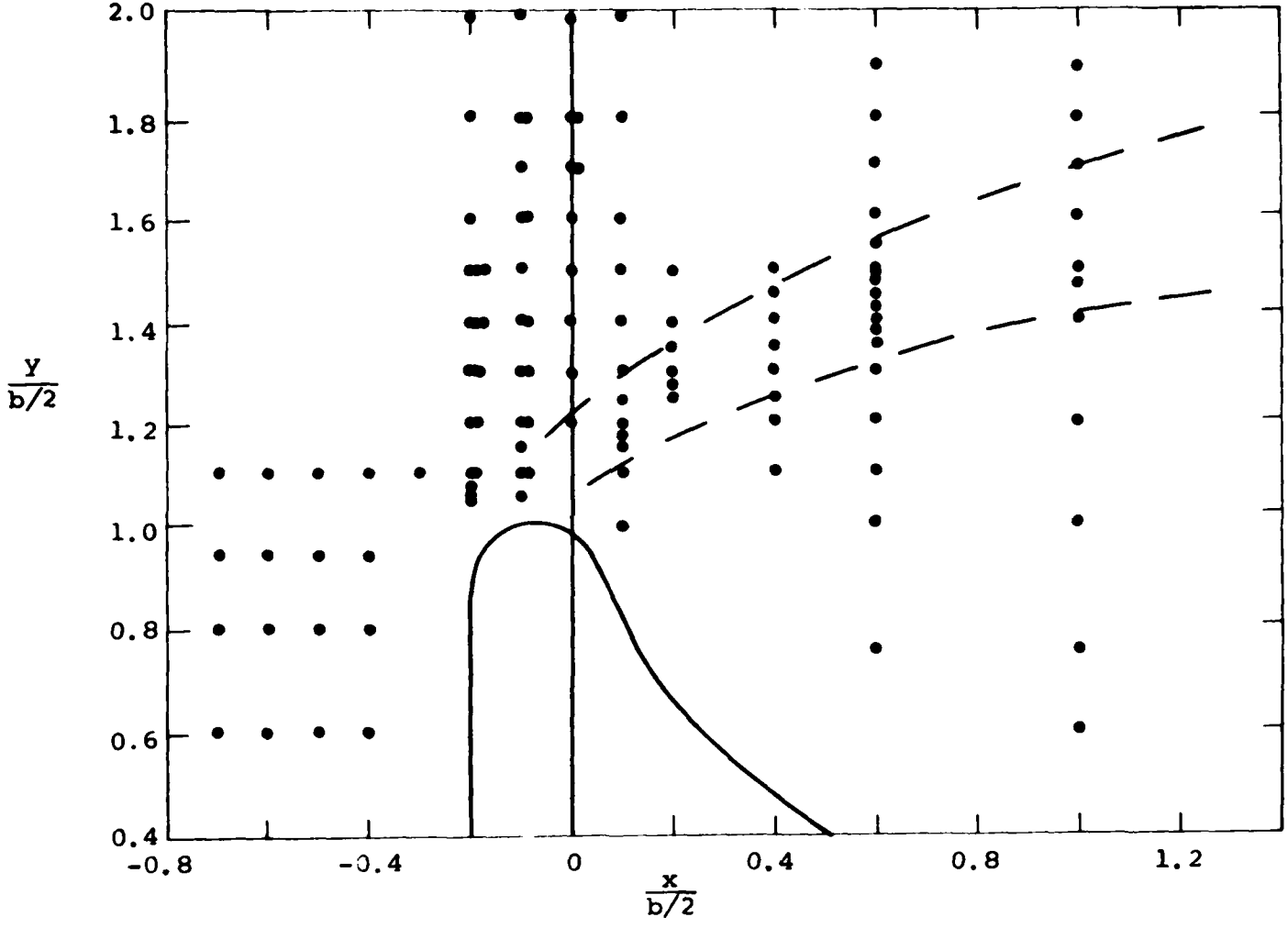

(e) Round edge model at M = 0.5 and Re = 0.15×10^6 (points 1094-1211).

Figure 15.- Concluded.

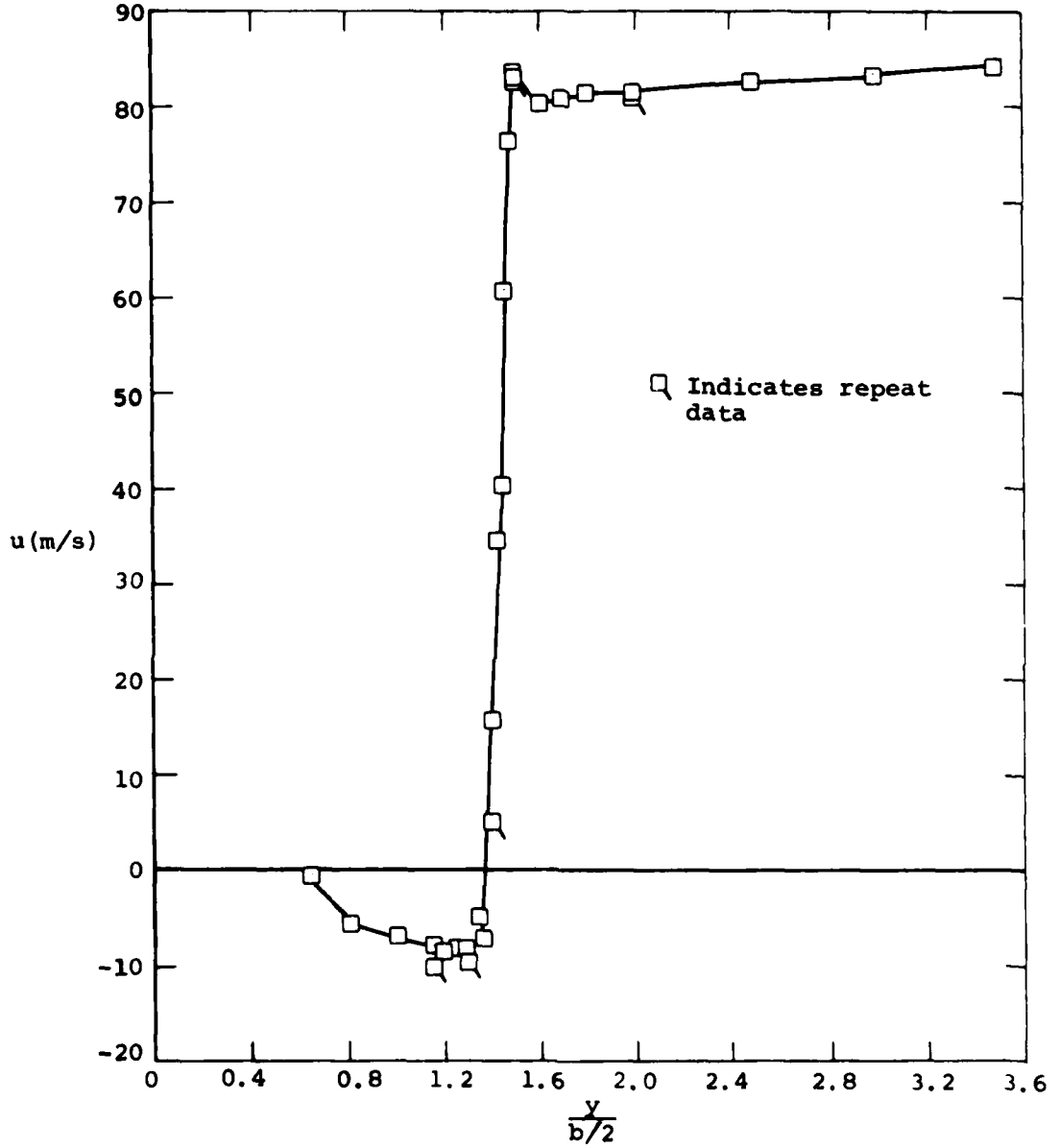

(a) Axial velocity variation with vertical position at $\frac{x}{b/2} = 0.5$.

Figure 16.- Measured velocities in the vicinity of the sharp edge model at $M = 0.25$, $Re = 0.25 \times 10^6$.

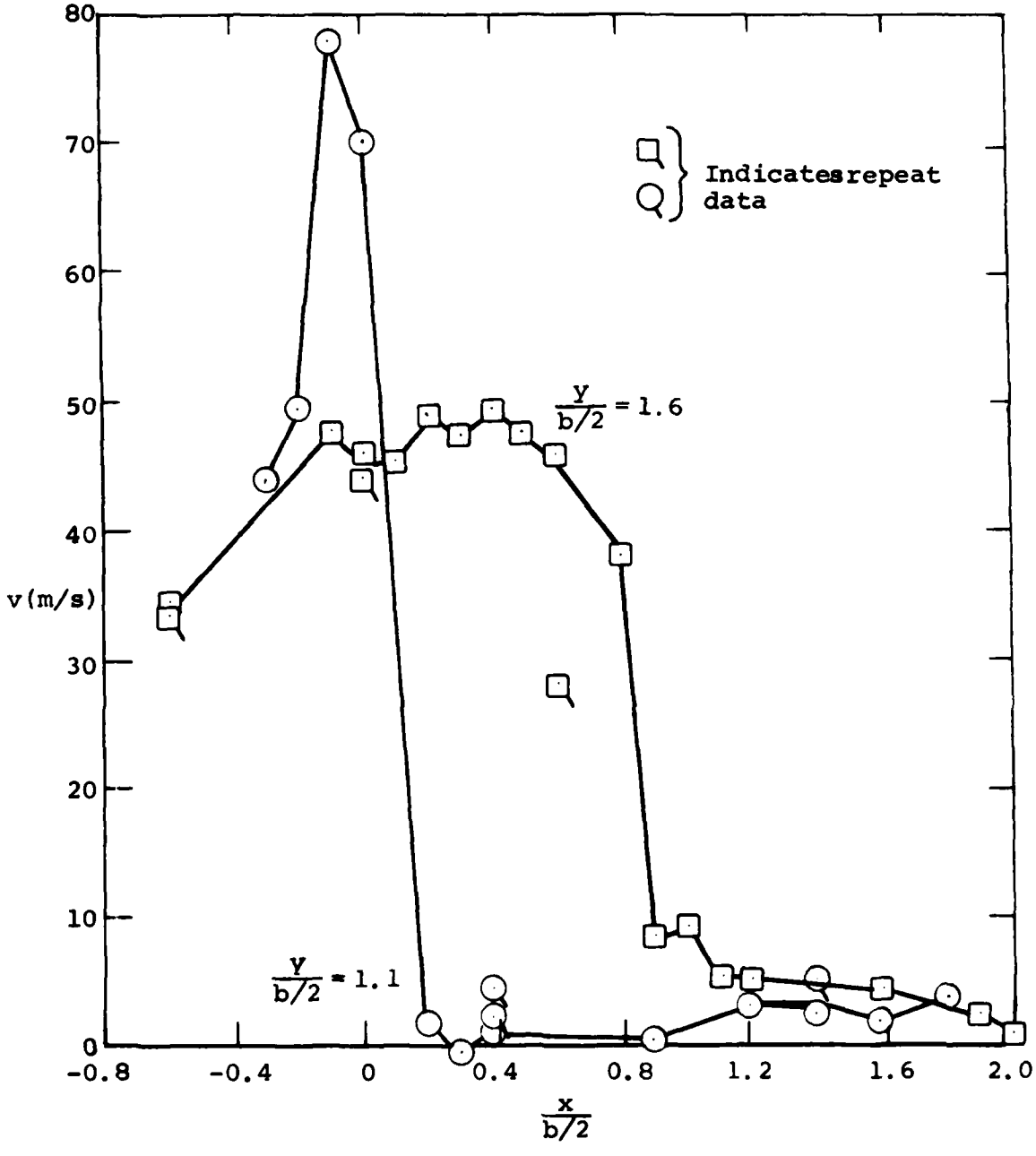

(b) Vertical velocity variation with axial position for $\frac{y}{b/2} = 1.1$ and 1.6.

Figure 16.- Concluded.

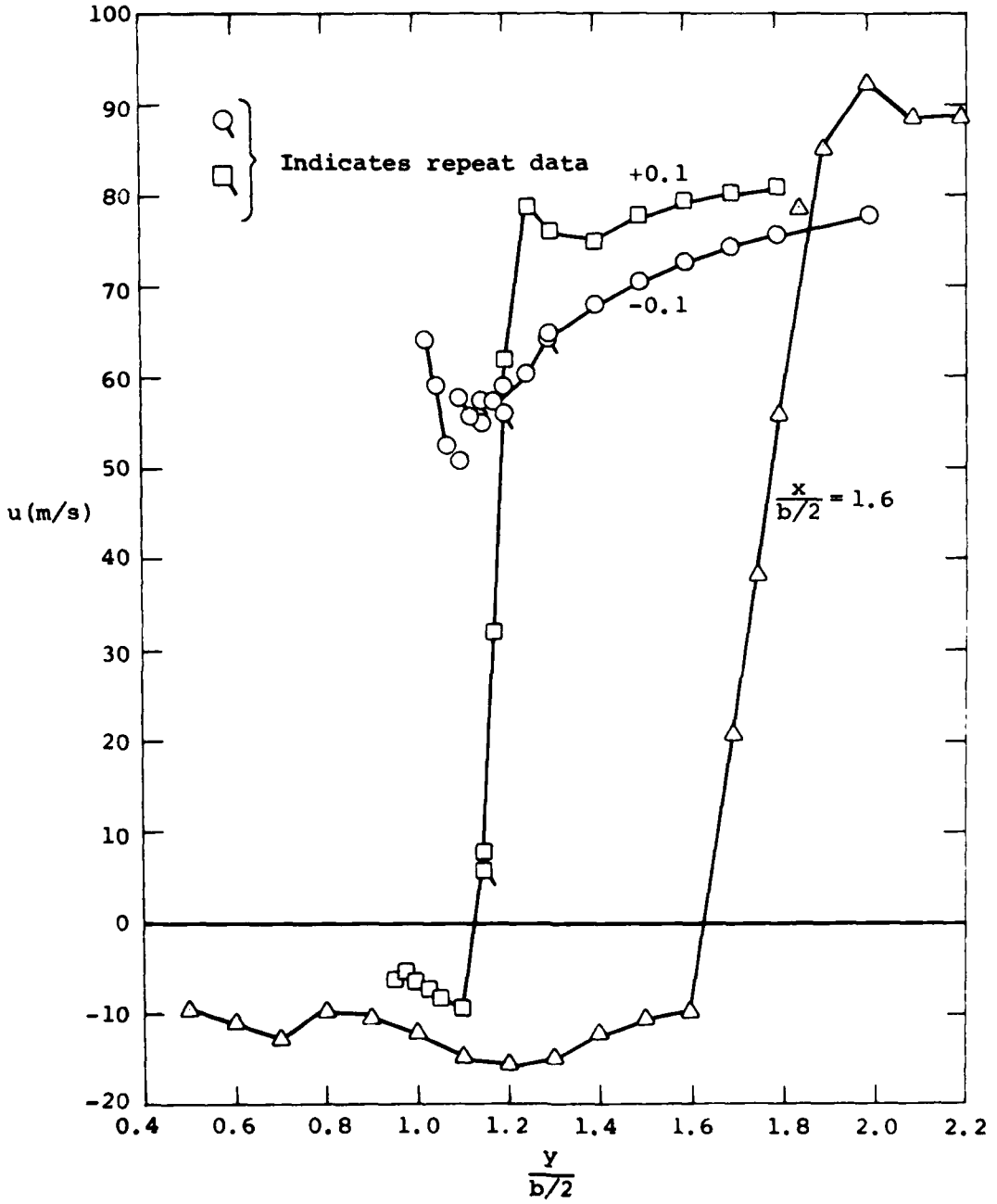

(a) Axial velocity variation with vertical position.

Figure 17.- Measured velocities in the vicinity of the round edge model at $M = 0.25$ and $Re = 0.25 \times 10^6$.

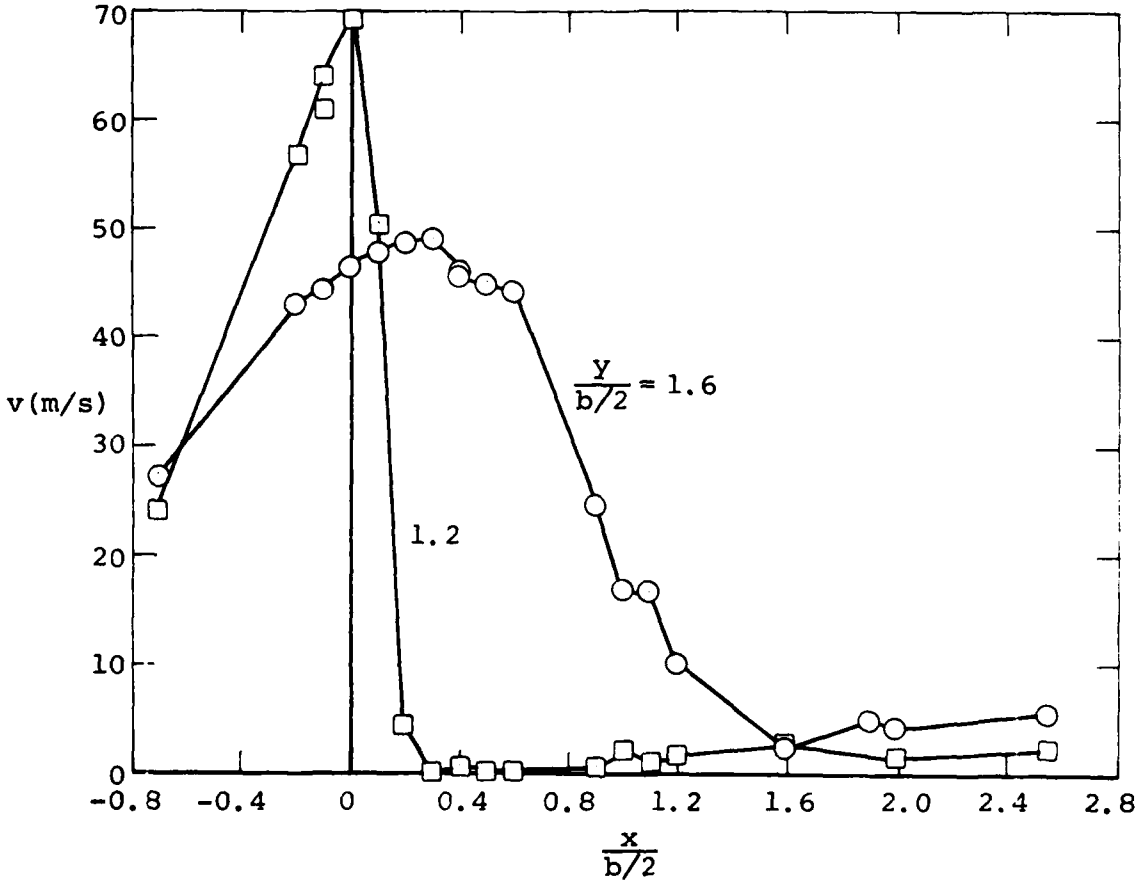

(b) Vertical velocity variation with axial position.

Figure 17.- Concluded.

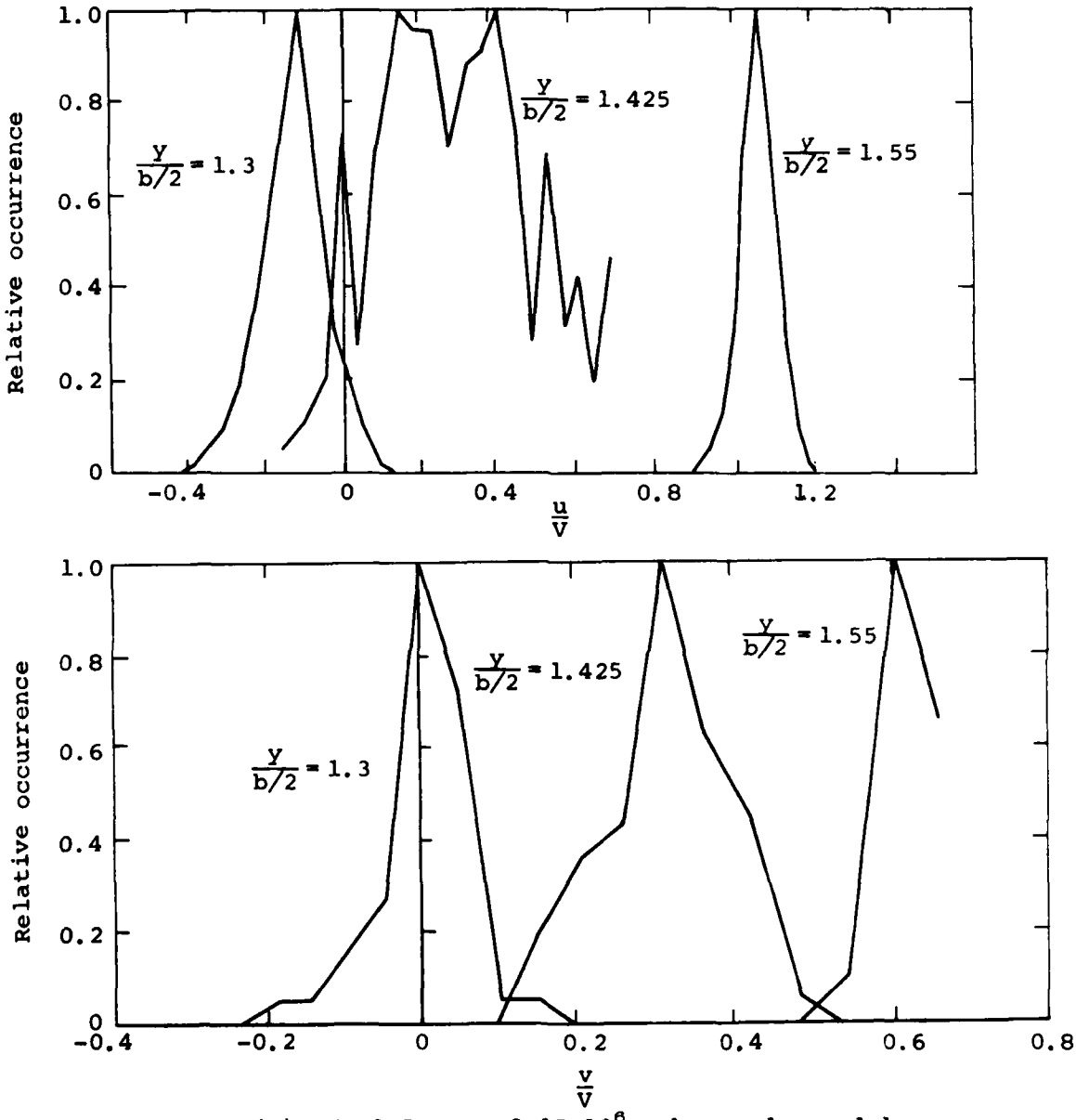

(a) $M = 0.5$, $Re = 0.15 \times 10^6$, sharp edge model.

Figure 18.- Velocity histograms through shear layer at $x/(b/2) = 0.5$

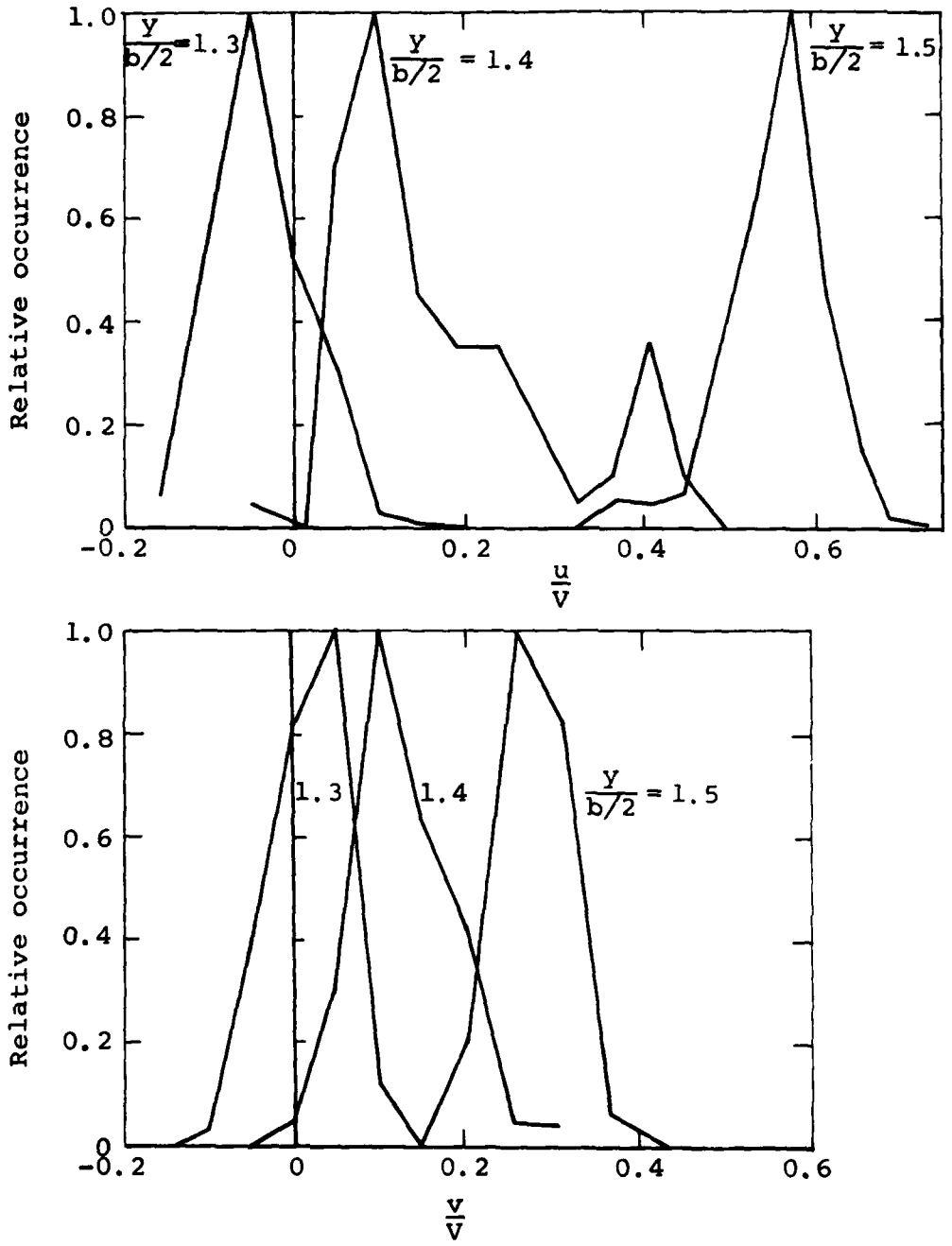

(b) M = 0.5, Re = 0.15×10^6, round edge.

Figure 18. - Concluded.

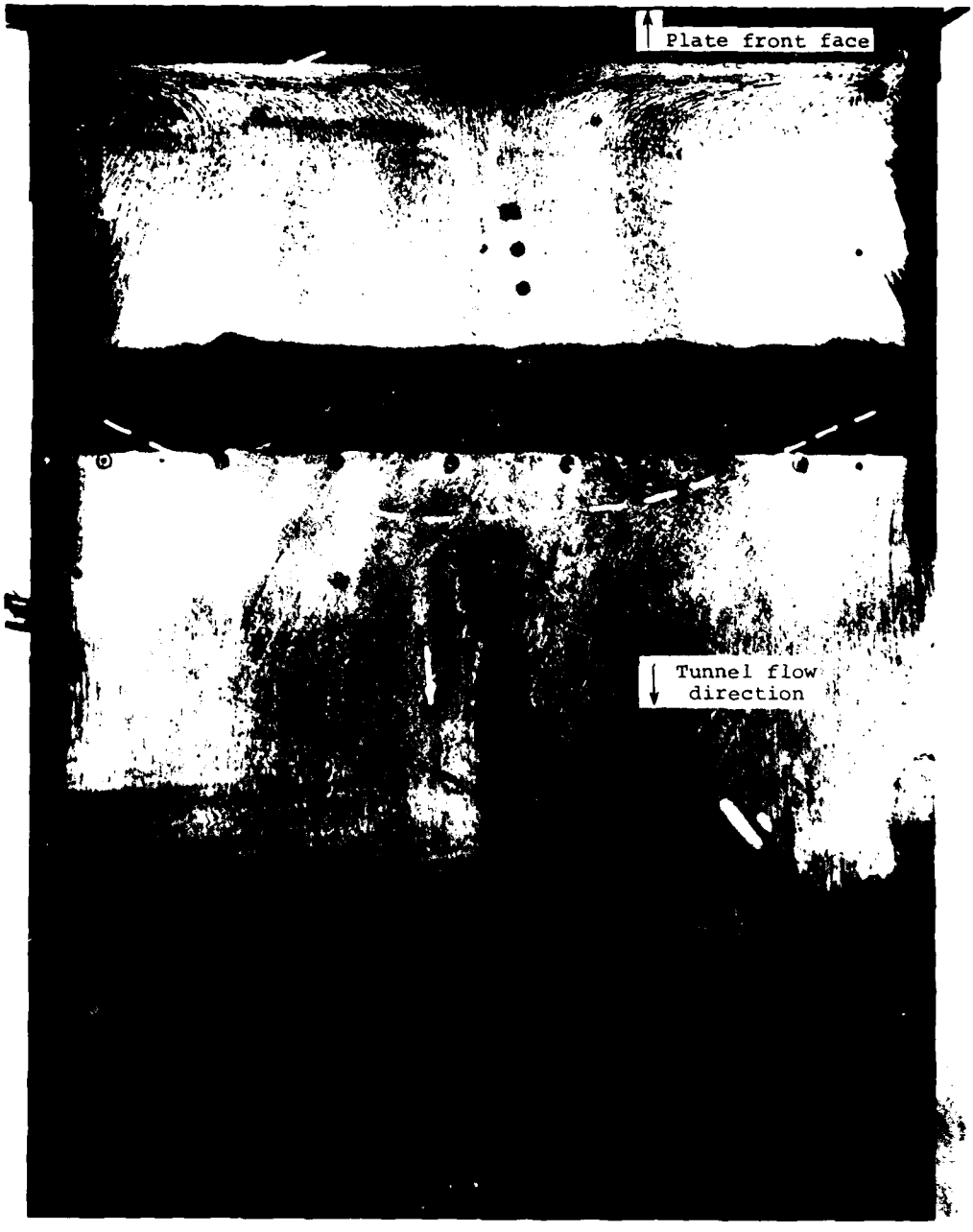

(a) Overall view.

Figure 19.- Flow visualization on round edge model.

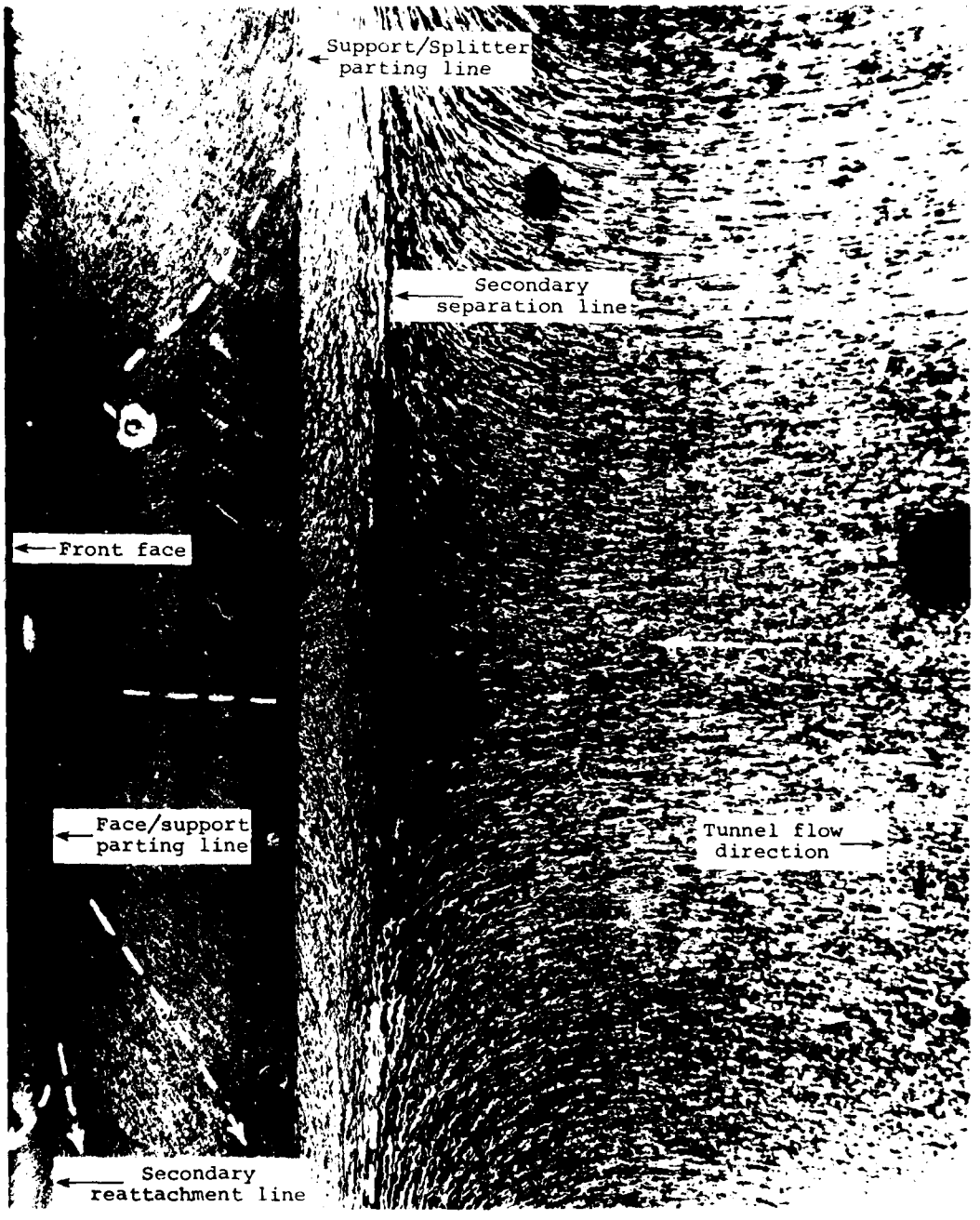

(b) Close up view of surface aft of the edge.

Figure 19.- Continued.

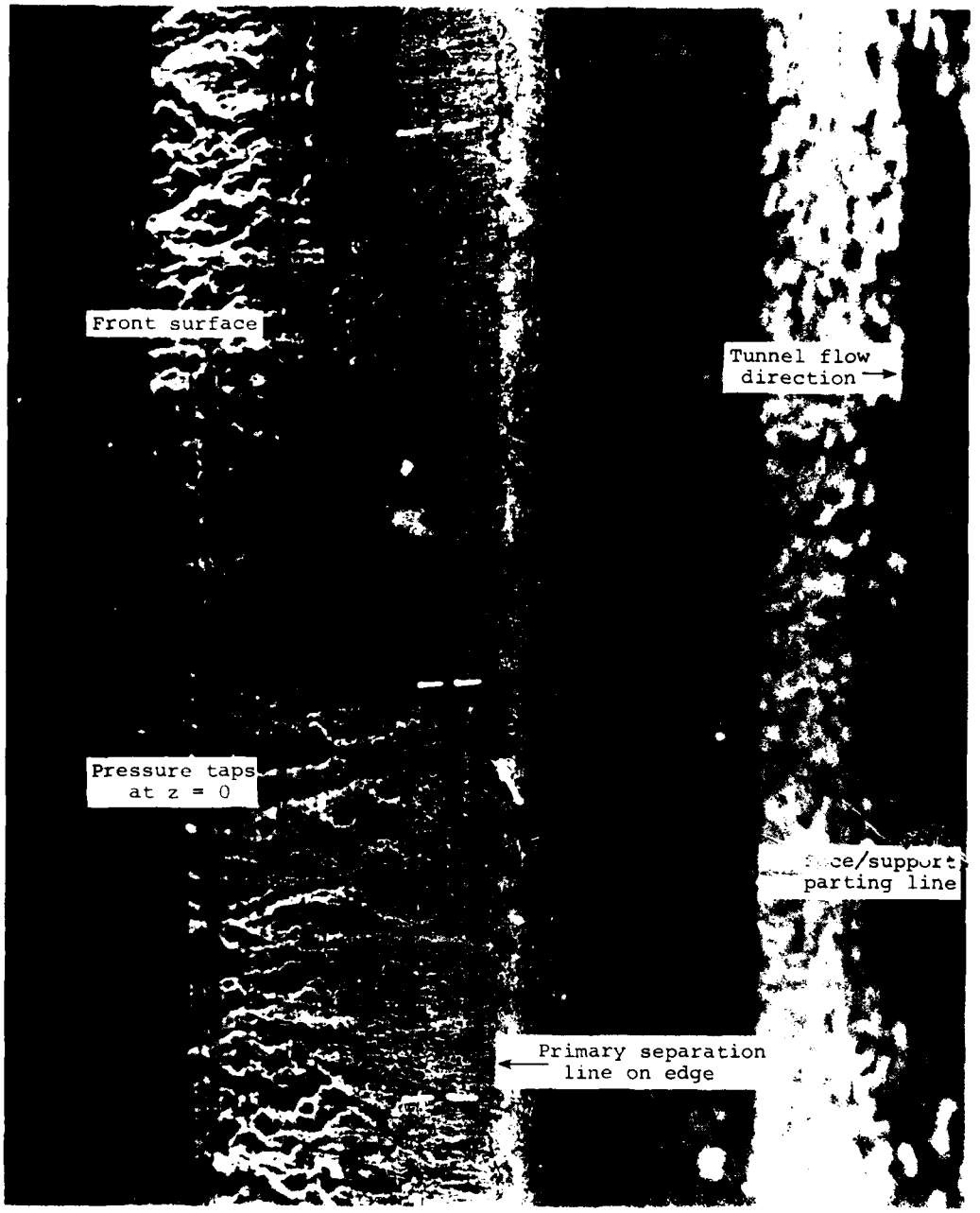

(c) Close up view of front surface and edge.

Figure 19.- Continued.

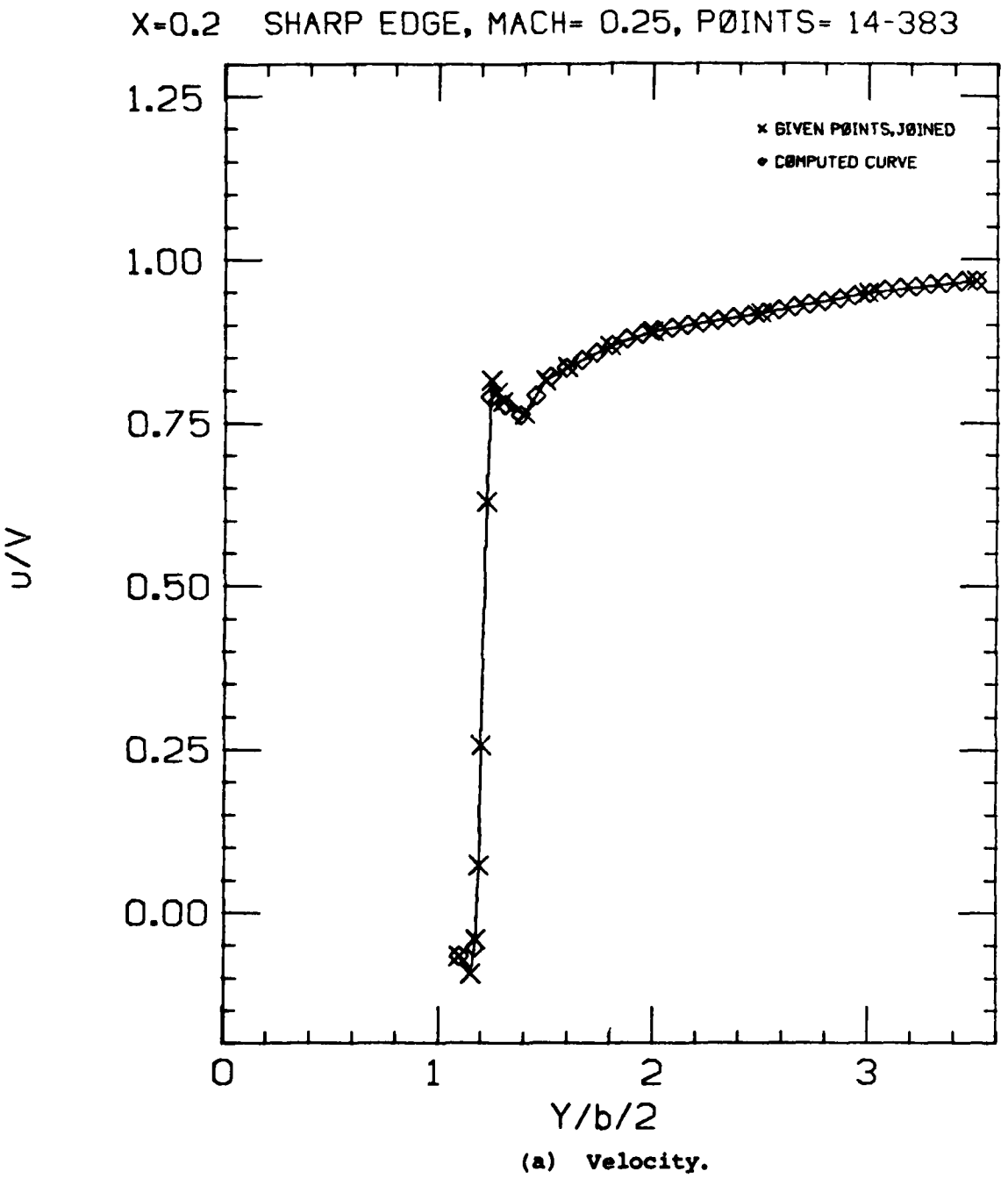

(a) Velocity.

Figure 20.- Spline fit to streamwise velocity component.

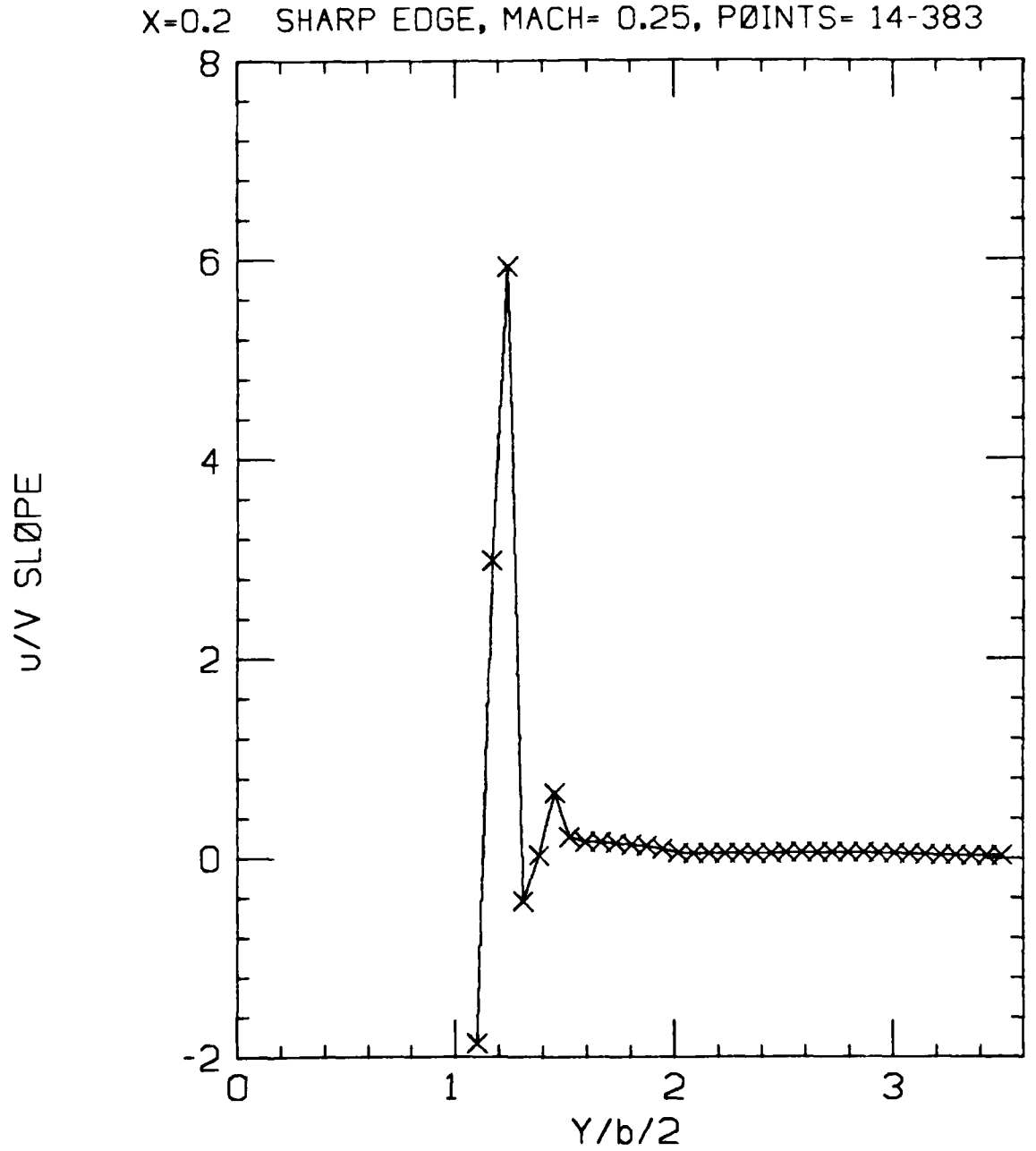

(b) Velocity derivative, $\frac{\partial \frac{u}{V}}{\partial \frac{y}{b/2}}$

Figure 20.- Concluded.

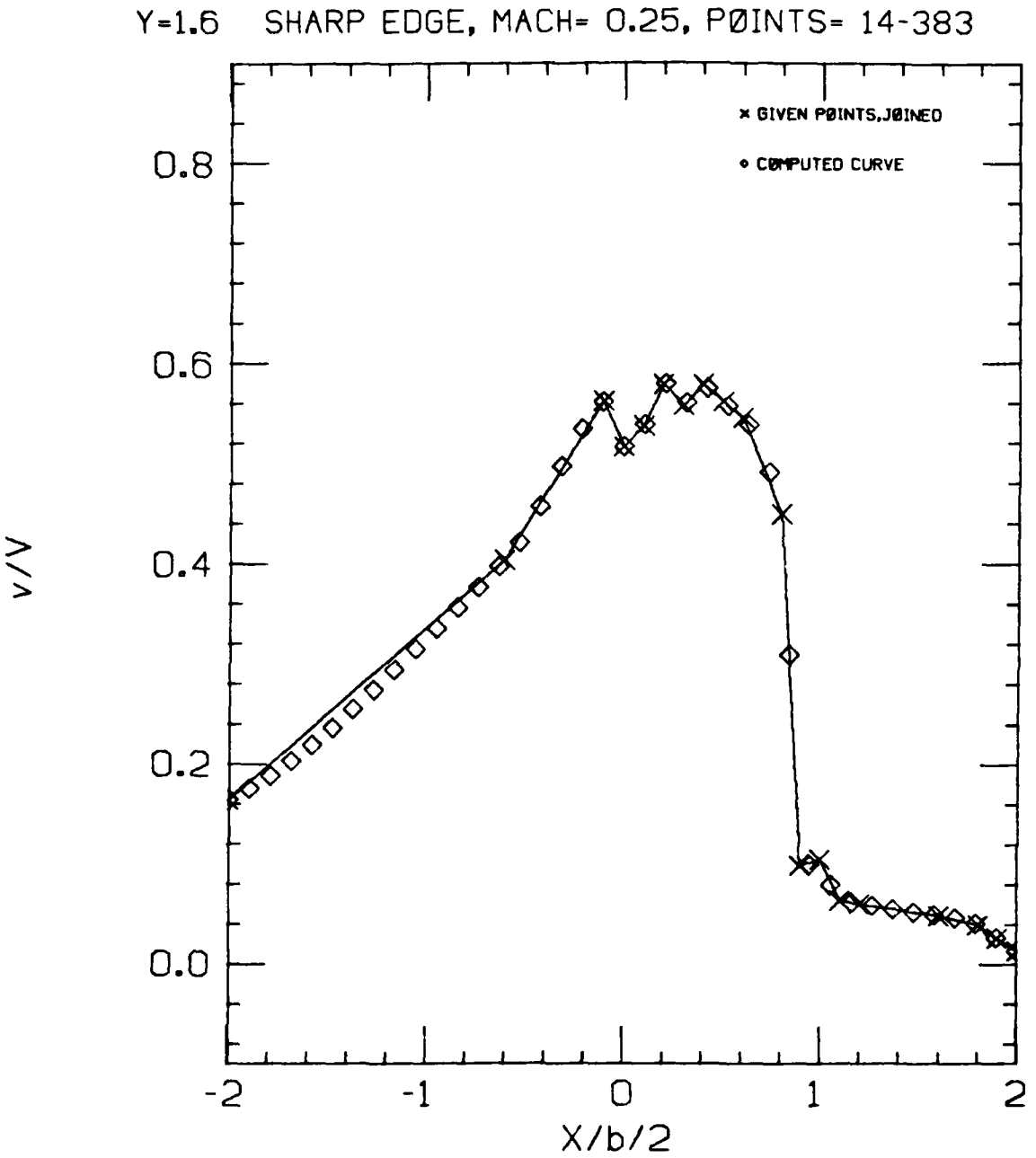

(a) Velocity.

Figure 21.- Spline fit to vertical velocity component.

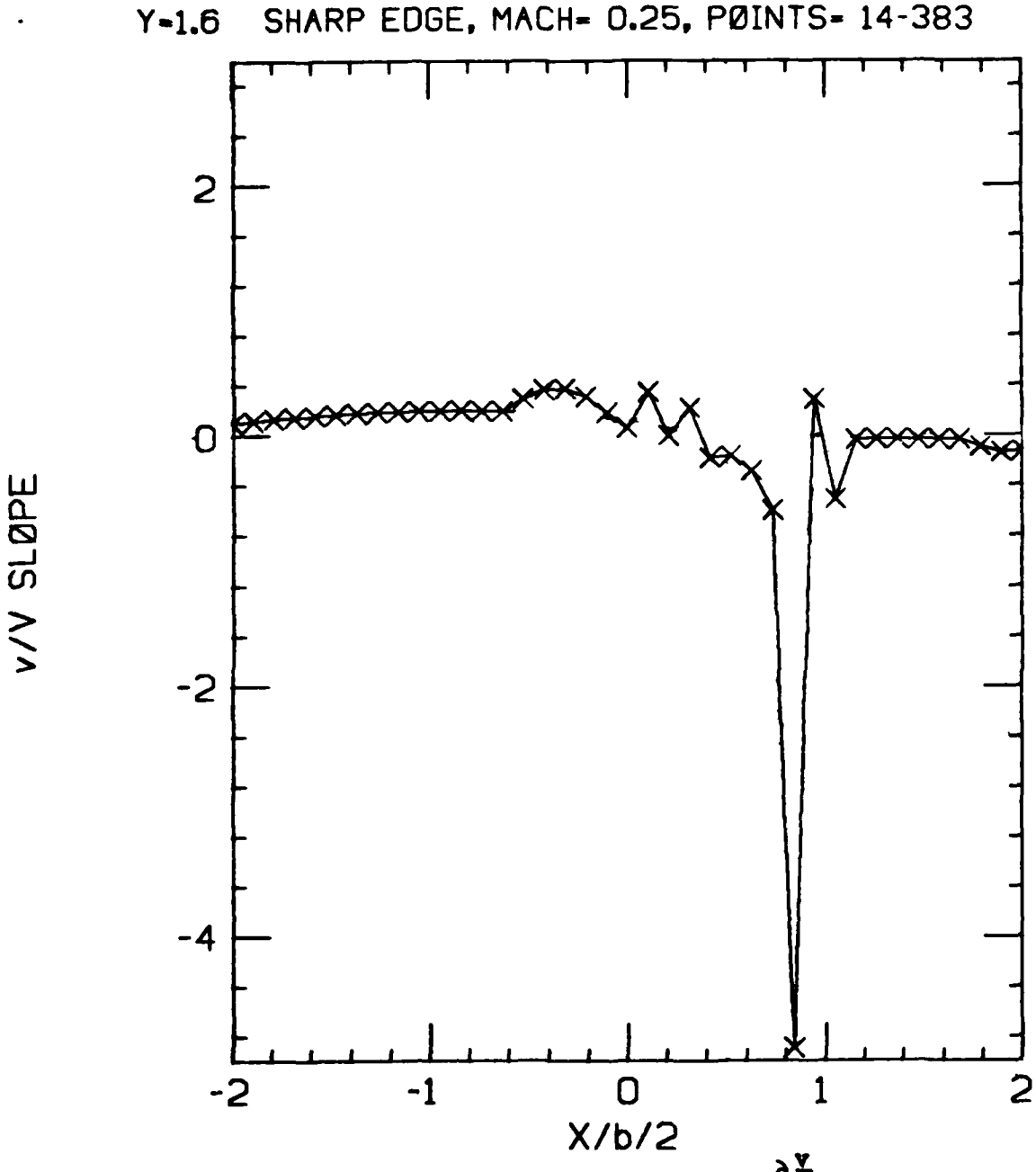

(b) Velocity derivative, $\frac{\partial \frac{v}{V}}{\partial \frac{x}{b/2}}$

Figure 21.- Concluded.

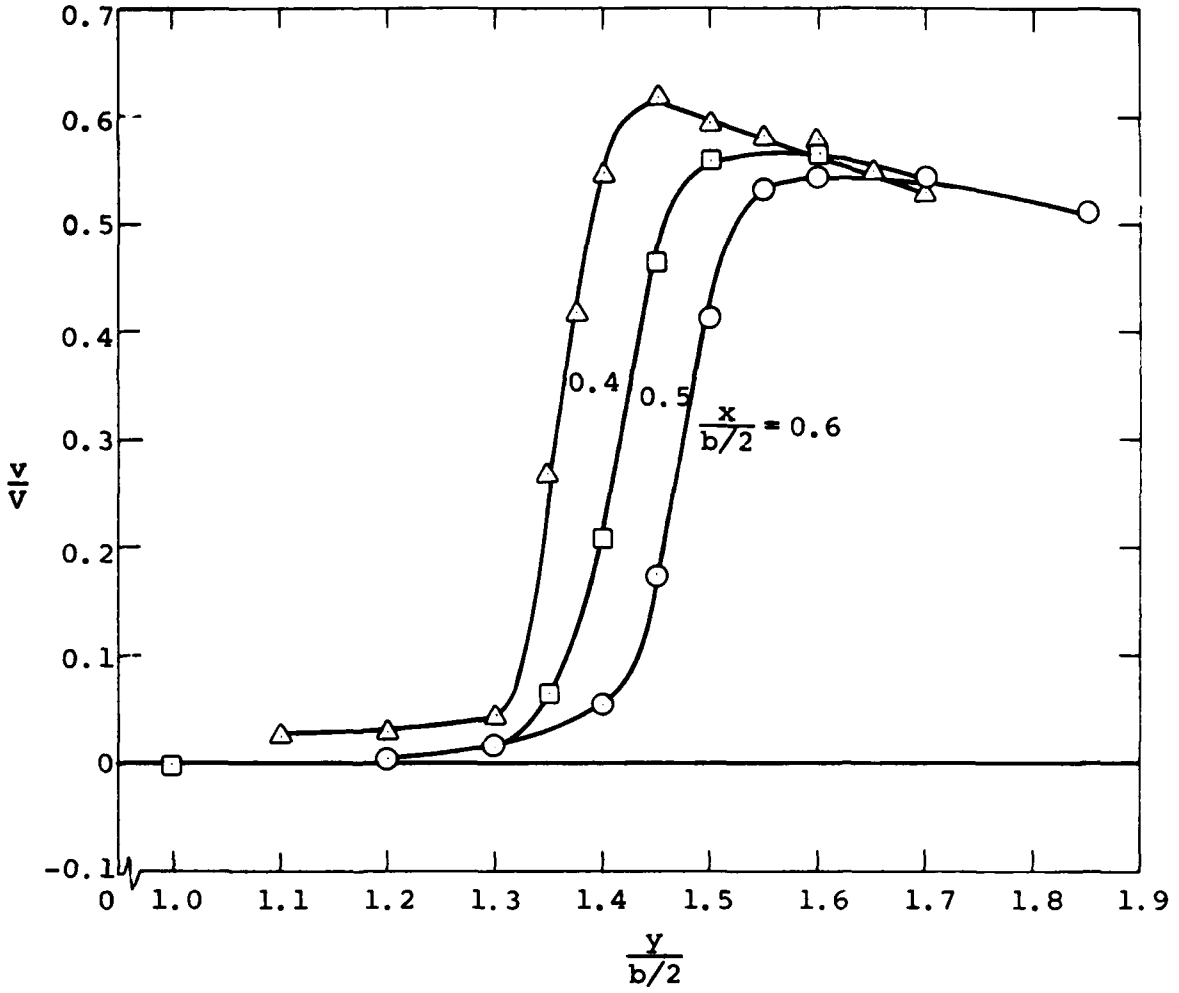

(a) Vertical velocity vs lateral position

Figure 22.- Vertical velocity derivative construction for sharp edge model, M = 0.25, Re = 0.25×10^6.

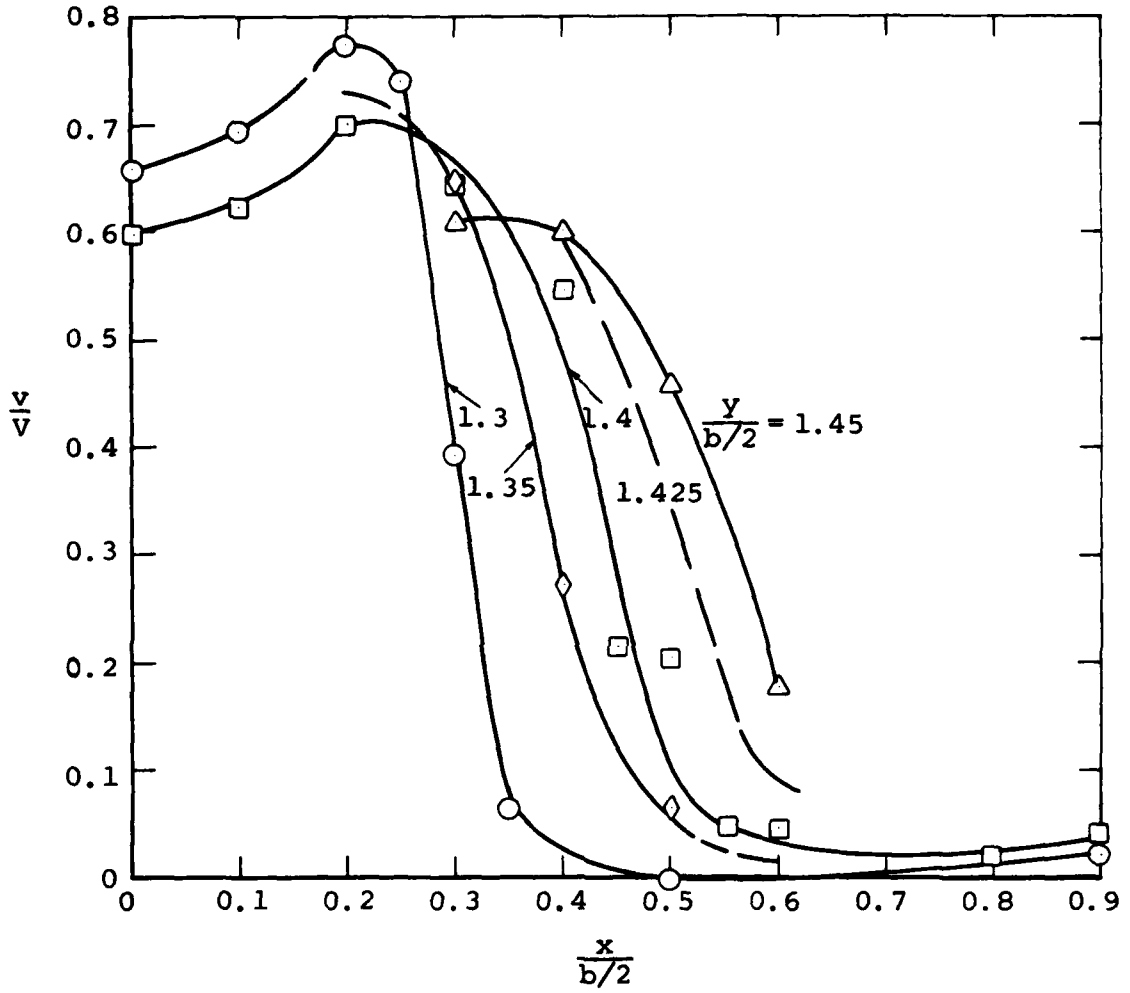

(b) Vertical velocity vs streamwise position

Figure 22.- Continued.

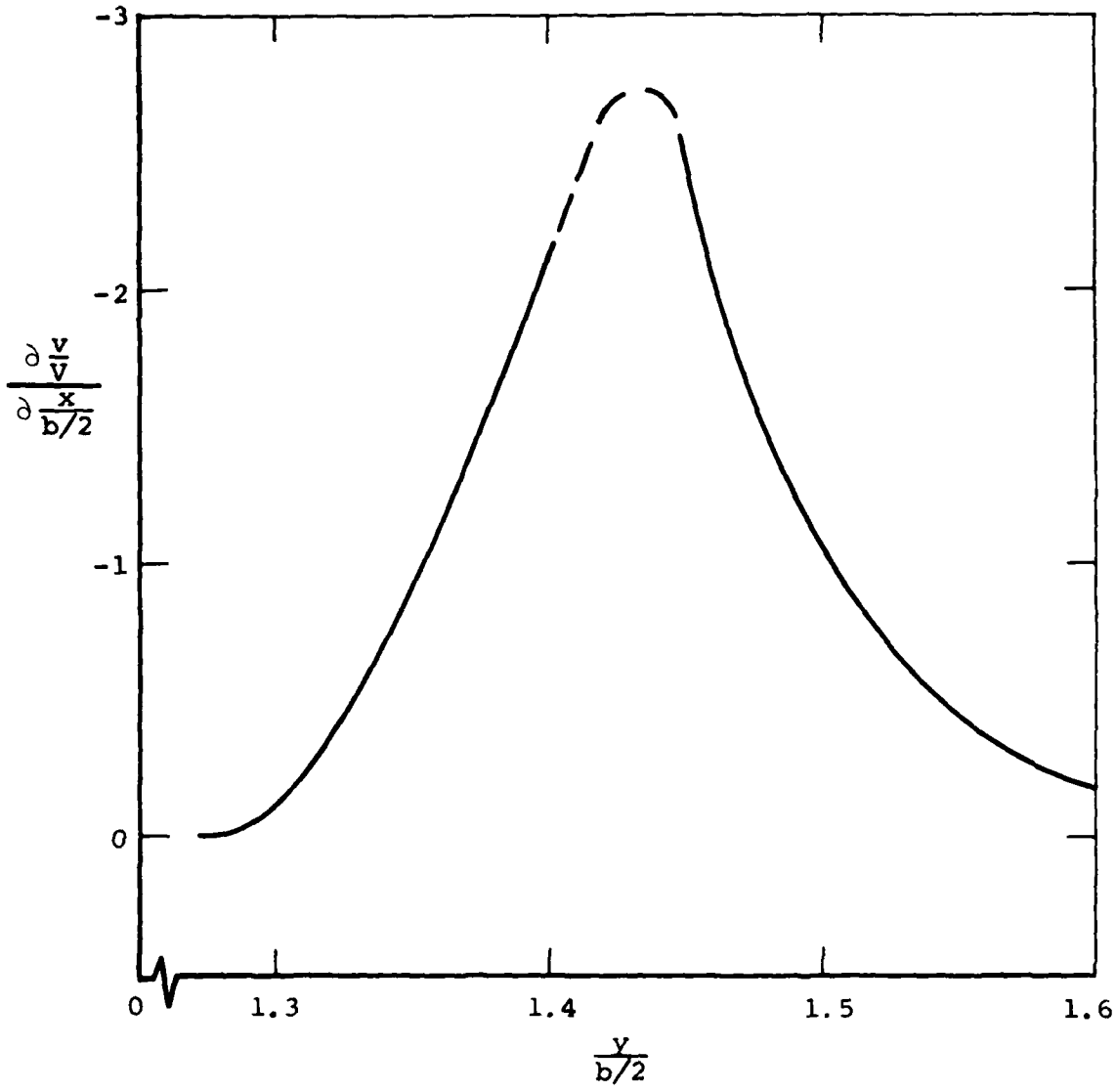

(c) Velocity derivative at $\frac{x}{b/2} = 0.5$

Figure 22.- Concluded.

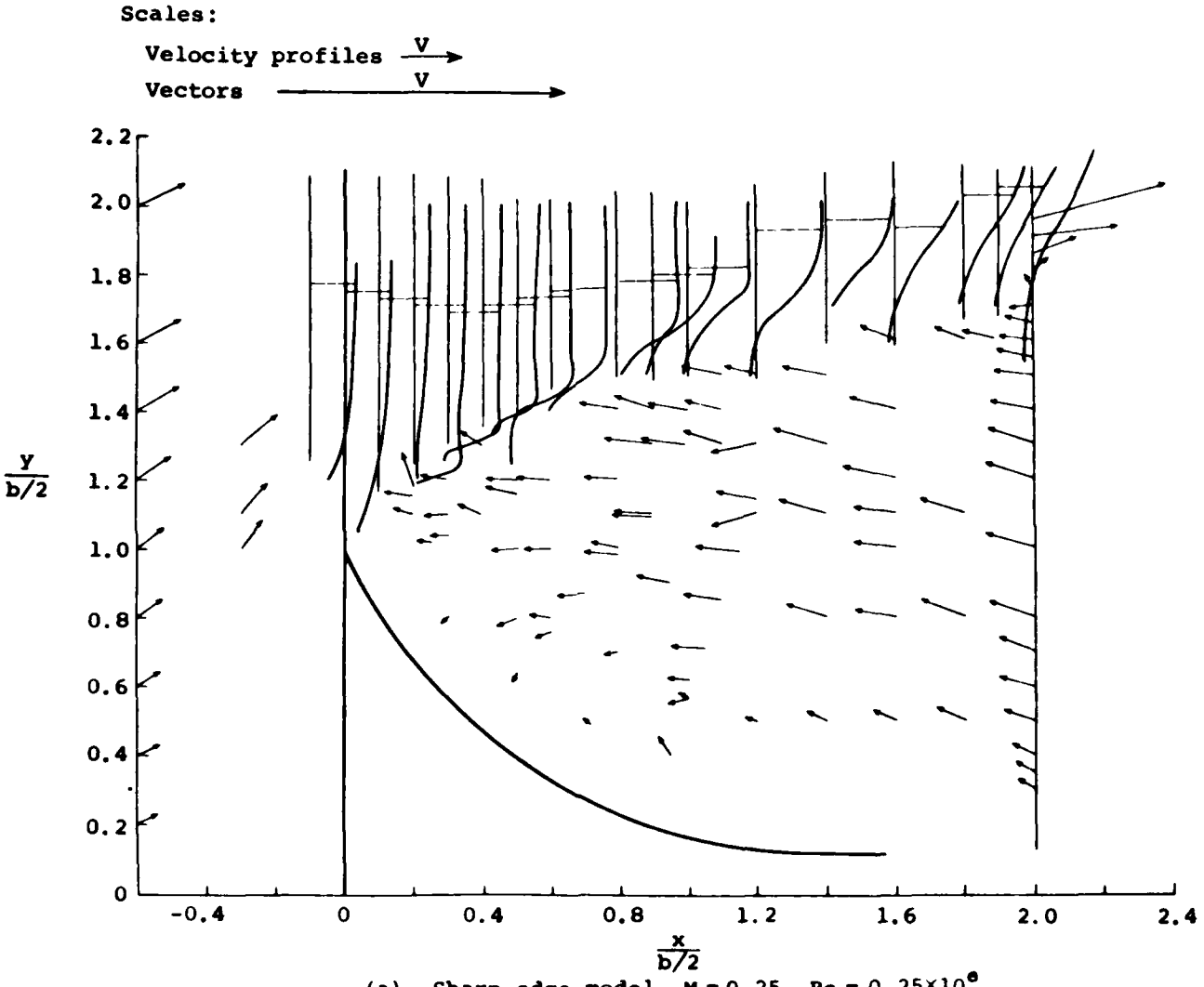

(a) Sharp edge model, M = 0.25, Re = 0.25×10^6

Figure 23.- Velocity profile and recirculation region velocity vector data.

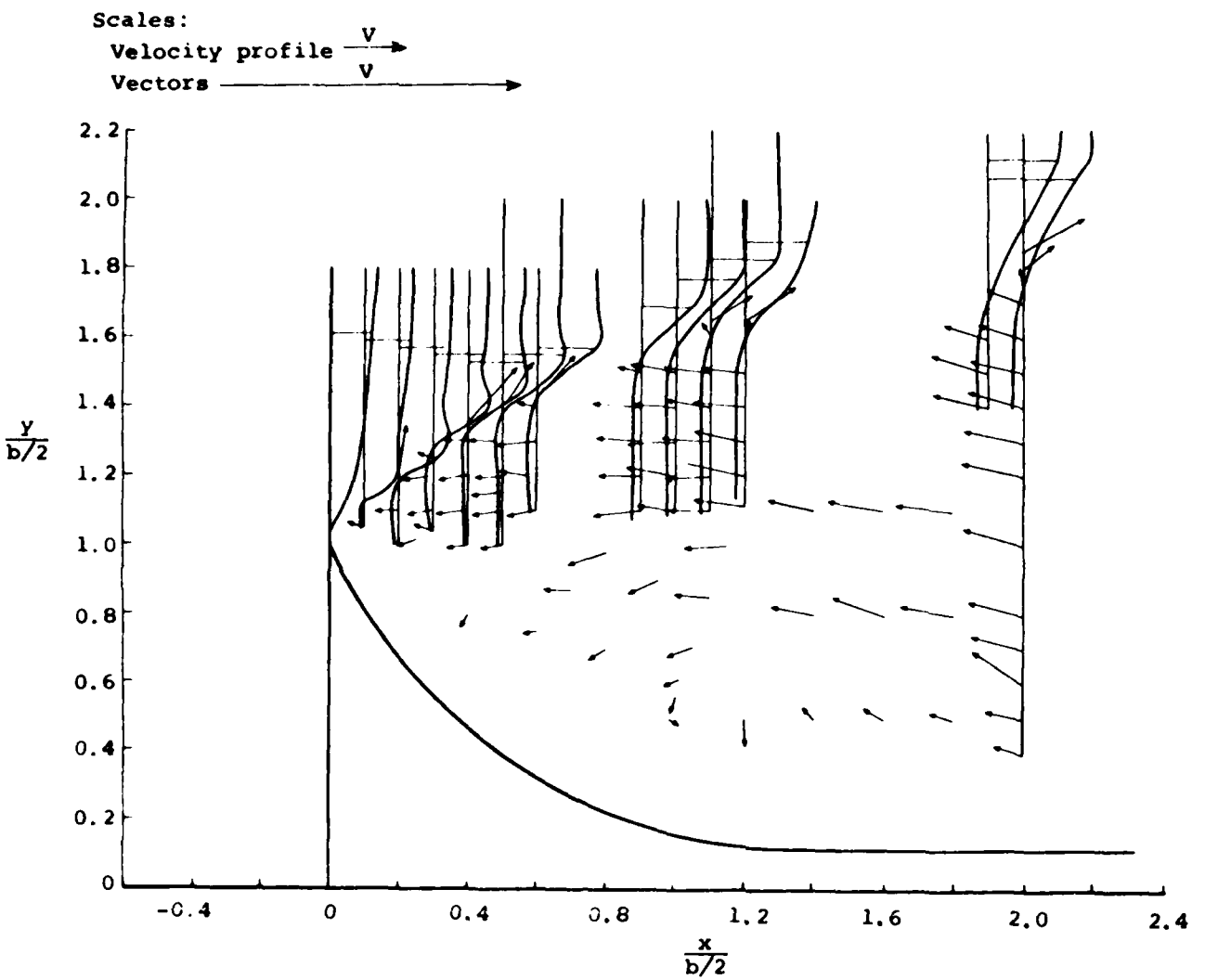

(b) Sharp edge model, M = 0.5, Re = 0.15×10^6

Figure 23.- Continued.

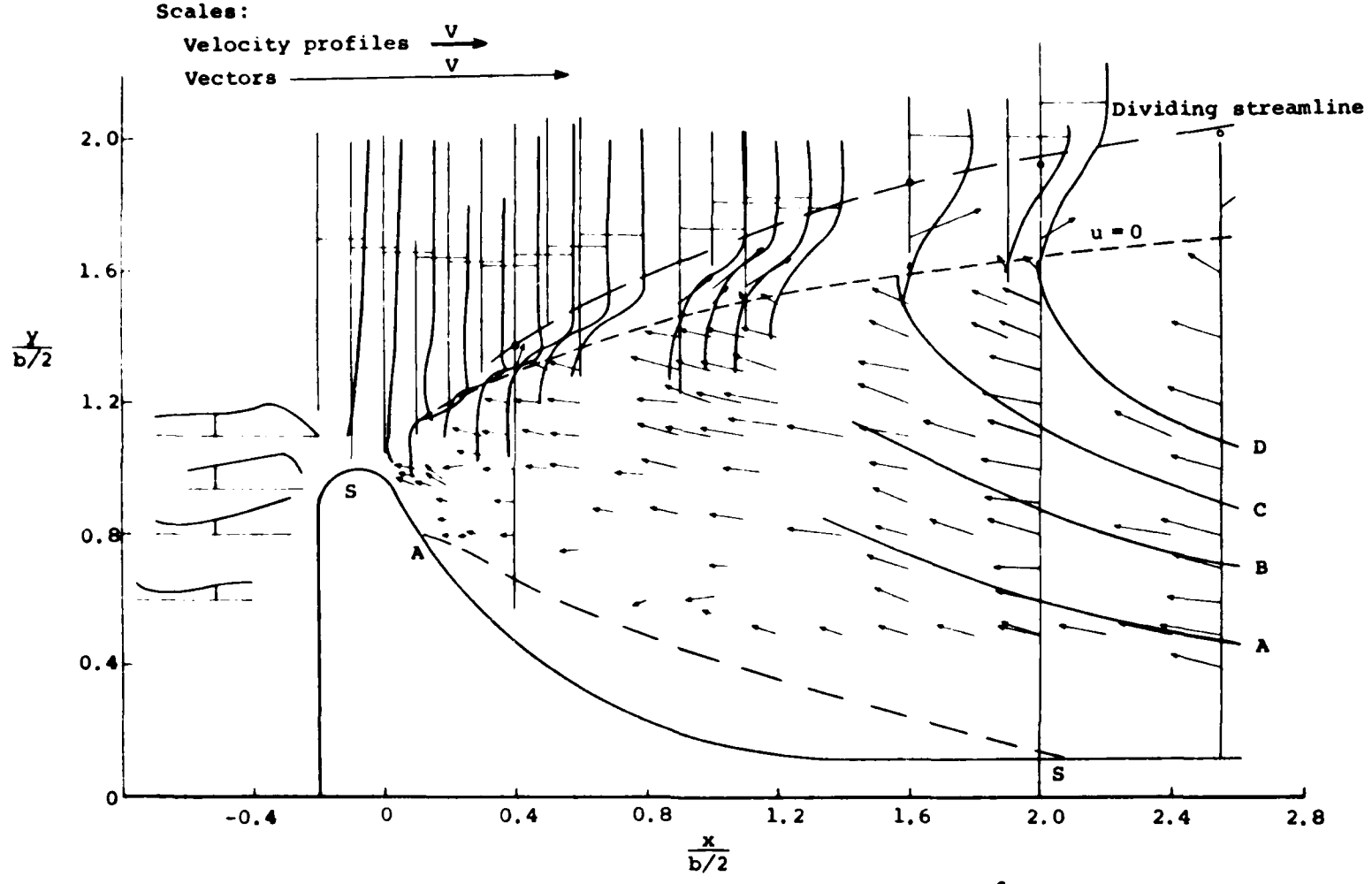

(c) Round edge model, M = 0.25, Re = 0.25×10^6

Figure 23.- Continued.

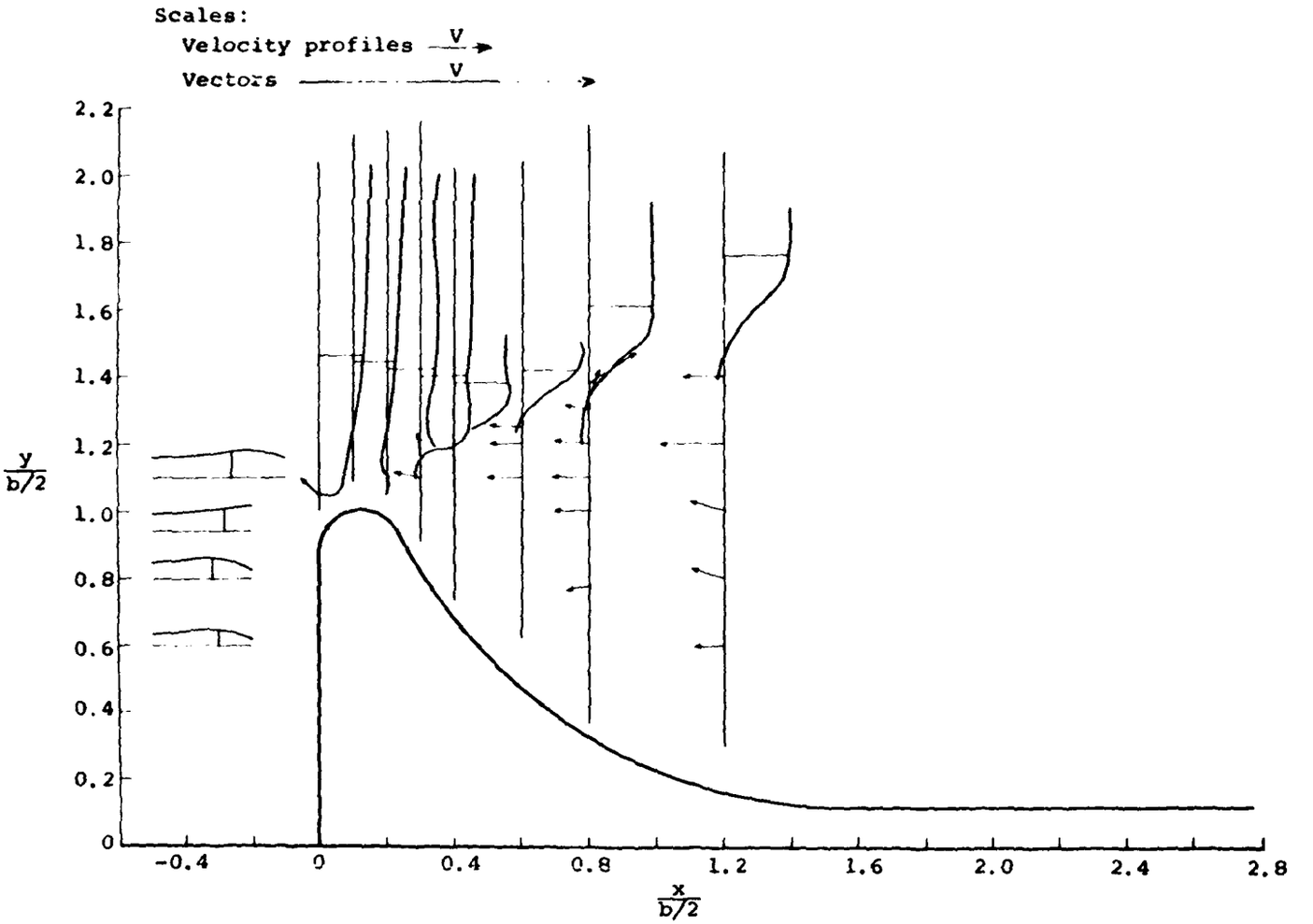

(d) Round edge model, M = 0.5, Re = 0.15×10^6

Figure 23.- Concluded.

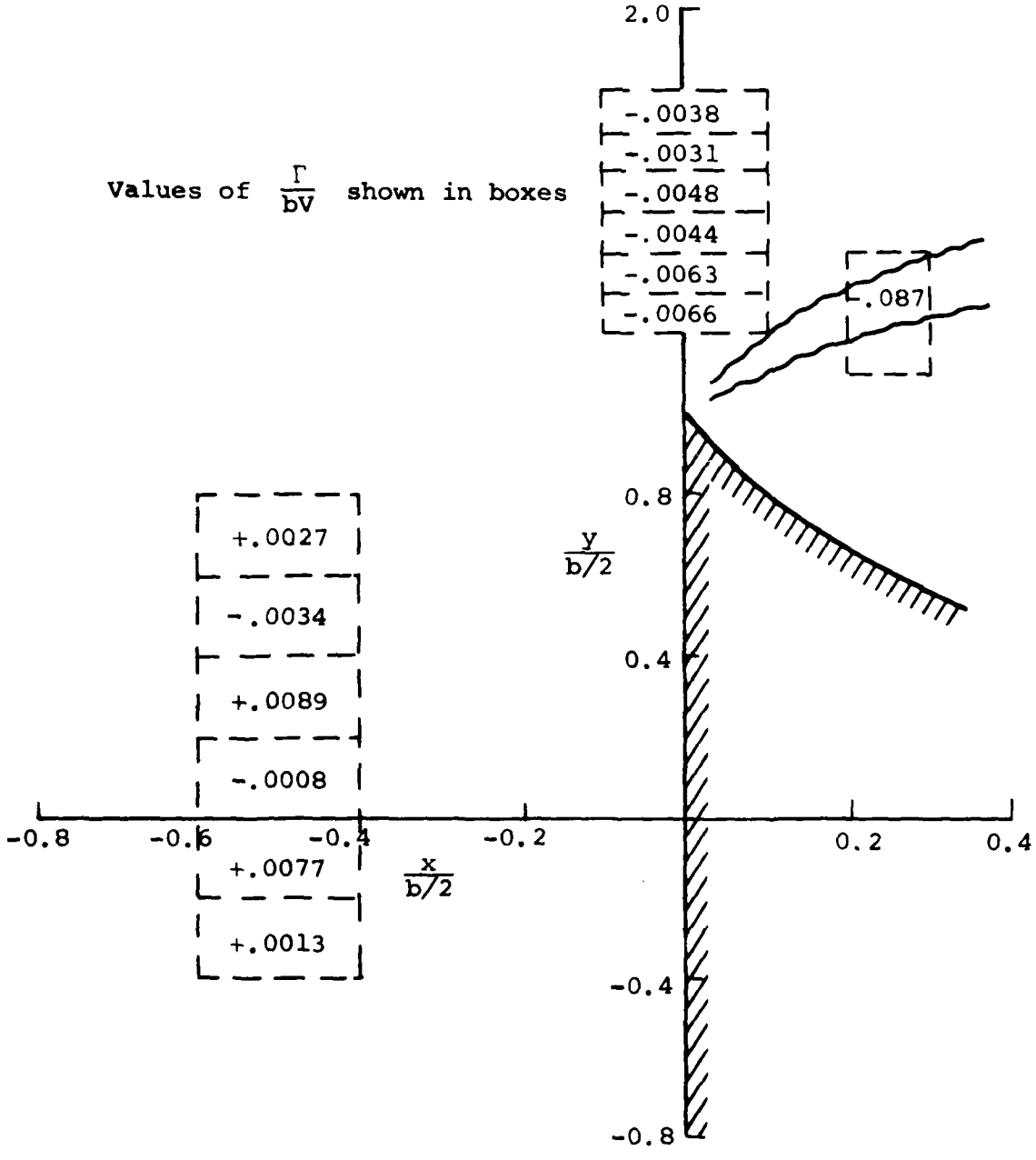

Figure 24.- Contour integration results in free stream; sharp edge model at M = 0.25.

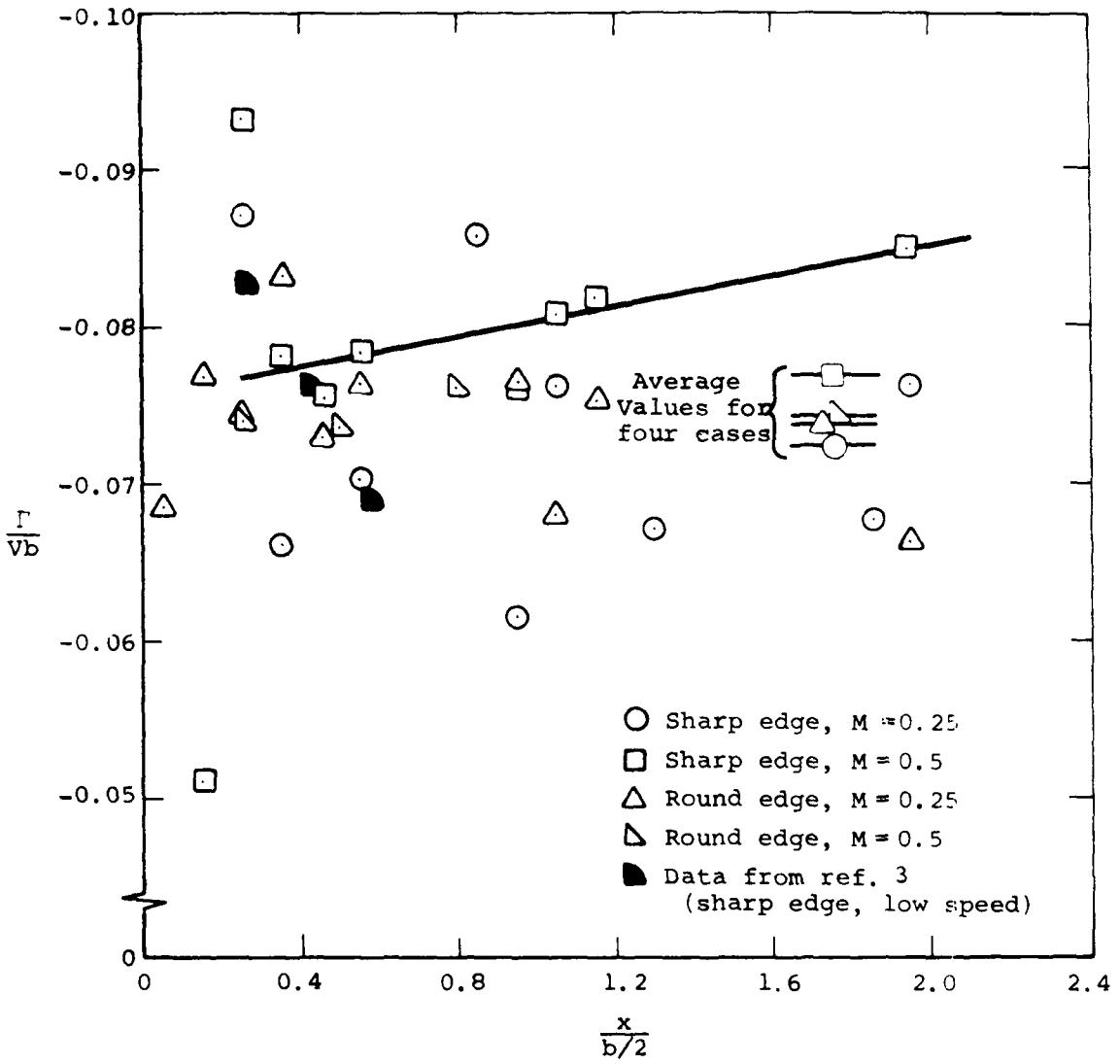

Figure 25.- Contour integration results for circulation.

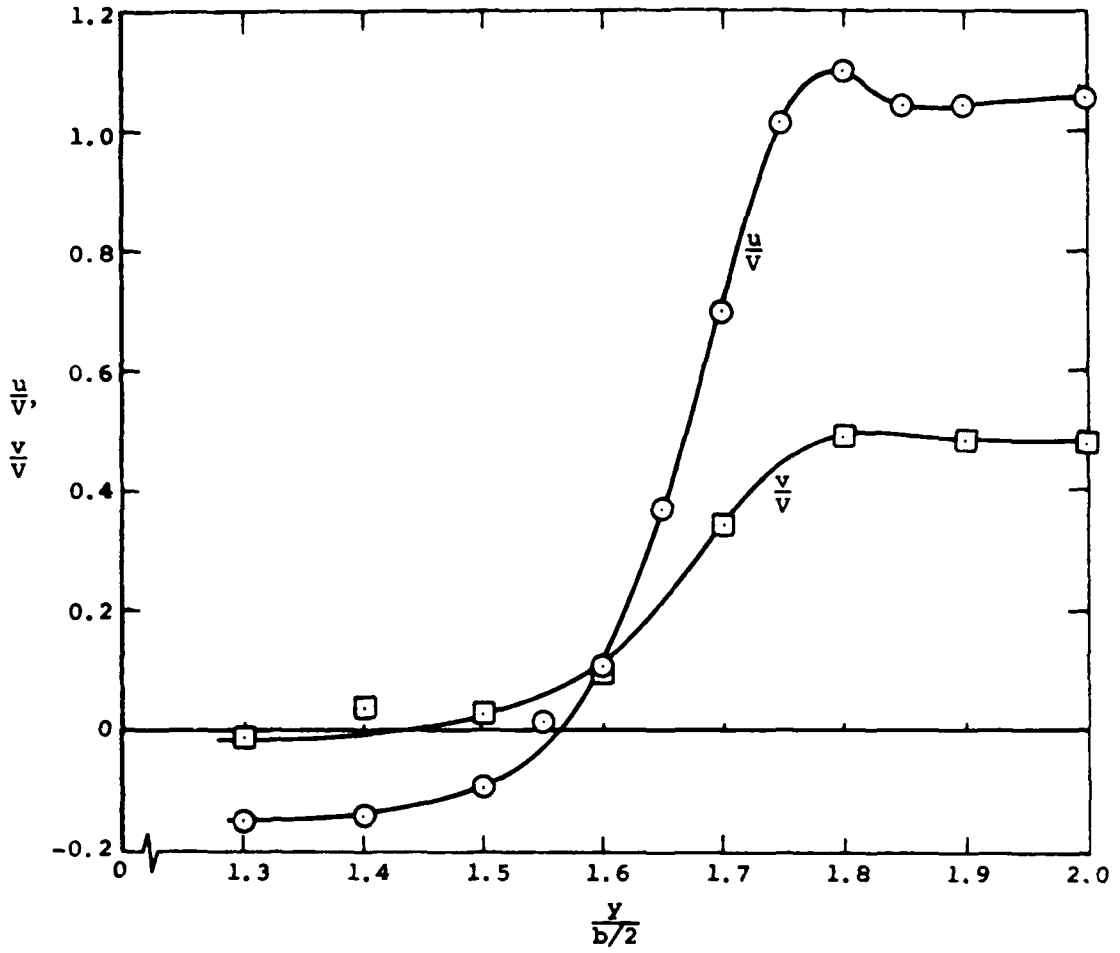

(a) Lateral variation of velocity

Figure 26.- Construction of vorticity distribution for sharp edge model at M = 0.25 for x/(b/2) = 1.0.

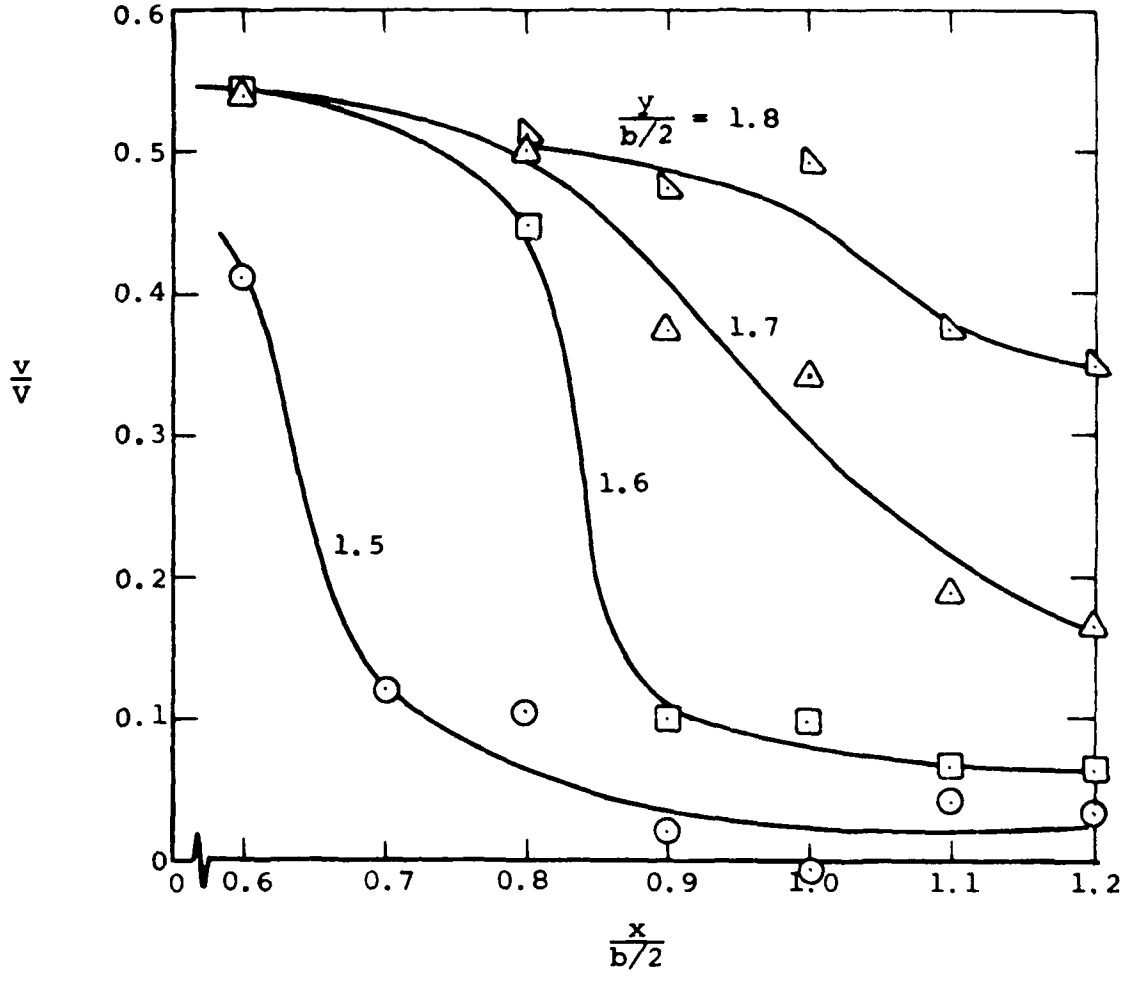

(b) Longitudinal variation of velocity

Figure 26.- Continued.

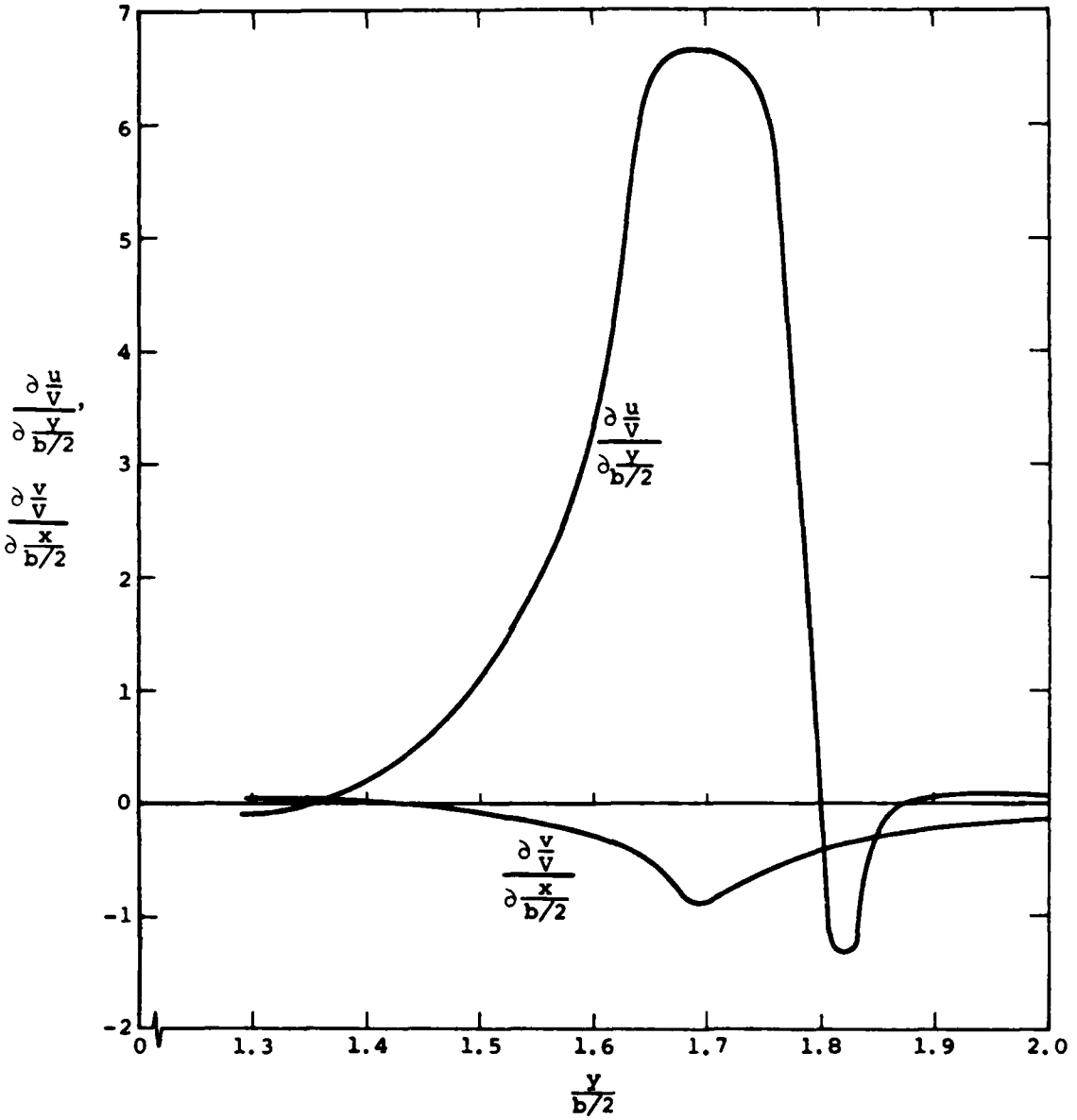

(c) Velocity derivatives

Figure 26.- Continued.

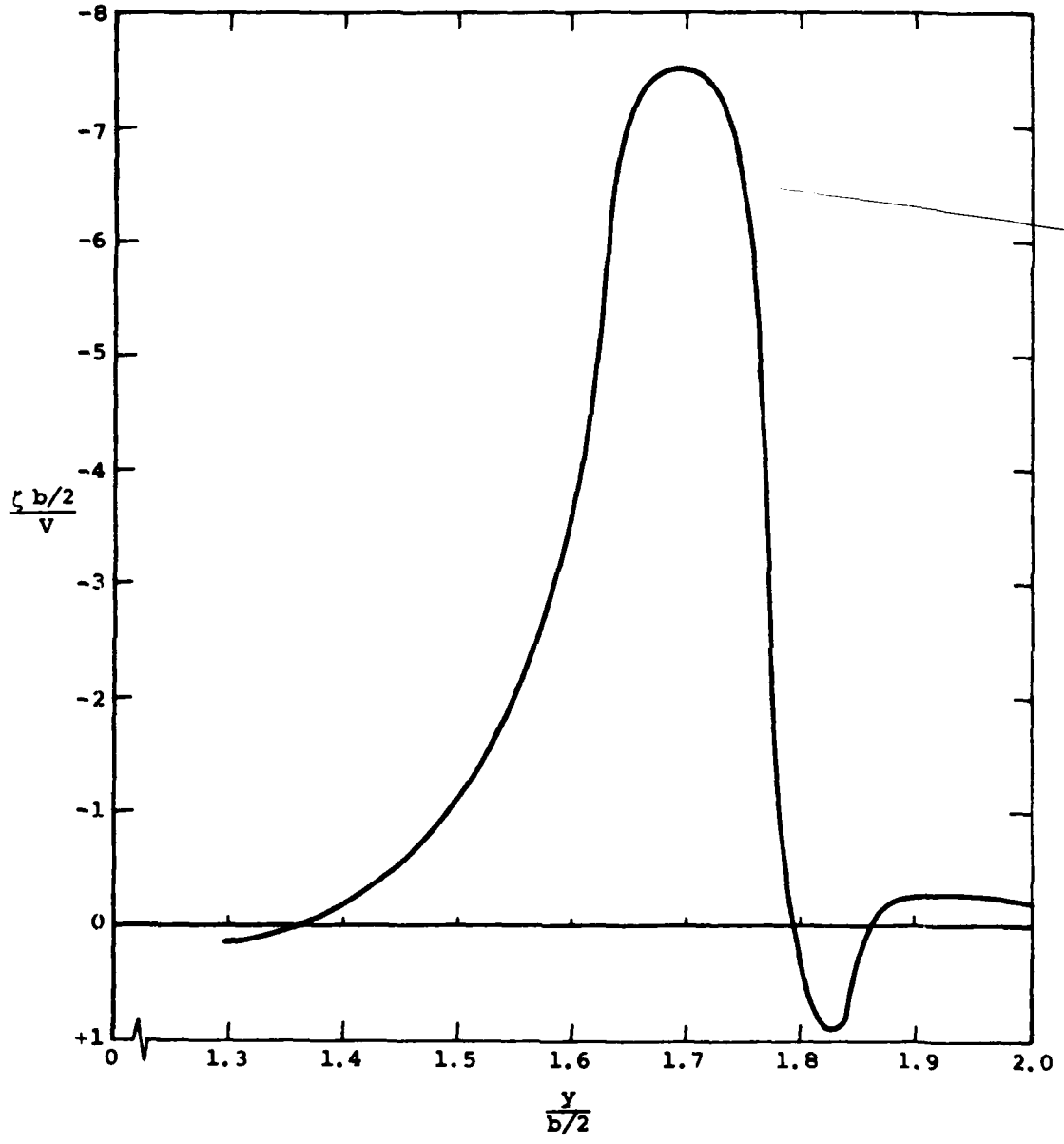

(d) Vorticity

Figure 26.- Continued.

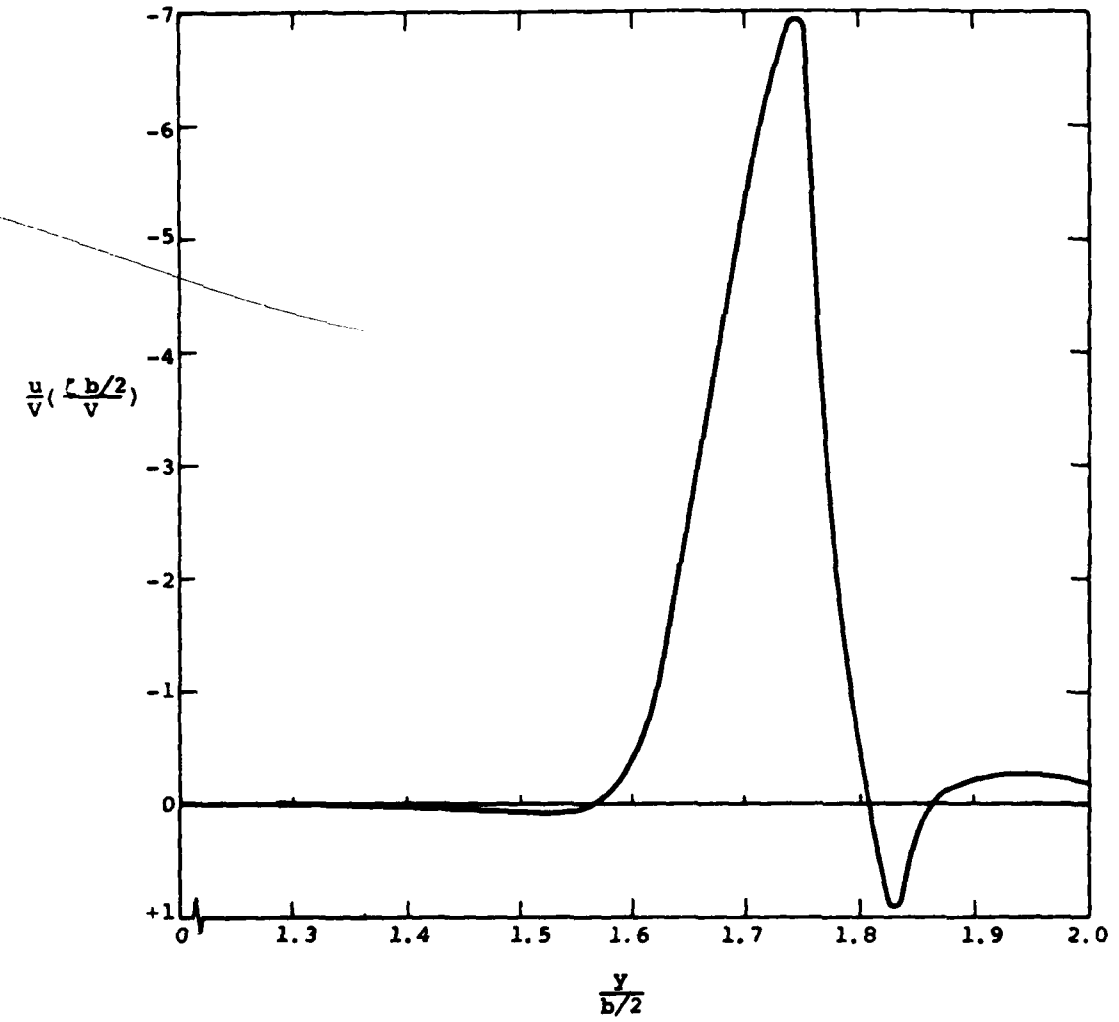

(e) Rate of transport of vorticity

Figure 26.- Concluded.

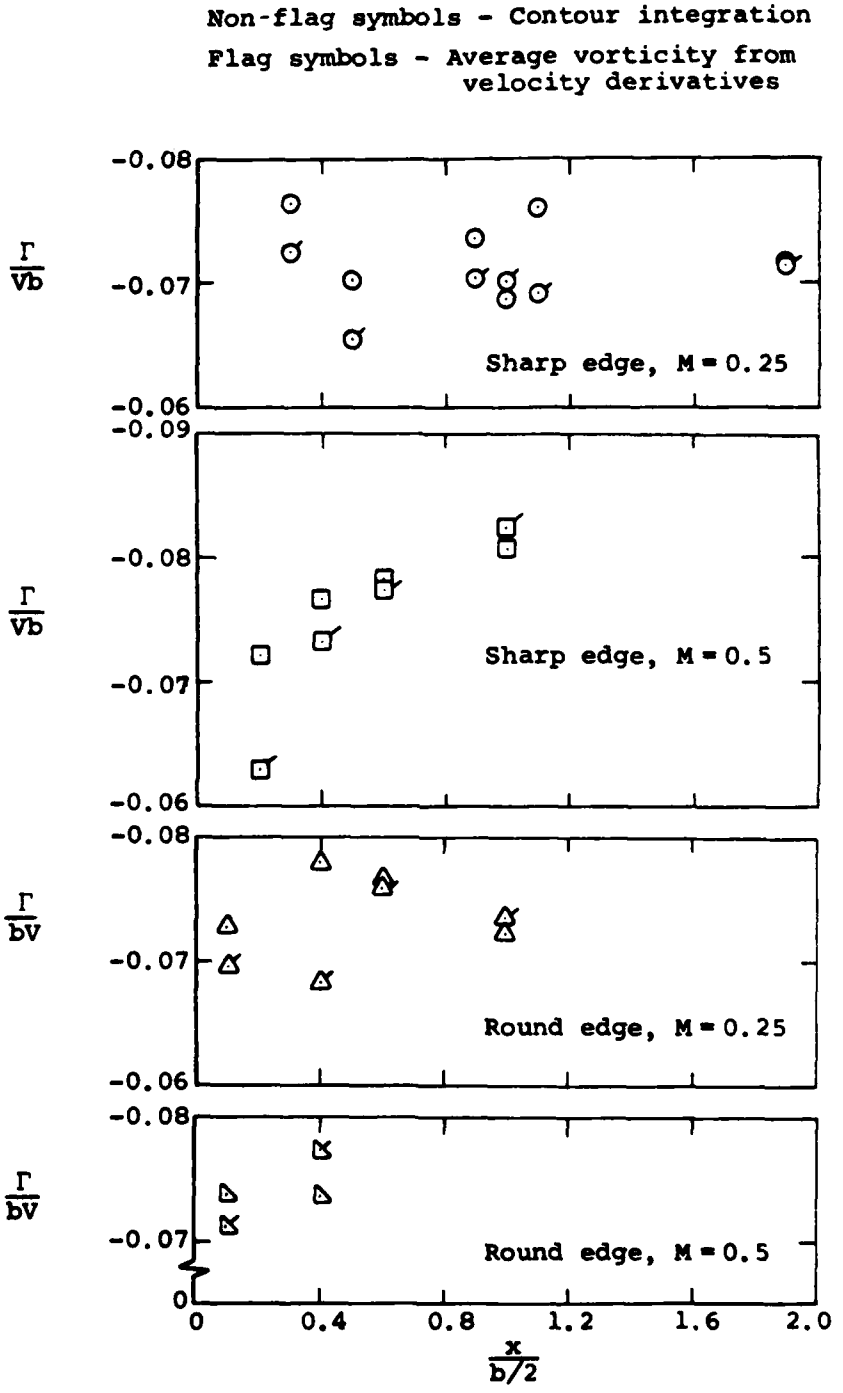

Figure 27.- Comparison of contour integration and velocity derivative results for circulation.

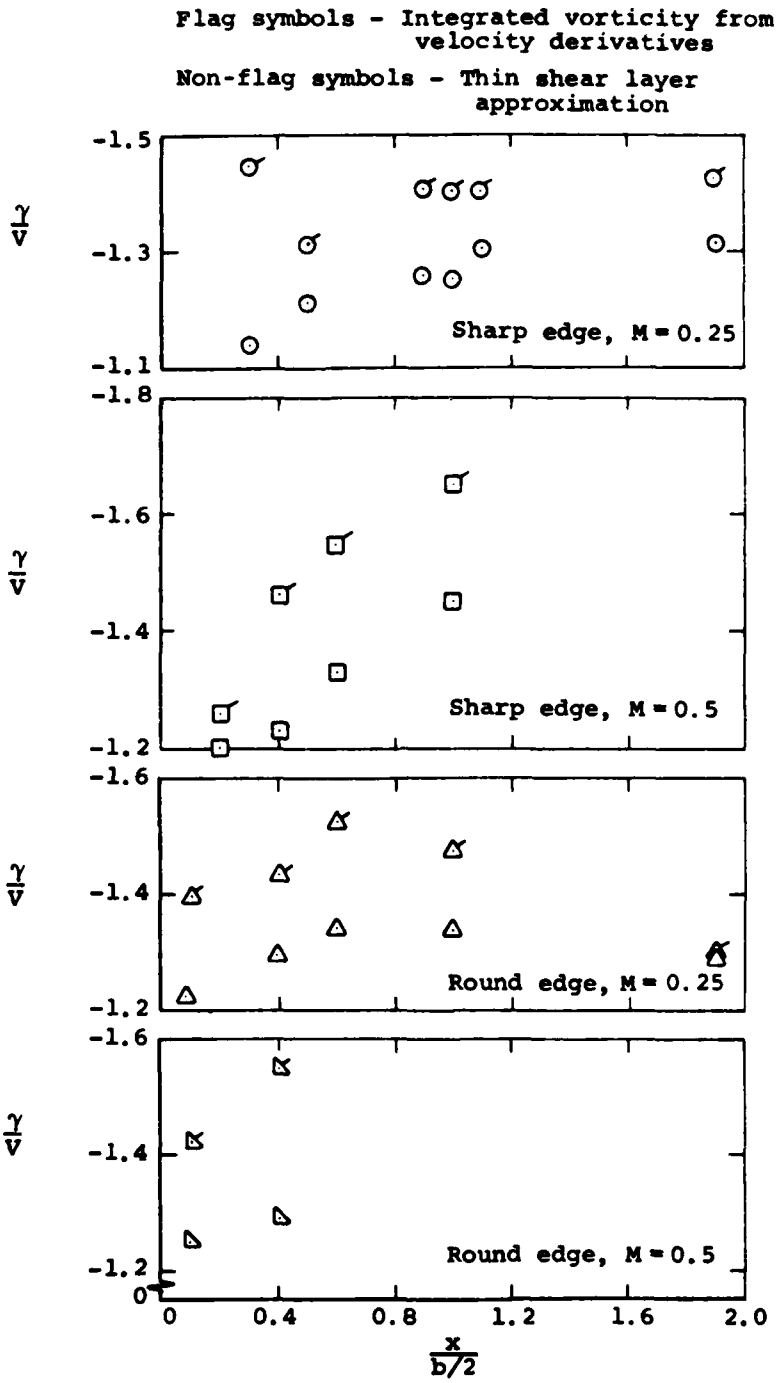

Figure 28.- Comparison of velocity derivative and thin shear layer approximation for total shear layer vorticity.

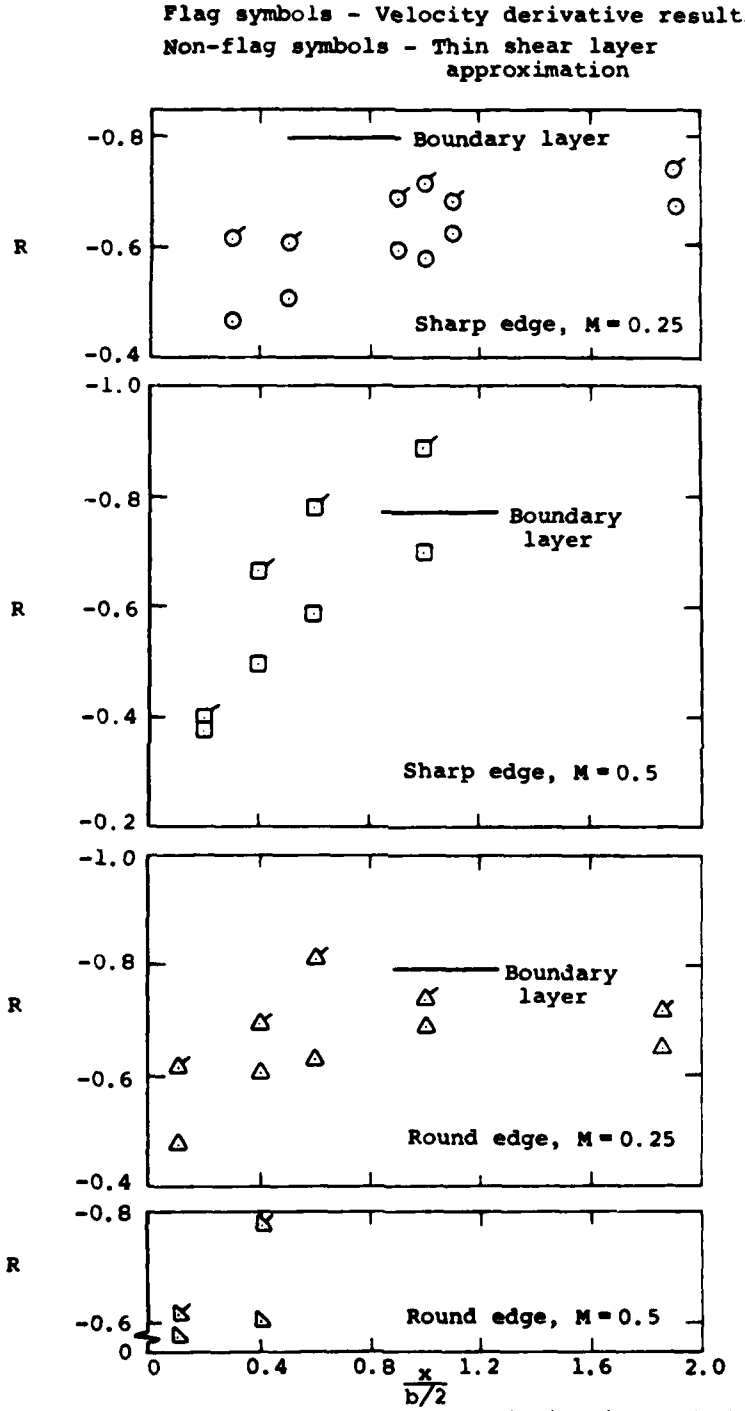

Figure 29.- Comparison of velocity derivative and thin layer approximation results for vorticity transport rate.

LIST OF SYMBOLS

b	width of model face
C_p	pressure coefficient, $(p - p_\infty)/q$
f	frequency
$\vec{n}$	unit vector normal to the contour element
N	the number of readings by the laser velocimeter of velocity components at a given location
p	static pressure
p_∞	free-stream static pressure
q	free-stream dynamic pressure, $1/2\rho V^2$
R	rate of transport vorticity, Eq. (16)
Re	Reynolds number, based on V and b/2
s	length along a contour
St	Strouhal number, fb/V
u_δ	velocity at edge of the boundary layer
u,v	velocity components in the x and y directions, respectively
u_i, v_i	the i^{th} reading by the laser velocimeter of velocity components at a given location in the flow
$\overline{u'^2}, \overline{v'^2}$	the mean square values of the turbulence intensity, Eqs. (3), (4)
V	free stream velocity
V_s	velocity at point in flow, $\sqrt{u^2 + v^2}$
Γ	circulatic
ρ	free-stream density
ζ	vorticity, defined in Eq. 13
$(\vec{\ })$	indicates vector quantity

DISTRIBUTION LIST

Technical Library
Building 313
Ballistic Research Laboratories
Aberdeen Proving Ground, MD 21005

Mr. Aviars Celmins
Ballistic Research Laboratory
Ballistic Modelling Division
Aberdeen Proving Ground, MD 21005

Dr. P. J. Roache
Ecodynamics Research Associates, Inc.
P. O. Box 8172
Albuquerque, NM 87108

Defense Technical Information Center
Cameron Station, Building 5
Alexandria, VA 22314 (12)

Library
Naval Academy
Annapolis, MD 21402

Director, Tactical Technology Office
Defense Advanced Research Projects Agency
1400 Wilson Blvd.
Arlington, VA 22209

Code 200B
Office of Naval Research
800 N. Quincy Street
Arlington, VA 22217

Code 438
Office of Naval Research
800 N. Quincy Street
Arlington, VA 22217 (2)

Dr. J. L. Potter
Deputy Director, Technology
von Karman Gas Dynamics Facility
Arnold Air Force Station, TN 37389

Professor J. C. Wu
School of Aerospace Engineering
Georgia Institute of Technology
Atlanta, GA 30332

Library
Aerojet-General Corporation
6352 North Irwindale Avenue
Azusa, CA 91702

NASA Scientific and Technical Information Facility
P. O. Box 8757
Baltimore/Washington International Airport, MD 21240

Dr. K. C. Wang
College of Engineering
San Diego State University
San Diego, CA 92182

Professor A. J. Chorin
Department of Mathematics
University of California
Berkeley, CA 94720

Professor M. Holt
Department of Mechanical Engineering
University of California
Berkeley, CA 94720

Dr. H. R. Chaplin
Code 1600
David W. Taylor Naval Ship Research and Development Center
Bethesda, MD 20084

Dr. Hans Lugt
Code 1802
David W. Taylor Naval Ship Research and Development Center
Bethesda, MD 20084

Dr. Francois Frenkiel
Code 1802
David W. Taylor Naval Ship Research and Development Center
Bethesda, MD 20084

Dr. T. C. Tai
Code 1606
David W. Taylor Naval Ship Research and Development Center
Bethesda, MD 20084

DISTRIBUTION LIST (Continued)

Dr. G. R. Inger
Dept. of Aerospace Engineering
Virginia Polytechnic Institute and
State University
Blacksburg, VA 24061

Professor C. H. Lewis
Dept. of Aerospace and Ocean Engrg.
Virginia Polytechnic Institute and
State University
Blacksburg, VA 24061

Professor A. H. Nayfeh
Dept. of Engineering Science
Virginia Polytechnic Institute and
State University
Blacksburg, VA 24061

Dr. A. Rubel
Research Department
Grumman Aerospace Corporation
Bethpage, NY 11714

Commanding Officer
Office of Naval Research
Eastern/Central Regional Office
666 Summer St., Bldg. 114, Section D
Boston, MA 02210

Dr. J. C. Erickson, Jr.
CALSPAN Corporation
Advanced Technology Center
P. O. Box 400
Buffalo, NY 14225

Dr. T. J. Falk
CALSPAN Corporation
Advanced Technology Center
P. O. Box 400
Buffalo, NY 14225

Dr. C. Witliff
CALSPAN Corporation
Advanced Technology Center
P. O. Box 400
Buffalo, NY 14225

Prof. R. F. Probstein
Dept. of Mechanical Engineering
Massachusetts Institute of Technology
Cambridge, MA 02139

Commanding Officer
Office of Naval Research Branch Office
536 South Clark Street
Chicago, IL 60605

Code 753
Naval Weapons Center
China Lake, CA 93555

Mr. J. Marshall
Code 4063
Naval Weapons Center
China Lake, CA 93555

Professor R. T. Davis
Dept. of Aerospace Engineering
University of Cincinnati
Cincinnati, OH 45221

Professor S. G. Rubin
Dept. of Aerospace Engineering and
Applied Mechanics
University of Cincinnati
Cincinnati, OH 45221

Library MS 60-3
NASA Lewis Research Center
21000 Brookpark Road
Cleveland, OH 44135

Dr. J. D. Anderson, Jr.
Chairman, Dept. of Aerospace Engrg.
College of Engineering
University of Maryland
College Park, MD 20742

Professor O. Burggraf
Dept. of Aeronautical and Astro-
nautical Engineering
Ohio State University
1314 Kinnear Road
Columbus, OH 43212

DISTRIBUTION LIST (Continued)

Technical Library
Naval Surface Weapons Center
Dahlgren Laboratory
Dahlgren, VA 22448

Dr. F. Moore
Naval Surface Weapons Center
Dahlgren Laboratory
Dahlgren, VA 22448

Technical Library 2-51131
LTV Aerospace Corporation
P. O. Box 5907
Dallas, TX 75222

Library, United Aircraft Corporation
Research Laboratories
Silver Lane
East Hartford, CT 06108

Professor G. Moretti
Polytechnic Institute of New York
Long Island Center
Dept. of Aerospace Engrg. and
Applied Mechanics
Route 110
Farmingdale, NY 11735

Dr. W. R. Briley
Scientific Research Associates, Inc.
P. O. Box 498
Glastonbury, CT 06033

Professor P. Gordon
Calumet Campus
Dept. of Mathematics
Purdue University
Hammond, IN 46323

Library (MS 185)
NASA Langley Research Center
Langley Station
Hampton, VA 23665

Professor A. Chapmann
Chairman, Mechanical Engineering Dept.
William M. Rice Institute
Box 1892
Houston, TX 77001

Technical Library
Naval Ordnance Station
Indian Head, MD 20640

Professor D. A. Caughey
Sibley School of Mechanical and
Aerospace Engineering
Cornell University
Ithaca, NY 14850

Professor E. L. Resler
Sibley School of Mechanical and
Aerospace Engineering
Cornell University
Ithaca, NY 14850

Professor S. F. Shen
Sibley School of Mechanical and
Aerospace Engineering
Cornell University
Ithaca, NY 14850

Library
Midwest Research Institute
425 Volker Boulevard
Kansas City, MO 64110

Dr. M. M. Hafez
Flow Research, Inc.
P. O. Box 5040
Kent, WA 98031

Dr. E. M. Murman
Flow Research, Inc.
P. O. Box 5040
Kent, WA 98031

Dr. J. J. Riley
Flow Research, Inc.
P. O. Box 5040
Kent, WA 98031

DISTRIBUTION LIST (Continued)

Dr. S. A. Orszag
Cambridge Hydrodynamics, Inc.
54 Baskin Road
Lexington, MA 02173

Dr. P. Bradshaw
Imperial College of Science and Technology
Department of Aeronautics
Prince Consort Road
London SW7 2BY, England

Professor T. Cebeci
Mechanical Engineering Department
California State University, Long Beach
Long Beach, CA 90840

Dr. H. K. Cheng
University of Souther California
Department of Aerospace Engrg.
University Park
Los Angeles, CA 90007

Professor J. D. Cole
Mechanics and Structures Department
School of Engineering and Applied Science
University of California
Los Angeles, CA 90024

Engineering Library
University of Southern California
Box 77929
Los Angeles, CA 90007

Dr. C. -M. Ho
Dept. of Aerospace Engineering
University of Southern California
University Park
Los Angeles, CA 90007

Dr. T. D. Taylor
The Aerospace Corporation
P. O. Box 92957
Los Angeles, CA 90009

Commanding Officer
Naval Ordnance Station
Louisville, KY 40214

Mr. B. H. Little, Jr.
Lockheed-Georgia Company
Department 72-74, Zone 369
Marietta, GA 30061

Professor E. R. G. Eckert
University of Minnesota
241 Mechanical Engineering Bldg.
Minneapolis, MN 55455

Dr. Gary Chapman
Mail Stop 227-4
Ames Research Center
Moffett Field, CA 94035

Library
Naval Postgraduate School
Monterey, CA 93940

Dr. J. L. Steger
Dept. of Aeronautics and Astronautics
Durand Building
Stanford University
Stanford, CA 94305

Dr. S. S. Stahara
Nielsen Engineering & Research, Inc.
510 Clyde Avenue
Mountain View, CA 94043

Engineering Societies Library
345 East 47th Street
New York, NY 10017

Professor A. Jameson
Mechanical and Aeronautical Engrg. Dept.
Princeton University
E Quad
Princeton, NJ 08540

DISTRIBUTION LIST (Continued)

Professor G. Miller
Dept. of Applied Science
New York University
26-36 Stuyvesant Street
New York, NY 10003

Office of Naval Research
New York Area Office
715 Broadway - 5th Floor
New York, NY 10003

Dr. A. Vaglio-Laurin
Dept. of Applied Science
New York University
26-36 Stuyvesant Street
New York, NY 10003

Mr. D. Farmer
Naval Ocean Research and Development Activity
Code 332
NSTL Station, MS 39522

Librarian, Aeronautical Library
National Research Council
Montreal Road
Ottawa 7, Canada

Lockheed Missiles and Space Company
Technical Information Center
3251 Hanover Street
Palo Alto, CA 94304

Commanding Officer
Office of Naval Research Western Regional Office
1030 East Green Street
Pasadena, CA 91106

Engineering Division
California Institute of Technology
Pasadena, CA 91109

Library
Jet Propulsion Laboratory
4800 Oak Grove Drive
Pasadena, CA 91103

Professor H. Liepmann
Department of Aeronautics
California Institute of Technology
Pasadena, CA 91109

Mr. L. I. Chasen, MGR-MSD Lib.
General Electric Company
Missile and Space Division
P. O. Box 8555
Philadelphia, PA 19101

Technical Library
Naval Missile Center
Point Mugu, CA 93042

Professor S. Bogdonoff
Gas Dynamics Laboratory
Dept. of Aerospace & Mechanical Sci.
Princeton University
Princeton, NJ 08540

Professor S. I. Cheng
Dept. of Aerospace & Mechanical Sci.
Princeton University
Princeton, NJ 08540

Dr. J. E. Yates
Aeronautical Research Associates of Princeton, Inc.
50 Washington Road
Princeton, NJ 08540

Professor L. Sirovich
Division of Applied Mathematics
Brown University
Providence, RI 02912

Redstone Scientific Information Center
Chief, Document Section
Army Missile Command
Redstone Arsenal, AL 35809

U.S. Army Research Office
P. O. Box 12211
Research Triangle Park, NC 27709

DISTRIBUTION LIST (Continued)

Editor, Applied Mechanics Review
Southwest Research Institute
8500 Culebra Road
San Antonio, TX 78228

Library and Information Services
General Dynamics-CONVAIR
P. O. Box 1128
San Diego, CA 92112

Dr. R. Magnus
General Dynamics-CONVAIR
Kearny Mesa Plant
P. O. Box 80847
San Diego, CA 92138

Office of Naval Research
San Francisco Area Office
One Hallidie Plaza, Suite 601
San Francisco, CA 94102

Library
The RAND Corporation
1700 Main Street
Santa Monica, CA 90401

Dr. P. E. Rubbert
Boeing Aerospace Company
Boeing Military Airplane Development
Organization
P. O. Box 3707
Seattle, WA 98124

Dr. H. Yoshihara
Boeing Aerospace Company
P. O. Box 3999
Mail Stop 41-18
Seattle, WA 98124

Librarian
Naval Surface Weapons Center
White Oak Laboratory
Silver Spring, MD 20910

Dr. J. M. Solomon
Naval Surface Weapons Center
White Oak Laboratory
Silver Spring, MD 20910

Professor J. H. Ferziger
Dept. of Mechanical Engineering
Stanford University
Stanford, CA 94305

Professor K. Karamchetti
Dept. of Aeronautics and Astronautics
Stanford University
Stanford, CA 94305

Professor O. Bunemann
Institute for Plasma Research
Stanford University
Stanford, CA 94305

Engineering Library
McDonnell Douglas Corporation
Department 218, Building 101
P. O. Box 516
St. Louis, MO 63166

Dr. R. J. Hakkinen
McDonnell Douglas Corporation
Department 222
P. O. Box 516
St. Louis, MO 63166

Dr. N. Malmuth
Rockwell International Science Center
1049 Camino Dos Rios
P. O. Box 1085
Thousand Oaks, CA 91360

Library
Institute of Aerospace Studies
University of Toronto
Toronto 5, Canada

Professor W. R. Sears
Aerospace and Mechanical Engineering
University of Arizona
Tucson, AZ 95721

Professor A. R. Seebass
Dept. of Aerospace and Mechanical
Engineering
University of Arizona
Tucson, AZ 95721

DISTRIBUTION LIST (Concluded)

Dr. K. T. Yen
Code 3015
Naval Air Development Center
Warminster, PA 18974

Air Force Office of Scientific
Research (SREM)
Building 410, Bolling AFB
Washington, DC 20332

Chief of Research and Development
Office of Chief of Staff
Department of the Army
Washington, DC 20310

Library of Congress
Science and Technology Division
Washington, DC 20540

Director of Research (Code RR)
National Aeronautics and Space
Administration
600 Independence Avenue, SW
Washington, DC 20546

Library
National Bureau of Standards
Washington, DC 20234

National Science Foundation
Engineering Division
1800 G Street, NW
Washington, DC 20550

AIR 320D
Naval Air Systems Command
Washington, DC 20361

AIR 950D
Naval Air Systems Command
Washington, DC 20375

Code 2627
Naval Research Laboratory
Washington, DC 20375

SEA 03512
Naval Sea Systems Command
Washington, DC 20362

SEA 09G3
Naval Sea Systems Command
Washington, DC 20362

Dr. Charles Watkins
Head, Mechanical Engineering Dept.
Howard University
Washington, DC 20059

Dr. A. L. Slafkosky
Scientific Advisor
Commandant of the Marine Corps (Code AX)
Washington, DC 20380

Director
Weapons Systems Evaluation Group
Washington, DC 20350

Research Library
AVCO Corporation
Missile Systems Division
201 Lowell Street
Wilmington, MA 01887

AFAPL (APRC)
AB
Wright-Patterson AFB, OH 45433

Dr. Donald J. Harney
AFFDL/FX
Wright-Patterson AFB, OH 45433

Mr. G. Malcolm
Mail Stop 227-8
Ames Research Center
Moffett Field, CA 94035